METHOD AND MECHANISM OF COLLOIDAL ASSEMBLY FOR SURFACE PATTERNING

by

Sayantan Das, M.S.

A dissertation submitted to the Graduate Council of
Texas State University in partial fulfillment
of the requirements for the degree of
Doctor of Philosophy
With a Major in Material Science, Engineering, and Commercialization
December 2015

Committee Members:

Gary W. Beall, Chair

Clois E. Powell

Mark Holtz

William Brittain

William Chittenden

FAIR USE AND AUTHOR'S PERMISSION STATEMENT

Fair Use

Duplication Permission

DEDICATION

To Baba, Ma

&

My sister Sanchaita

ACKNOWLEDGEMENTS

I will like to thank Partnership for Research and Education in Materials (PREM) NSF Grant # DMR-1205670 for providing the funds for this research. This dissertation work is highly indebted to College of Science and Engineering department of Texas State University for letting me use their facilities. Special thanks to Eric Schires and Dr. C. Smith and ARSC staff to help me get trained on several equipment's.

During the course of my doctoral study, I had several shortcomings. Although, my advisor Dr. Gary Beall had always believed in me and helped me move forward on every occasions. I cannot thank him enough for his support and guidance that helped me in several ways.

Dr. S. Duraia and Dr. C. Powell had been instrumental in completing my research work. I also thank my committee members Dr. Mark Holtz, Dr. William Brittain and Dr. William Chittenden for their valuable inputs.

Thanks to Dr. Bob Davis and Dr. William Chittenden for extending help and guidance during my commercialization and business classes. Special gratitude to my high school science teacher Mr. SKD, who had been my mentor and guided me, and Mr. Kamal Sarkar from UTRGV who recommended me to join the MSEC program and guided me throughout my studies here in USA, and Dr. Tom Myers and fellow selection committee for accepting me into this program and giving me an opportunity.

I will take this opportunity to thank other people that have crossed my path during this degree and helped me in several ways: Dr. D. Oliver, Dr. F. Starr, Dr. D. Bhatta, Dr. D. Riahi, Dr. Debnath, Dr. M. Chakraborty, Sanchari Kar, Suman Bhattacharya, Paul Jacob, Poulami Gupta , Stephanie Polk, Javad Rezanejad, Maedeh Dabbaghianamiri, Jijo Kurian, Priti, Dr. T. Nash, Dr. M. Goss, Dr. B. Henderson, Dr. A. Douglas, Dr. H. Chen, Dr. T. Cantu, Dr. R. Cook, Mike Gardner, Karla Pizanna, Robin Yuvon, Jennifer Partida, Dan Millikan, Katie Blazek, Mark Riggs, Edith, Dr. W. Geerts, Dr. R. Droopad, Dr. K. Lewis, Dr. T. Betancourt, Dr. S. Strickland, Dr. Juan Ramirez, Dr. Sorto, Dr. Y. Lee and Dr. A. White.

Thanks to Cecy and Parna for being there as great support in this journey.

Finally, my sincere thanks and gratitude goes to my Father: Late Satya Kumar Das, and mother Late Ila Das, for bestowing their love and protection; throughout.

TABLE OF CONTENTS

LIST OF FIGURES

Figure **Page**

LIST OF ABBREVIATIONS

Abbreviation	Description
DOD	Drop on Demand
DLVO	Boris Derjaguin and Lev Landau, Evert Verwey and Theodoor Overbeek (nl).
vDW	van der Waals
2D	Two Dimensional
3D	Three Dimensional
LS_N	L; Large, S; Small, N is the number ratio of the small to large spheres
RCA	Reverse Convective Assembly
NaCl	Sodium Chloride
+ve,-ve	positive, negative
Vol.	volume
Dia.	diameter
nm	nano-meter
SDS	Sodium Do-decyl sulfate
SEM	Scanning Electron Micrograph
PS	Polystyrene
DEG	Di-Ethylene Glycol
NMP	N-methyl 2-Pyrolidone
FA	Formamide
PVP	Poly-vinyl Pyrolidone
DMP	Dimatix Material Printer
Rpm	Revolutions per Minute
sec	Seconds
mm	millimeter
Sccm	Standard Cubic Centimeters per Minute
RF	Radio Frequency
DI	De-ionized
$CaSO_4$	Calcium Sulfate
Hz	Hertz (unit of Frequency)
V_{p-p}	Peak to peak Voltage
CAGR	Compound Annual Growth Rate
TFT-LCD	Thin-film Transistor Liquid Crystal Display
LED	Light Emitting Diode
MIMIC	Micro Molding in Capillaries
UV	Ultra-violet

ABSTRACT

In the field of self-assembly of colloids, there are a number of unanswered questions; can creation of surface patterns be merely achieved by the design of the process? What is the mechanism behind the formation of spontaneous surface patterns? In addition, how to control these patterns? These questions were answered in this work. In particular, we study the self –assembly of nanoparticles into monolayers as a means to build hierarchical structures that will exhibit new functionality. The techniques utilized include convective self-assembly and DOD inkjet printers. For uniform and controlled colloidal monolayers with reduced defects, we present a study on different solvent compositions and use of external modifiers such as vibration and surface coatings during the self-assembly process. These monolayers can be used in colloidal lithography, to prepare high quality metallic nanostructures. Moreover, the live view of particles during self-assembly and modelling of capillary interaction between the colloids, helps to unravel the mechanism behind colloidal phase segregation. This work has produced novel surface patterning using simple scalable methods, which can be used for various applications. One of the promising applications includes use of phase segregated stripe pattern array of mixed colloids as color filters for display devices.

I. INTRODUCTION

The appearance of order from disorder is a fundamental topic of investigation and interest shared by a wide range of scientific and industrial disciplines. An essential part of nanotechnology is self-assembly; owing to its practicality and convenience in making ensembles of nanostructures. Whiteside (1) defines self-assembly as "autonomous organization of components into ordered structures or patterns as a result of specific interactions among the preexisting components themselves, without human intervention". Self-assembly is relevant in numerous dynamic, multicomponent systems, to name a few; smart materials (2), self-healing structures (3), computer networks (4) (5), etc.

Static and dynamic are the two main kinds of self-assembly (1) based on the thermodynamics of the process. A system that is at equilibrium and does not dissipate energy is known as static self–assembly process. An example of static self-assembly process is molecular self-assembly. If a system dissipates energy for the formation of structures or patterns between components, then it is termed as dynamic self-assembly. In other words, dynamic self-assembly is a non-equilibrium process, which occurs in an open system and requires external energy.

It is important to note, as per the second law of thermodynamics, the entropy of a closed system is not at all reduced in any process. In an open system, the decrease in entropy

(ordering of particles) is made possible due to the compensated entropy increase in the surrounding (environment).

An example of dynamic self-assembly process is colloidal self-assembly. In particular, for an evaporating solution drop, the ordering of the particles happen due to the evaporation of the solvent to the surrounding, which in turn drives energy into the system, enabling work to be done over the particles to self-assemble. In addition, external mechanical or electrical forces could be used to direct these solute/particles to form desired surface patterning.

The way these mesoscopic (colloidal) particles act or interact in suspension, and in air-water interface during self-assembly have been a growing interest because of the size of these particles (mesoscopic; ranging from approx. ~1nm-1000nm). This enables bridging of the molecular and macroscopic scales (6) (7) (8) (9) (10) .Usually, top-down and bottom-up, are classified as the two main approaches used to assemble colloidal particles, in desired orientation.

A few of the main top-down approaches are photolithography and electron ion beam. These methods are known to be extremely precise and controllable but expensive and time consuming. The bottom up approach, on the other hand, is not as precise or controllable as top down, but cheaper, more convenient and time efficient. Gaining insight to the mechanism of self-assembly via bottom up approach, to control the process

enables precise and consistent structures over different surfaces. This is very attractive to a broad horizon of researchers and industry.

Currently, the main drawbacks of colloidal surface patterning are the inherent constraints on limited structural designs, which is defined by the colloidal monolayer .This thesis is geared to extend the accessible structures that can be formed by colloidal monolayers. Utilizing the monolayer as a template to obtain desirable structure, first we focused on controlled formation of monolayers over large areas via different techniques.
Special attention is paid towards understanding the mechanism of phase segregation of binary colloidal particles during self-assembly and spontaneous stripe pattern formation.

II. MOTIVATION AND OUTLINE

Ordered microstructures using colloidal particles have a plethora of applications. For example, potential use in display devices (photonic devices) (11), biosensors, acoustic materials, optical communications, catalytic supports (12) (13), 2D sensor arrays, next generation hybrid metamaterials (14), super-hydrophobic and self-cleaning surfaces, and controlled adhesion of cells. (15) (16) (17)

One of the major applications of self-assembled colloidal particles is to produce patterned microstructure for photonic crystals, which can be potentially used on micro/macro display devices, integrated photonic chips (18) (19) (20). Periodic structure of colloidal assembly is capable of reflecting colors due to interference of light, a real life example is a mineraloid called precious opals (21). These opals are internally composed of regular, hexagonally close packed silicon dioxide spheres of size ranging from 150-300nm. When light passes through these structures due to interference and diffraction effects, colors are produced, these colors are termed as structural color.

The motivation of this thesis is to contribute towards the further development of flexible and versatile colloidal patterns on surface, which can be used in various applications. After accidentally discovering particle segregation in polydisperesed mixture of silica nano-particles, an effort was launched to find the cause of such phenomenon. Using bottom up self-assembly technique, we provided novel surface patterning features that could be useful for new applications. The aim of this work was not detailed study of the application; rather the findings are available for further

development into applications. The overall goal of this work is to use colloidal particles, to understand the mechanism of self-assembly and in turn be able to generate novel surface patterns.

This thesis is broken down into : first, the brief Introduction, second, the motivation and outline of this work, third, a brief survey of the theoretical concepts relevant to this work are presented discussing the forces involved in colloidal stabilization and colloidal assembly followed by review of literature on relevant topics, fourth, results and discussion is subdivided into three parts; monolayer self-assembly processes, nano sized hierarchical structures on surfaces and binary colloidal surface pattern mechanism, fifth, experimental methods used discussed in detail, including reverse convective and inkjet printing, sixth, a chapter on relevance of this work for application and commercialization is presented.

III. THEORY AND BACKGROUND

3.1 Forces at Work in Colloidal Stability and its Assembly

3.1.1 Colloids in Dispersion

The colloidal stability in a dispersion is fundamental to understanding dispersed matter; the stability of the colloids is usually governed by the combination of the van der Waals interaction (attraction) and electrostatic interaction (repulsion). As described by the DLVO theory, combining the electrostatic interactions, and the van der Waals interaction and hard sphere (Born) repulsion potential for two like charged particles at a distance d, sums up the complete interaction potential as (22):

$$U_{DLVO}(d) = U_{vdW}(d) + \Psi(d) + U_{BORN}(d) \quad (7)$$

Using Derjagun approximation for two sphere of radii R_1 and R_2, with separation between two spheres (D) being substantially smaller than the radii of the sphere, van der Waals force can be approximated as:

$$U_{vdW}(d) = -\frac{A_H}{6D} \cdot \frac{R_1 R_2}{(R_1 + R_2)} \quad (8)$$

The existence of electrostatic fields arises from charged surfaces, charged surfaces occur by chemical manipulation of the surface properties, dissociation of the surface groups or by adsorbing ions. The existence of charged surface enables attraction of counter ions, which in turn creates an electric double layer around surface of the particle. Many theories had been proposed to describe the distribution of charges in these layers. Stern (23) had successfully combined all the existing theories and presented a model for charged surfaces with rigid layers of adsorbed counter ions, in closest vicinity to the surface and also includes non-bound ions (diffuse layer) at larger distances from the

surface. It has been reported that surface potential decreases linearly in the rigidly adsorbed stern layer, but for the diffused layer the potential decays exponentially. The electrostatic interaction potential $\Psi(d)$ for the diffused layer can be represented by the combination of Boltzmann and Poisson distribution. The Boltzmann distribution can be used for describing the freedom of movement of ions in solutions that arises from the electrostatic interaction and thermal motion. Poisson Equation, is used for describing the three dimensional potential distribution. By linearizing the Poisson-Boltzmann equation (22), yields the electrostatic interaction potential $\Psi(d)$:

$$\Psi(d) = \Psi_0 \exp(-\kappa d) \quad (9)$$

Where,

$$\kappa = \sqrt{\frac{2c_0 e^2}{\varepsilon \varepsilon_0 k_B T}} \quad (10)$$

$c_0 = ion\ concentration,$

$\varepsilon, \varepsilon_0 = dielectric\ constants\ of\ the\ bulk\ electrolyte\ solution\ and\ of\ vacuum$

$k_B = Boltzman\ constant$

$\kappa^{-1} =$ *Debye length describes the thickness of the double layer, which is limited to* $1/e$ *of the surface potential*.

The born repulsion occurs when distance between two particles is less than their diameter, preventing the particles from overlapping; its potential is given by:

$$U_{BORN}(d) = \frac{1}{d^{12}} \quad (11)$$

Combination of these electrostatic potential (Equation 8, 9 & 11) results in DLVO potential in respect to interparticle distance d (See figure 3.1.1.1). Plotting the potential against the distance from the surface gives three important regimes. First, the primary

minima caused by van der Waals forces at close proximity of the particle. From colloidal stability standpoint, if the particles reaches this minimum they are irreversibly joined together, forming a coagulate system. Second, is the primary maximum at larger distance, which if high enough acts as a barrier to prevent coagulation. Finally, an existence of secondary minima exists at even higher distance, which causes particles to join reversibly.

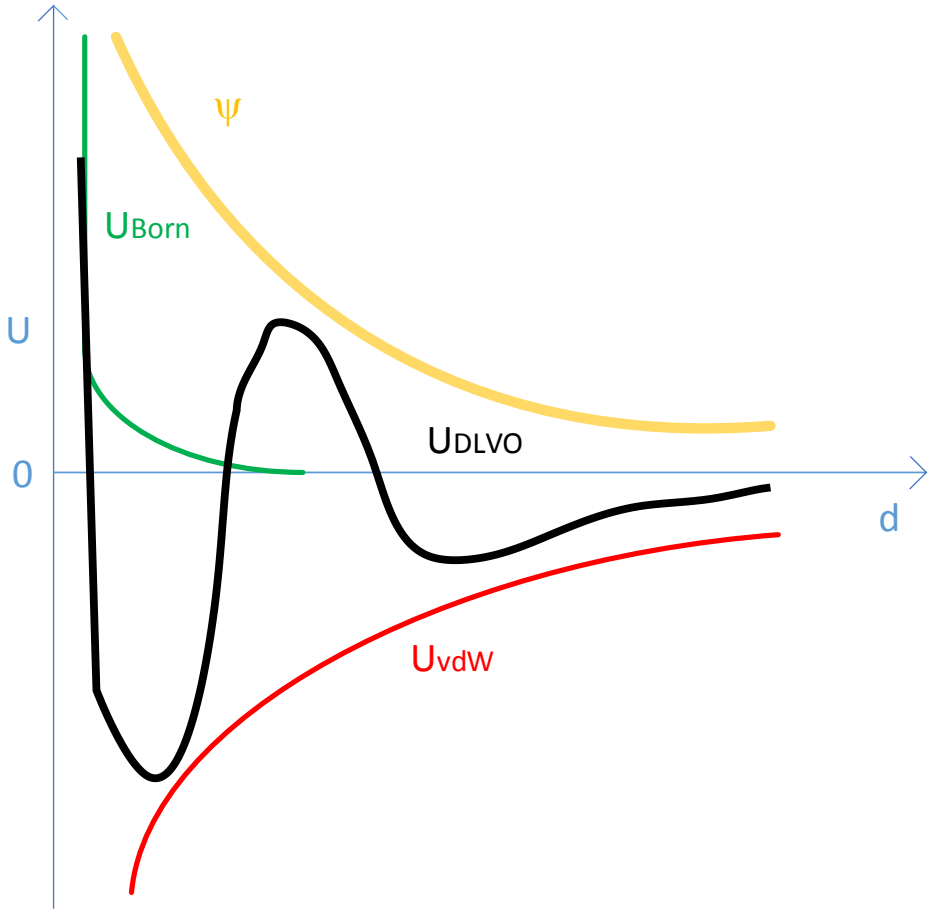

Figure 3.1.1.1 DLVO theory based total interaction potential between two particles in respect to distance

3.1.2 Colloids at the interface of Two Phases

Colloids at the interface of two phases (for example; air and water) is subjected primarily to two forces, the capillary force that occurs due to the deformation of liquid surface around the colloids and dipole interaction force that occurs due to differences in dielectric constants between two phase.

Dipole Interaction is the long-range repulsive force that onsets on the air-water interface, responsible for the non-close packed monolayer formation. The dipole-dipole interaction between similarly charged particles at interface is given by:

$$U_{dip-dip}(d) = \frac{(z.e.\kappa^{-1})}{4\pi\varepsilon\varepsilon_0}.\frac{1}{d^3} \qquad (12)$$

Capillary forces are of two types, namely flotation capillary forces and immersion capillary forces, unlike air-water interface mediated self-assembly of particles, the capillary interaction prevalent for directed self-assembly is immersion based capillary forces (See Figure 3.1.1.1).

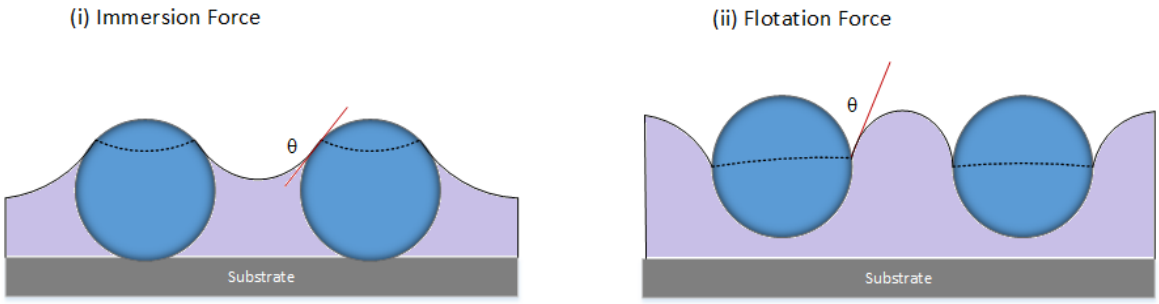

Figure 3.1.2.1 Attractive Capillary forces between two colloidal particles (i) Immersion Force, and (ii) Floatation Force

According to Kralchevsky *et al.* (24) the capillary force acting between two particles is given by:

$$F \sim -2\pi\sigma Q_1 Q_2 q K_1(qL) \quad (13)$$

One can derive the interaction energy between two particles from equation (13) by integrating F with respect to small increment in length (dl), the interaction energy (W) obtained is:

$$W \sim -2\pi\sigma Q_1 Q_2 K_0(qL) \quad (14)$$

Here,

$Q_i(capillary\ charge) = r_i sin\varphi_i.$

$r_i, \varphi_i = radii\ of\ the\ contact\ line\ and\ slope\ angle\ respectively$

$K_0 = modified\ bessel\ function\ of\ the\ second\ kind\ and\ zero\ order,$

$K_1 = modified\ bessel\ function\ of\ 1st\ order$

$\sigma = surface\ tension\ of\ the\ liquid\ film$

$q^{-1}(capillary\ length) = \frac{\Delta\rho g}{\sigma};$

$\Delta\rho = differene\ in\ mass\ density\ of\ mediums(liquid), g = gravity$

Simplified Immersion forces between two colloid is given by:

$$F \sim -(2r)^6 q^{-1} K_1(qL) \quad (15)$$

From equation15, Capillary force is indicative of long-range attraction force, and it is reported (25) to govern close packing of the particles during self-assembly.

3.2 Two Dimensional Colloidal Self-Assembly

3.2.1 Close Packed monolayer using Directed Self-Assembly

Drying of latex and silica colloidal particles for self-assembly has been practiced since the beginning of the 20th century (26). Several bottom up self-assembly processes are used for colloidal self-assembly, including; electrophoretic deposition (27), self-assembly

with physical confinement cells (28), capillary force assisted deposition via controlled evaporation (29) (30), spin coating (31), horizontal deposition (32), sedimentation (33), electrostatic deposition (34), and Langmuir type (35). In our work colloidal self-assembly is primarily driven by solvent evaporation, this process is very simple, robust, and scalable (36). The mechanism that governs this deposition is the convective assembly of the particle. This evaporation driven process is also referred to as "convective self-assembly" (37) (30) (38) (39), or "evaporation-induced self-assembly" (40). The first to introduce the concept of convective self-assembly was Denkov et.al (30) (41). The first to demonstrate a continuous deposition process where Dimitrov and Nagayama (42), Prevo et.al (36) was successful in developing a scalable process for industrial applications (e.g. anti-reflective coating). Using convective self-assembly, structured thin films from nano particles in solution are prepared by dragging a liquid meniscus unidirectional at constant velocity along a solid surface (See figure 3.2.1.1).

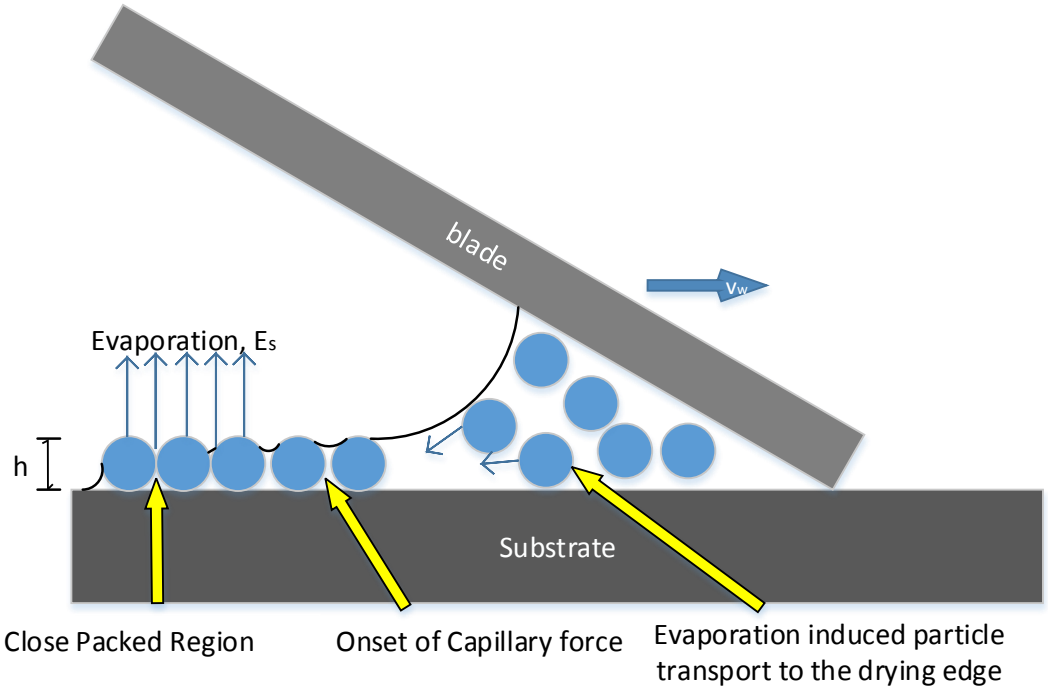

Figure 3.2.1.1 Schematic of drying region of thin wetting film, being dragged at a rate v_w on a substrate. The colloidal assembly of thickness h is deposited at a growth rate, v_c.

As shown in Figure 3.2.1.1, the blade is usually placed at an acute angle above the substrate, a small volume of colloidal suspension is placed in the trapped corner formed between the blade and the substrate. The blade is withdrawn at a desired velocity and the phenomenon; evaporation induced self-assembly, takes place at the three phase contact line of the meniscus of the evaporating liquid films/drying front. The particles in the thin films are drawn together due to the combination of hydrodynamic flux (39) and capillary forces (43). Hydrodynamic flux occurs due to evaporation of water in the drying front, which makes the dispersed particles in the liquid drawn to the edge of the growing monolayer. Lateral immersion capillary force sets in when the height of the water film is either equal or below the top surface of the particle(s). It is reported (43), the close

packed structures and self-assembly occurs primarily due to the dominance of capillary forces.

Using material flux balance equation for array formation at the leading edge, the rate of monolayer formation for a monodispersed system is given as (36).

$$v_c = \frac{K\emptyset}{h(1-\epsilon)(1-\emptyset)} \quad (1)$$

Where, K is constant depending on relative humidity, $\emptyset$ is the concentration of particles, h is the thickness of the film, ϵ and is the packing fraction. For a given particle concentration, and fixed K, if the drag speed (v_w) of the blade matches the rate of assembly (v_c), i.e. $v_c = v_w$, one can be able to coat specific structure characterized by a unique value of $h(1-\epsilon)$.

This process is simple and robust in producing ordered monolayers, but in addition to the local concentration variation issue of non-equilibrium process, meniscus pinning due to the surface tension effect, causes sudden jumping of meniscus, hinders the homogeneity of the coating. Also in this process, the number of parameters involved is large, which makes the control of this process very complicated, few of the parameters include withdrawal speed, substrates surface energy and pressure, temperature and humidity. If any of these parameters are not tuned correctly, undesirable coating is produced (44). Instead of moving the blade in the conventional direction as shown in Figure 1, one also can move the blade in reverse direction. In previous work by Chen *et al.* (45), the blade is adjusted at a certain height above the substrate using a precision stage, and moved in opposite direction, it was reported there was no significant changes found in the outcome of the film quality. Using reverse direction, the yield rate of the film growth at the three-

phase contact line was doubled due to the difference in vapor diffusions, which means film formation using reverse direction is faster compared to conventional methods.

3.2.2 Inkjet Printing

One of the most promising methods for selective deposition of functional material is Ink-jet Printing (46). The capability of the inkjet printers to directly write patterns and deliver precise amount of various kinds of materials at a precise location is immensely attractive for various applications (47). Specifically Inkjet Printers has been used to fabricate organic transistors (48), self-assembled thin Nano composite barrier films (49), full color emissive polymer displays, controlled release drug delivery devices in pharmaceuticals and functional ceramics (50) (51) (52) (53). Colloidal deposition via evaporation of drops has various potential applications, which include manufacturing of micro and nanowires (54) (55), cosmetics, explosive crystalline layers and nano-crystals (56). Here we will discuss fundamental principles associated for droplet formation followed by ink behavior on the surface and current drawbacks of inkjet technology for producing uniform films over larger areas.

Figure 3.2.2.1 is a typical example of drop on demand inkjet print head. At first, as voltage being applied to the piezo electric actuator, pressure waves are created due to the sudden change in volume, which in turn causes the fluid to propagate throughout the capillary. As the positive pressure wave nears the nozzle (See Figure 1.2.2.1), the fluid is pushed outward. If the kinetic energy transferred outward is greater than the surface energy to form a droplet, then a droplet will be ejected. Finally, the speed of the droplet is

dependent on the amount of kinetic energy that has been transferred outward (57) (58). For completion of the trajectory intended for the droplet, the initial velocity of the droplet has to be high enough to overcome the air drag in its path. The velocity of ejection and the droplet size can be controlled in the piezo DOD print heads by manipulating the driving voltage. Since the droplet ejection is completely dependent on the propagation of the pressure waves, the viscosity of the fluids used is crucial.

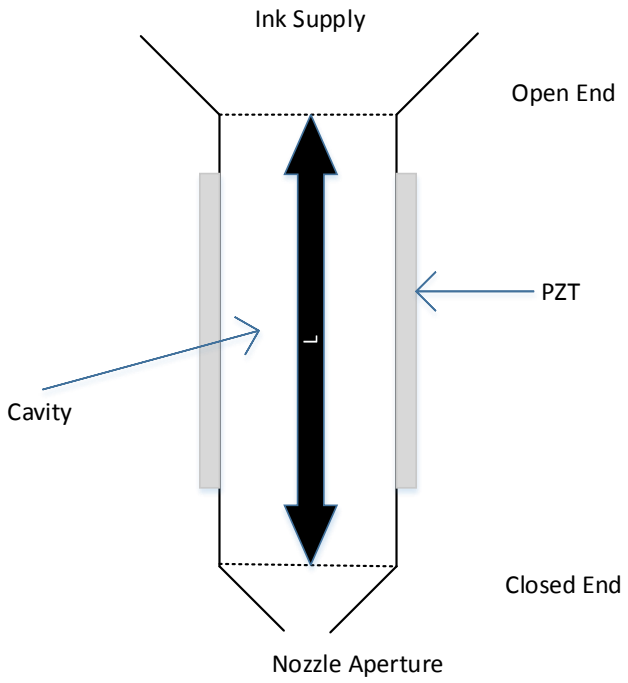

Figure 3.2.2.1 Illustration of piezoelectric print head

According to Dam *et al.* (59) the process of the impact of fluid on the surface can be divided into three steps, at first the drop impacts the surface, then the radius of the fluid–surface interface increases (the length is dependent on the substrates surface energy and the weber number of the ink) due to radial flow of the particles. Finally, the fluid comes to rest due to the viscous dissipation.

For most applications mentioned above and specifically for functional coatings, printings and paint coating, a uniform homogeneous film is highly desired. The commonly observed coffee ring effect and central bump of particles due to evaporation of a droplet had been an obstacle for creating homogeneous films, which in turn is the concern for this technology to provide larger area of uniform coating. A lot of work has been done previously to understand the effect and cause of coffee ring and central bump (60) (61) (62) (63). Very little work has been done with colloids. Work done by Park and Moon were successful in creating a homogenous film of silica particles by varying the chemical composition of the fluid. They attributed the formation of homogeneous film to the use of mixed solvent (of high and low boiling point) to suppress coffee ring effect by reducing drying rate and counteracting the radial flow of the particle. Hydroxyapatite particles were used to create uniform monolayer on top of Titanium substrate by Sommers et al (64) (65) and they attributed the uniformity of the deposition to the competitive force between the hydrodynamic and van der Waals forces. Yan et al. studied effects of the surfactants and surface charges, for formation of continuous films.

3.3 Non Close Packed Monolayers

For colloidal lithographic applications, close packed structure of monolayer colloids can only provide features based on the interstitials. There are a whole lot of possible complex structures that are possible if non-close packed monolayer structures can be formed using colloids. Currently there are few different methods to produce non-close packed

monolayers from close packed monolayers. Mechanical means to separate the particles spatially by using elastomeric substrates or plasma etching to reduce the size of the particle (66) (67) (68). Other methods include selective removal of polymer additives after the spin coating process (69) (70). Also using oil-water interface, colloidal assembly into non-close packed structure has been realized (71) (72) (73) (74).

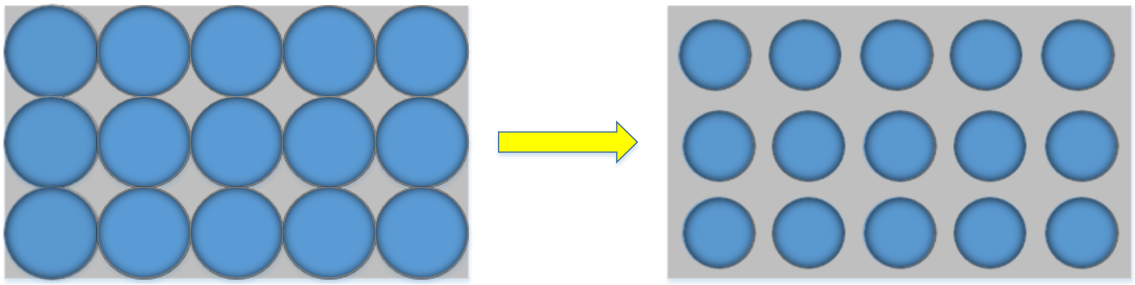

Figure 3.3.1 Process of formation of non-close packed structure from close packed structure using plasma induced size reduction of colloids

The most straightforward process of making non-close packed structure from close packed structure is via plasma treatment. This method enables size reduction of individual colloids without altering the lattice spacing (66). This process is very useful for providing different structural patterns; clearly, the size reduction is dependent on different controllable parameters during plasma etching. One of the main drawbacks of this process is elongated plasma treatment can degrade the quality of the individual particles (surface corrugations and deviations from spherical shape).

3.4 Binary Colloidal Assembly and Phase Segregation

In this section, we will briefly describe the relevant work that has been done with binary colloid particles to form stoichiometric patterns, and phase segregation during self-assembly of binary colloids.

Two- dimensional monolayer assembly comprising of two different sizes of colloidal particles are termed as binary colloidal monolayers. Large (L) and small (S) sized colloids form binary arrangements with variety of structural symmetries and different stoichiometry, contrasting to a single-sized 2D assembly (75) (See Figure 3.4.1). The variations in stoichiometry and the assembly structure are dependent on the size ratio and concentration (76).

Two methods are used for the assembly of binary particles to produce variety of LS_n structures (Figure 3.4.1), sequential assembly (two-step processes) (77) (78) (79) (80) and co-assembly (one-step process) (81) (82) (83) (84) (85) (86). von Blaaderen (77) (with size ratio ($\frac{S}{L}$=0.5)) used the sequential assembly method to develop a non-equilibrium layer by layer growing process. Large areas of binary monolayers were first fabricated. Then using the first layer of monodispersed particle as substrate, small spheres are deposited via evaporation process. The interstitial sites of the larger particle acts as energy minima for smaller particles hence they gets trapped in them and assemble with a high degree of order. The concentration of the smaller particles determines the assembly structure, changing concentration of the smaller particles during the drying process leads to change in the stoichiometric ordering. This method was found to be time consuming,

due to the change of concentration of particle during assembly (See Figure 3.4.2) and due to meniscus pinning effect non-uniform coatings were observed.

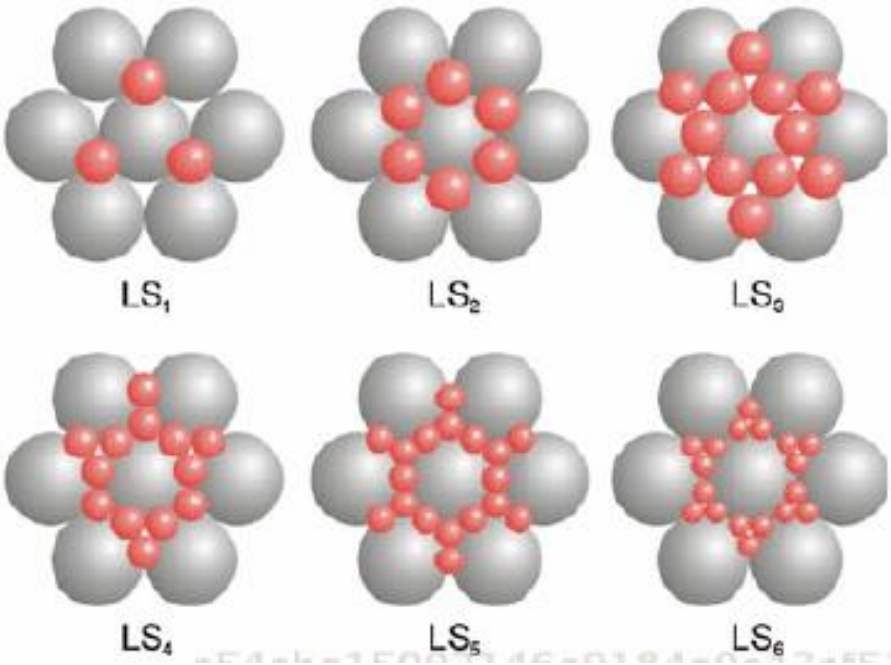

Figure 3.4.1 Examples of possible structures in binary colloidal monolayers. Picture obtained from reference (75)

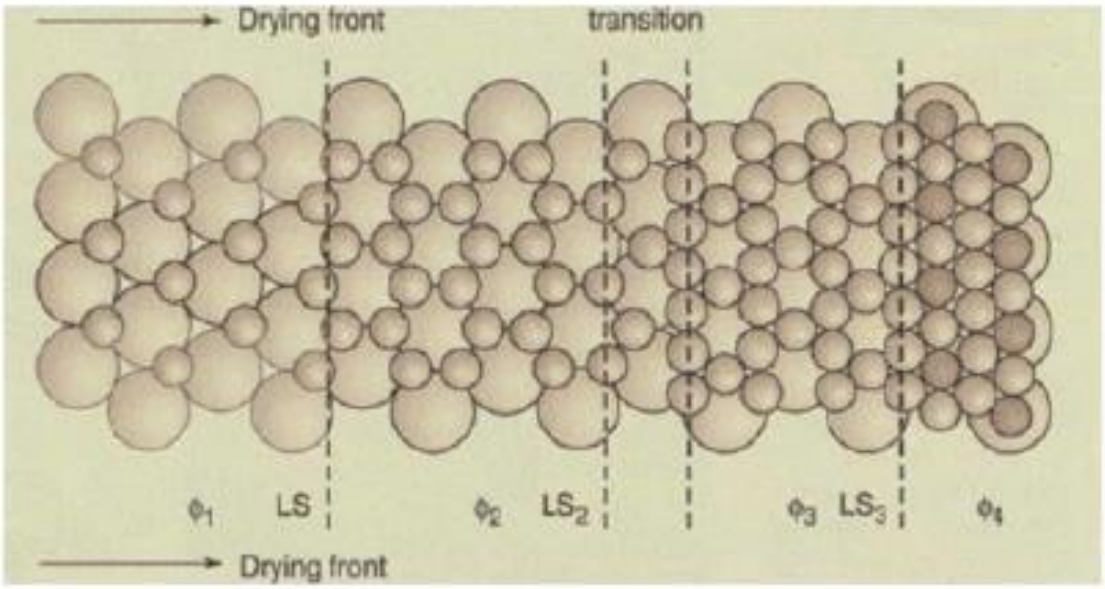

Figure 3.4.2 Binary colloidal monolayers using sequential convective assembly of small particles in the interstitial sites of a close packed monolayer of large particles [30] with size ratio of $\frac{S}{L}$=0.5. An example of stoichiometry inconsistency due to changing small particle concentration during deposition. Picture obtained from reference (75)

To overcome one of the above limitations, stepwise spin - coating was introduced by Wang *et al*. (87) for size ratios ($\frac{S}{L}$=0.25-0.6). The stoichiometry of the binary colloids was affected by the spin speed and the diameter ratio of the particles. This method was found to be rapid but failed to produce precise stoichiometry.

Kim *et al.* (78) were the very first to use confined convective assembly and they fabricated $LS_{2,3,4,5}$ configurations using size ratio ($\frac{S}{L}$=0.3-0.65). Huang *et al.* (80) used electrophoretic assembly of like charged binary and ternary particles to fabricate monolayers using a wide variety of size ratio ($(\frac{S}{L})$ =0.1-0.9). Control over stoichiometry was a problem in both processes, due to inherent nature of non-equilibrium processes.

An alternative approach of fabricating binary colloidal structure is co-assembly process. A rapid vertical evaporation process is implemented by Kitaez and Ozin (81). They successfully produced a variety of stoichiometry with size ratio above $(\frac{S}{L})$ 0.225. This process produced variations of assembled structure as a function of the concentration of smaller particles (82), but consistency of these varied structures became a problem over a wide area. Luis-Liz Marzan (83) reported symmetric co-crystallization patterns using anisotropic gold rods.

The first to use a horizontal deposition method for the coassembly process was Kumnorkaev and Gilchrist (with $(\frac{S}{L})$ =0.1) (84). They attempted to fill in large spherical monolayers interstices with a large number of small spheres, this process failed to produce stoichiometric structures. Nicolas Vogel (75) produced monolayers by compression and surface lowering transfer method using a Langmuir trough. Adjustment of the two particle types at the air-water interface were found to give a higher degree of control. Yu et.al. (86) produced direct assembly of binary structures at the air/water interface. The interface-mediated processes uses the concept of high lateral mobility of particles. Sufficient time for the smaller particles to find their minimum free energy position at the interstitial sites of the larger spheres is the driving mechanism in this process. Yu et.al (86) used polystyrene particles with size ratios ranging from ($(\frac{S}{L})$ =0.147 -0.194) to form LS_2 and LS_6 configurations.

These above mentioned methods produce different stoichiometric structure by using binary colloids are well established. Current effort in this field are focused on producing different stoichiometric structures consistently over large area for industrial applications.

The experimental work on phase segregation of binary particles was conducted by Hachisu *et al.* (88) & Yamaki *et al.* (89). Hachisu *et al.* (88) utilized 1000nm & 600 nm polystyrene particles in a suspension. These suspensions were allowed to dry for a period of 50 hours, and reported phase segregation of particles without any further clarification .Yamaki *et al.* (89) reported a size dependent separation of colloidal particles during 2D convective self-assembly of a liquid film on a mercury surface. The larger particles were gathered in the center and smaller particles surrounded them on the outer edge, as shown in Figure 3.4.3. It was reported the degree of separation between the particles is found to be more distinct for the radii ratio (($\frac{S}{L}$)) close to 0.5. They reported, the major forces involved in this process were lateral capillary forces and convective forces, these forces govern the 2D assembly and the size dependent separation (89). The convective flow is dominant for the larger particles in the early stage of the assembly. However, the random motion (Brownian motion) of the smaller particles dominates the convective flow during this stage of the process. The Monte Carlo simulation further validates the process. The simulation considered only two governing forces; capillary and convective. The results of the simulation did correlate with the experimental observations. They concluded that more experimental and theoretical work is needed to clarify the segregation mechanism.

Liang et al. (90) used the lattice Boltzmann pseudo solid model to simulate binary colloidal particles during self-assembly, similar to evaporation induced self-assembly of a drop of liquid containing particles on a solid substrate. They reported the key factor for separation of particles is particle size ratio. At size ratio of ($\frac{S}{L}$) 0.5, they also found phase segregation similar to Yamaki *et al.* (89), and Liang *et al.* (90) claims the modelling

process used is better than any contemporary models, as it enables full consideration of solid-fluid interactions, unlike the Monte Carlo simulation.

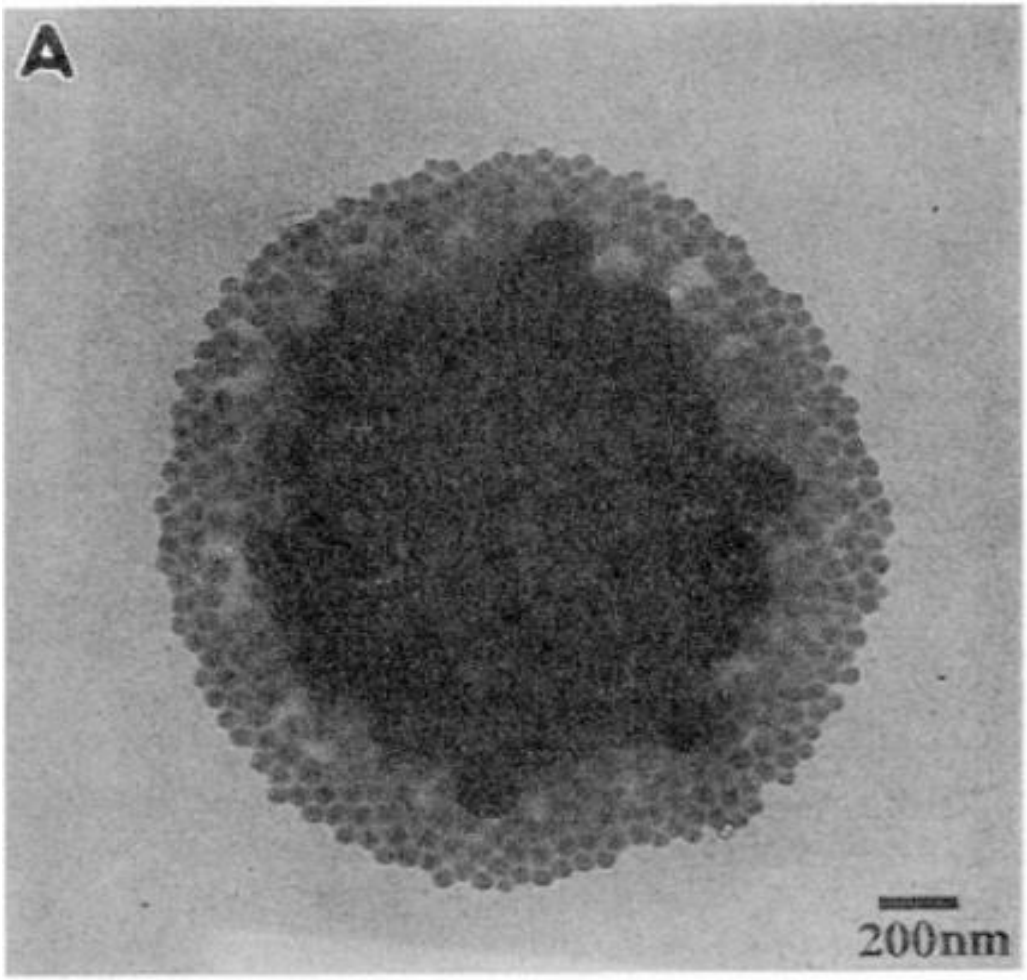

Figure 3.4.3 Transmission electron microscope image after 2D self-assembly of polystyrene particles of size 55 and 144 nm in diameter. Picture obtained from reference (89).

Barrat *et al.* (91) uses density functional theory to explain the phase segregation of particles for variety of size ratio of hard spheres, they conclude that size ratio $(\frac{S}{L}) < 0.92$ during freezing results in partial phase segregation, for size ratio $(\frac{S}{L})$ close to 0.85, approximately 25% of small spheres were present in the domain of the larger spheres.

Below the size ratio 0.85 calculation predicted different stoichiometry formation and few phase segregations depending on number ratio or volume fraction.

Another study on binary colloidal hard spheres by Murray and Saunders (92) explored the stability of several non-interstitial binary structures. For size ratios ($\frac{S}{L}$) > 0.62, the mixtures of hard spheres were predicted to segregate into two pure crystalline phases, with less than 1% miscibility. This prediction by Murray and Saunders were experimentally verified by Bartlett *et al.* (93). Using hard spheres of size ratio of 0.61, where the colloidal suspensions were prepared at either end of the composition range (concentration range: x_L =0, xS=1 to x_L =1, xS=0) and was dried for over a period of days, to counteract gravitational sedimentation they rotated the sample at very slow speed. The small spheres in the assembly of large spheres was found to be less than 1%. A complete segregation of each pure component was verified for particular composition range of (x_L =0.66-1, x_S=0-0.057), but for composition ranging from (x_L=0.43-0.58) they see partial mixing with few areas of segregation.

Based on the results obtained for size ratio (0.61) and varied composition range, Bartlett (93) summarizes the factors that relate to the relative stability of these phases as the volume fraction, number fraction of the species, and the relative diameter ratio. Charged particles interact through long-range screened Coloumbic potential, which is different from hard spheres, but Bartlett *et al.* (93) predicted similar phase behavior. Lorenz *et al.* (94) predicted that phase segregation can be affected by the charge ratio of two differently sized particles. On flat capillary cells, Lorenz et.al. let the deionized charged colloidal sphere to self-assemble over period of weeks, but they failed to conclude

anything in regards to the effect of charge ratio on phase segregation, rather they suggested future experiments using a charge variable species.

Kaplan *et al.* (95) describes entropy driven phase separation for nearly hard sphere (electrically charged polystyrene spheres, screened by the ions in solution) binary colloidal mixtures. They constructed phase diagrams for nine different size ratios of hard spheres (($\frac{S}{L}$) =0.068-0.29), with different low volume fractions (<0.30) and salt concentrations (of NaCl) as low as 0.1-0.2 M. The mixtures were placed in 1 mm thick cuvettes and observed over a period of weeks. A distinct phase separation between two sizes were observed after crystallization and in the wall of the cells for size ratios (($\frac{S}{L}$) <= 0.4). They concluded that the mechanism of phase separation in bulk could be due to the entropy driven transitions, where the smaller spheres mediates an entropic attraction force between larger particles, enabling phase separation. In bulk before phase segregation or aggregation (95), due to the presence of the larger sphere the total available volume for smaller spheres is reduced. As the center of smaller spheres are not allowed in the vicinity of larger spheres, and that vicinity is defined by the sum of the small and large sphere diameters; termed as excluded volume of smaller sphere: See Figure 3.4.4. Although, when two large hard sphere in bulk approach each other due to the attraction force in presence of smaller particles, an overlap of the spheres excluded volume occurs. The exclusion of volume increases the overall volume available for the smaller spheres enabling reduction of free energy (energy minimization) of the system hence the particles segregate. Kaplan *et al.* predicts similar entropic effect occurs if smaller particles dominates the contribution of free energy to the system, the large particle comes in

contact with the substrate or wall, the excluded volume gets doubled and they attach themselves near the surface (See Figure 3.4.4(c)).

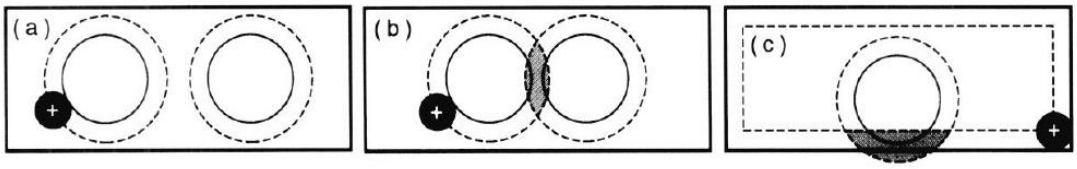

Figure 3.4.4 Free energy of smaller particles is dependent on the volume accessible to the center of each particle (a) An example of excluded volume of the spheres, (b) While large particles approach each other, excluded volume gets overlapped and overall volume for small particles increase(c) When larger particles come in contact with the cell wall or substrate, the volume availability of smaller particles increases. Picture taken from Kaplan *et al.* (95)

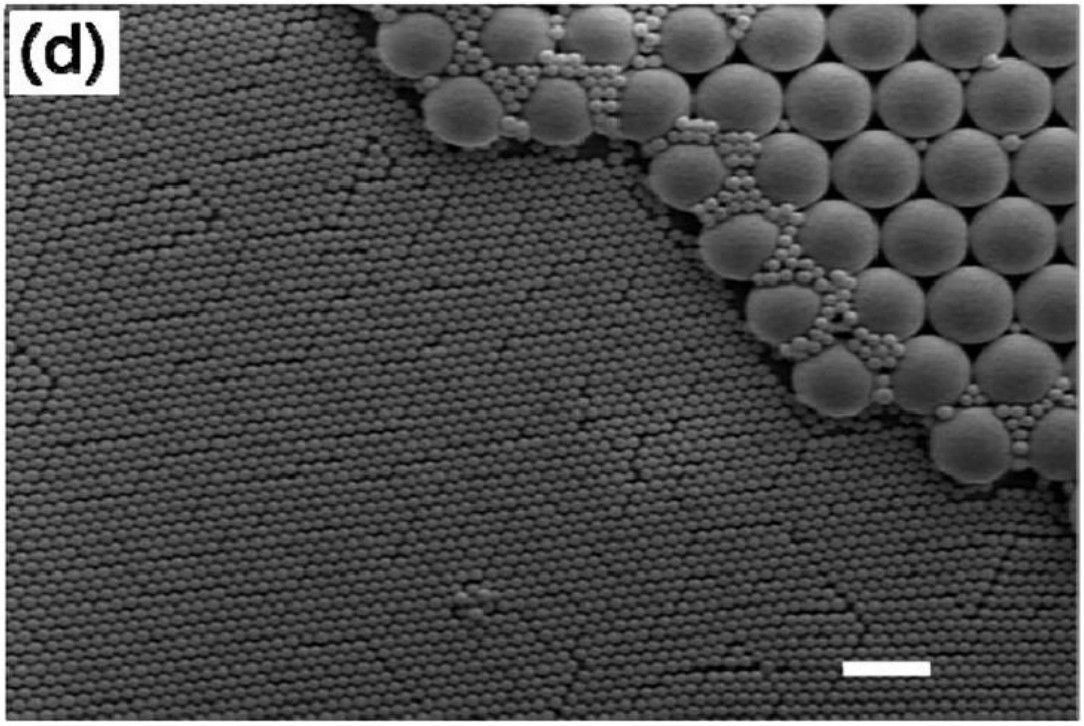

Figure 3.4.5 Structural nonuniformity due to segregation of the small and large PS spheres during self-assembly. Scale bars = 2 µm .Picture obtained from reference (96)

Dai.etal. (96) while evaluating phase diagrams and designs of monolayers for different stoichiometric (LS_n) structures found few defects observed during the assembly (See Figure 3.4.5). They termed the phase segregation as defects and predicted the cause to be insufficient mixing of the two different sizes or the substrate not being cleaned properly.

IV. RESULTS AND DISCUSSION

In this section, the results of the research will be presented in two major sections:
At first, we present different methods used for self-assembly of commercially available colloidal particles into monolayers over a significantly larger area. Convective self-assembly method and drop on demand piezo actuated printing method is used to produce single sized colloidal monolayer. Using colloidal monolayers, we present different surface patterning via plasma etching and metal deposition. Finally, the mechanism of phase segregation for binary colloids and control of the spontaneous periodic stripe pattern formation on surface is investigated and presented.

4.1 Colloidal Monolayer Assembly Methods

In this chapter, methods and parameter optimization required for significantly large areas of assembly of single sized colloidal particles.
First, directed evaporation induced self-assembly is used for the assembly of close packed monolayer of monodispersed particles. In general, there are several self-assembly methods known in the literature, convective self-assembly process used here significantly reduces cost and time to produce two-dimensional structures on a surface. This process also yields large areas of quality films on a variety of substrates, with minimal waste.
Another method used for producing close packed two-dimensional self-assembly is a drop on demand piezo-inkjet printer. An inkjet printing process is very accurate, it allows different structure patterns on the surface with high accuracy, time saving and easily scalable with minimal waste.

4.1.1 Directed Self-Assembly Method enabling Close Packed Monolayers

4.1.1.1 Introduction

In our study, the methods used for directed evaporative self-assembly was convective self-assembly. Practically there are several different self-assembly process for creating colloidal monolayer, for instance the self-assembly process can be classified into two types direct self-assembly and interface mediated self-assembly. Even though interface mediated self-assembly via Langmuir trough can provide a large area monolayer with reduced multilayer formation and better packing due to enhanced relaxation time available for the particle to pack in hexagonal packing: in our study we preferred direct self-assembly. Direct self-assembly process is easier and cheaper to implement than the Langmuir trough method. Additionally, the external force that direct the self-assembly helps us to create patterns, which we can control easily. Hence directed self-assembly process enables us to be independent on inherent properties of the system as in air water interface mediated self-assembly (Langmuir Trough Method).

In this chapter we present the results obtained using directed self-assembly to produce monolayer of significantly larger areas for different sizes of commercially available polystyrene particles. The process presented here uses convective self-assembly, but contrary to conventional direction of motion of the blade (+ve x direction), we move the blade in the opposite direction (-ve x direction), although both the process (as mentioned in Sect. 3.2.1) yields similar results, 2but with the latter direction of motion the growth rate of the film is higher. As seen in Figure 4.1.1.1.1 the upper contact line of the meniscus from which the colloidal assembly (at drying front) occurs, is attached along the outer edge of the blade.

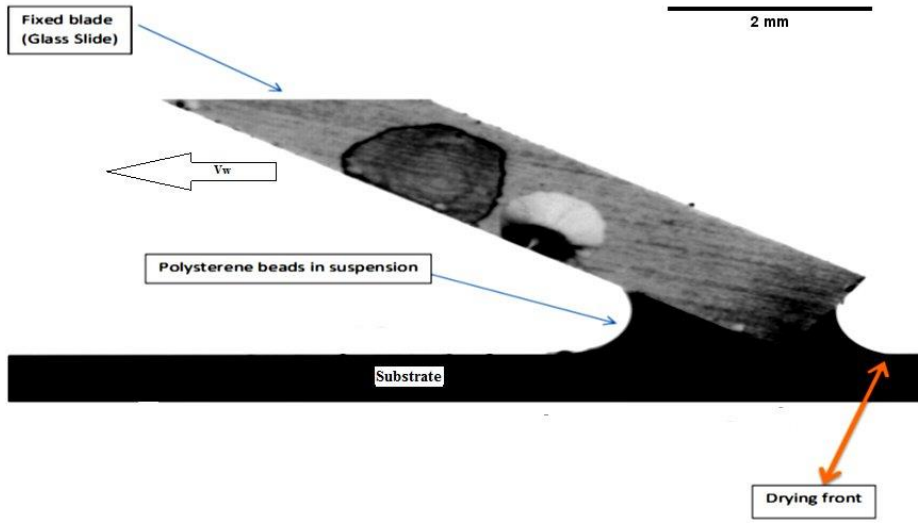

Figure 4.1.1.1.1 Image of the three phase contact line (drying front), formed during Reverse Convective Assembly. Picture was taken using a goniometer setup.

This allows capturing video of the drying front during the self-assembly of the colloids as the reverse convective assembly process enables an uninterrupted path for the reflected light (See figure 4.1.1.1.1; drying front). Figure 4.1.1.1.1 is showing the side view image of the glass blade at an angle, placed immediately above the substrate. The dispersed polystyrene colloids in suspension, is placed at the corner of the blade and substrate. The assembly onsets at the drying front, enabling videography of the particles during assembly.

4.1.1.2 Results and Discussion

Figure 4.1.1.1.2 shows the setup of the reverse convective self-assembly process for colloidal self-assembly on a substrate.

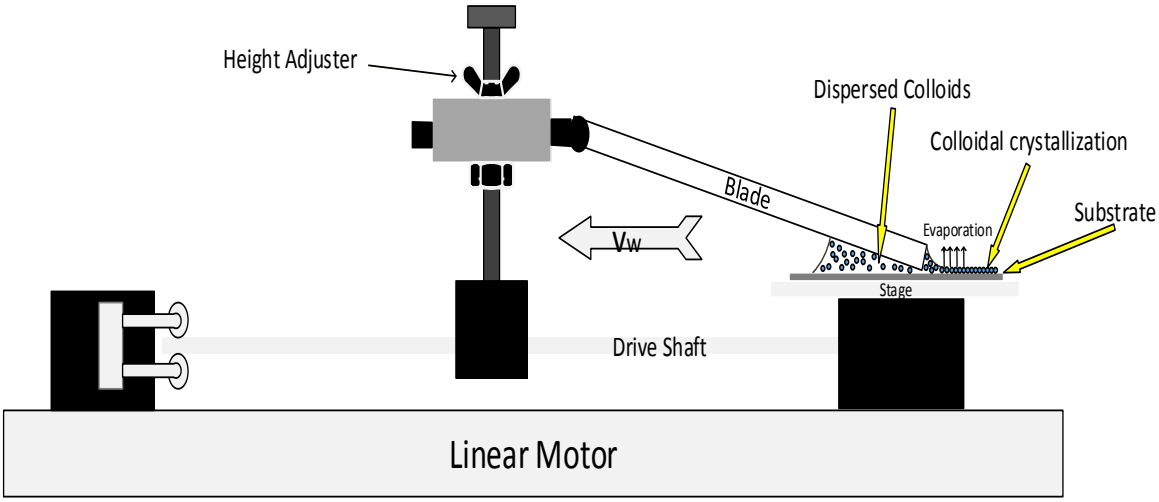

Figure 4.1.1.1.2 Schematic of the coating apparatus

The commercially available polystyrene particles were pre-dispersed at 1 vol. % loading, while further dispersions were carried out using ultrapure water for desired solid loading of 0.1-1 vol. %. Before every use for self-assembly process, the dispersed solution was ultra-sonicated for 1-2 min. Addition of 20 µl colloidal suspension between the wedge of the blade and substrate was performed via a micropipette, the angle between the blade and the substrate were kept fixed at 20º-25º. The whole setup was inside a humidity-controlled box with humidity kept fixed at 65% RH, and the blade was dragged at a desired speed (v_w).

Following is the description of the stages of the above self-assembly process; (a) Initially, the suspension creates a meniscus between the blade and substrate; (b) Upon moving the blade at a designated speed in the preferred direction, the meniscus gets stretched and eventually thinned at the drying front, and due to evaporative flux the particles gets pulled towards the drying front. Moving the blade too fast or too slow caused either voids or multilayer formation. At a particular speed, formation of multilayer or voids is mostly dependent on the concavity of the meniscus near the drying front and the particles concentration near that region. With meniscus stretching and evaporation of water from the drying front the (c) viscosity of particles (onset of viscosity depends on the size of the particle in suspension and drying rate) increases near the drying front and as the meniscus thins and the height lowers below the height of the particles, the particles gets pinned or immobilized, forming non close packed assembly, (d) and with the onset of the capillary interaction finally a close packed structure is formed on the substrate. As the blade is being dragged, the process of forming close packed structure is repeated for the entire region.

The individual monolayer domains are distinguishable by their distinct coloration. The effect of a lower speed results in buckling (multilayers); these multilayers are visibly noticeable again by their coloration.

This process is quite versatile with respect to the size of the colloidal particle. Polystyrene particles with diameter between 100 and 900 nm were successfully used in this process. The substrate has to be well cleaned (free of external particles) preferably with higher surface energy (hydrophilic) for well ordering of particles into monolayers.

To study the effect of speed on quality of the film, the speed of withdrawal of the blade were varied between 0.6 and 1.5 ml. /hr. while keeping all other parameters fixed. Other parameters include colloidal particles of diameter 600 & 900 nm at solid loading of 1 vol. %, fixed relative humidity of 65%, and blade angle at 20^{o}. The percent of multilayer, monolayers and voids coverage with varying speed was quantified.

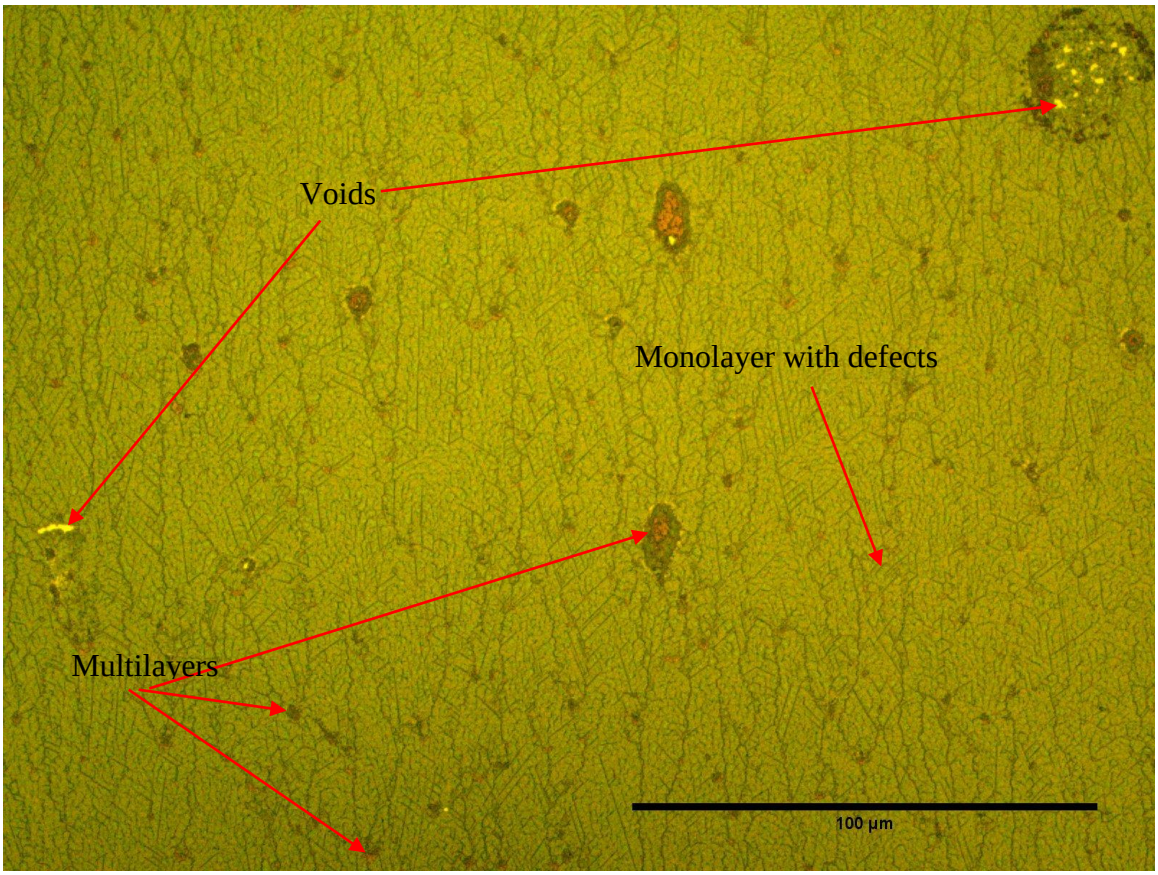

Figure 4.1.1.1.3 50X Magnification Optical Image of 600 nm (diameter) Polystyrene Film on Silicon substrate after Reverse Convective Self Assembly at 3.58 µm/s. Different color represent different domain of self-assembly.

For quantitative analysis on the coating, we used optical microscope images, vivid color formation due to Bragg's reflection of different assembly domains and packing. This helps us to analyze the exact quality (monolayer, multilayer, and voids) of the film over an area using optical images (See figure 4.1.1.1.3). Exact analysis of the image is done

using a commercially available software Image J, and qualitative analysis was done using scanning electron microscope.

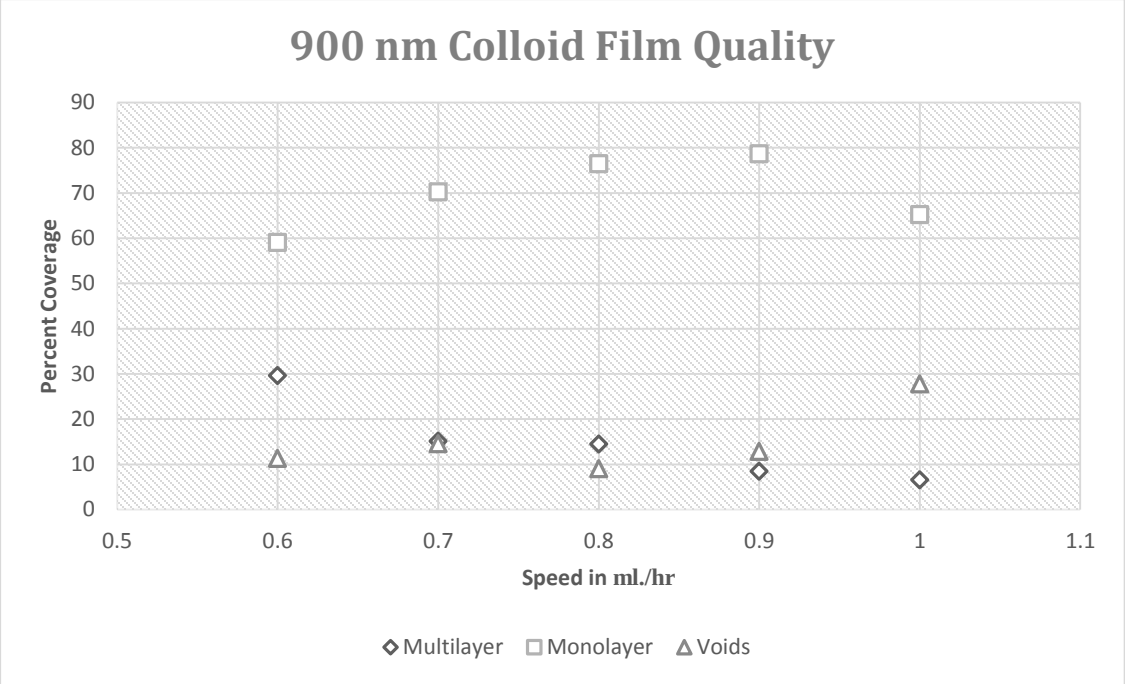

Figure 4.1.1.1.4 900 nm Polystyrene Film quality analysis with respect to the speed of blade

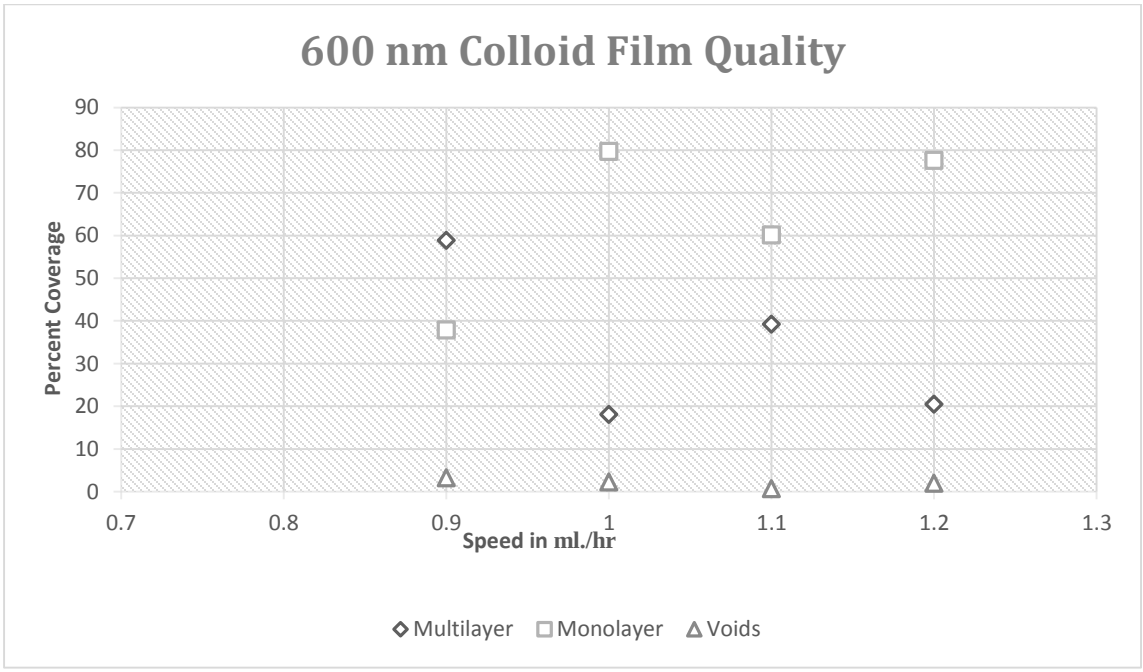

Figure 4.1.1.1.5 600 nm Polystyrene Film quality analysis with respect to the speed of blade

Figure 4.1.1.1.4 shows that withdrawal speed of the blade closer to 3.22µm/s. the quantity of monolayer coverage for 900 nm (dia.) particles over the area is at a maximum. When the speed is increased more than 3.22µm/s., more voids are present, and below 3.22µm/s., more multilayers are formed. In Figure 4.1.1.1.5 for the blade speed closer to 3.58µm/s., we have the maximum monolayer coverage for 600 nm (dia.) particles. When the speed is below 3.58µm/s. larger amount of multilayer occurs, whereas speed above 3.58µm/s exhibits increased voids.

For a particular solid loading (1 vol. %) of 600nm and 900 nm particles, the concentration (number of particles) of 600 nm particles are higher than 900 nm particles. In particular 8.393239E+10 number of particles/ml for 600 nm were present for solid loading 1vol.% compared to 2.486886E+10 number of particles/ml for 900 nm with solid loading 1vol.%. Eqn.1 of Sect 3.2.1 indicates the speed of colloidal monolayer formation is inversely proportional to the height of the particle and directly proportional to the concentration of the particle.

Number of particles is obtained using, the following equation:

$$\frac{\#\ of\ particles}{ml} = \frac{6\rho_f}{\pi {D_p}^3(\rho_f + \frac{\rho_b}{C} - \rho_b)} \quad (1)$$

ρ_f=1gm/cc, ρ_b=1.05 gm/cc,C=%solids/100=0.01,D_p=particle diameter (97).

The video of self-assembly at the drying front during the reverse convective self-assembly process enables us to unravel the cause of many important features of the film formation and its quality. One of the most notable findings include the origin of formation of defects (point and line defects). It is noticed that pinning of particles on the substrate is one of the primary causes of defect origination. In order to reduce these defect formations, we pre-coated the substrate with different loading (vol. %) of SDS

(Sodium Do-decyl Sulfate). SDS is a negatively charged surfactant, which after coating on substrate induces a repulsive layer for the particle, which in turn impedes the pinning process. As colloidal self-assembly occurs in presence of capillary forces among the particles, with addition of a surfactant to the surface induces a lowering of the surface tension of the solvent, as capillary force is directly proportional to the interface tension or surface tension. Therefore, lowering the surface tension by adding SDS reduces the capillary force (98) . The reduction of particle pinning onto the substrate enables monolayer growth with no sudden obstacle in its path and the reduced capillary force enables higher relaxation time for the particle. This enables a better packing with less defects along the growth of the film. As shown in the figure 4.1.1.1.6 we see a significant reduction in line defects with increase in SDS concentration.

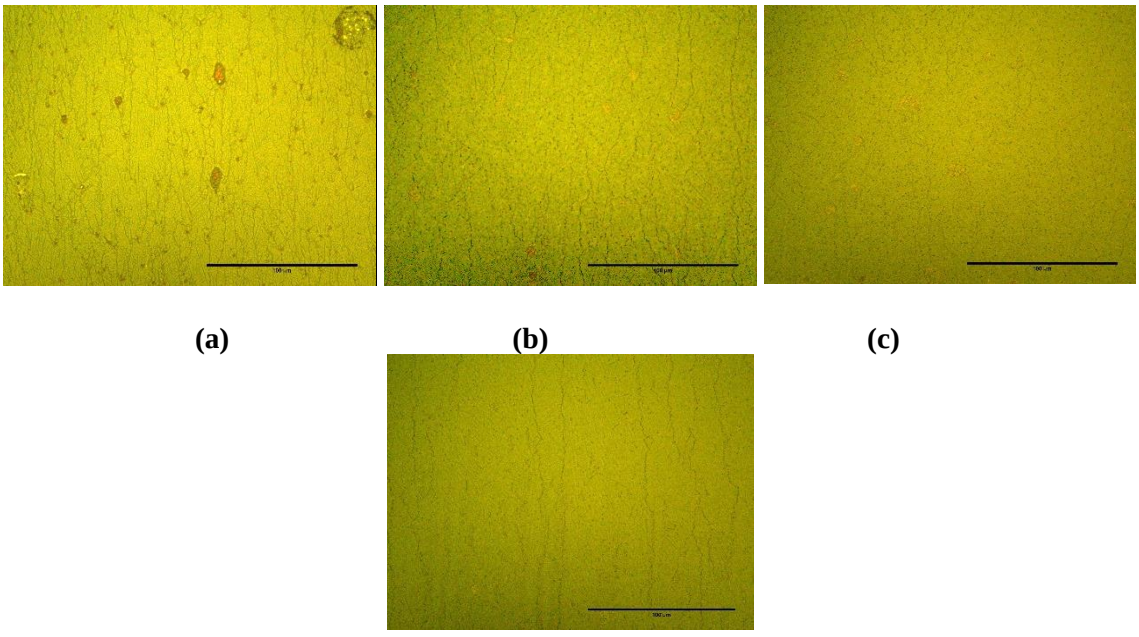

(a) **(b)** **(c)**

(d)

Figure 4.1.1.1.6 50 X Magnification Optical Image of 600 nm Polystyrene for film quality analysis with respect to % SDS precoated on substrate.(a) 0% SDS (b)0.1% SDS,(c) 0.5% SDS, (d) 1% SDS

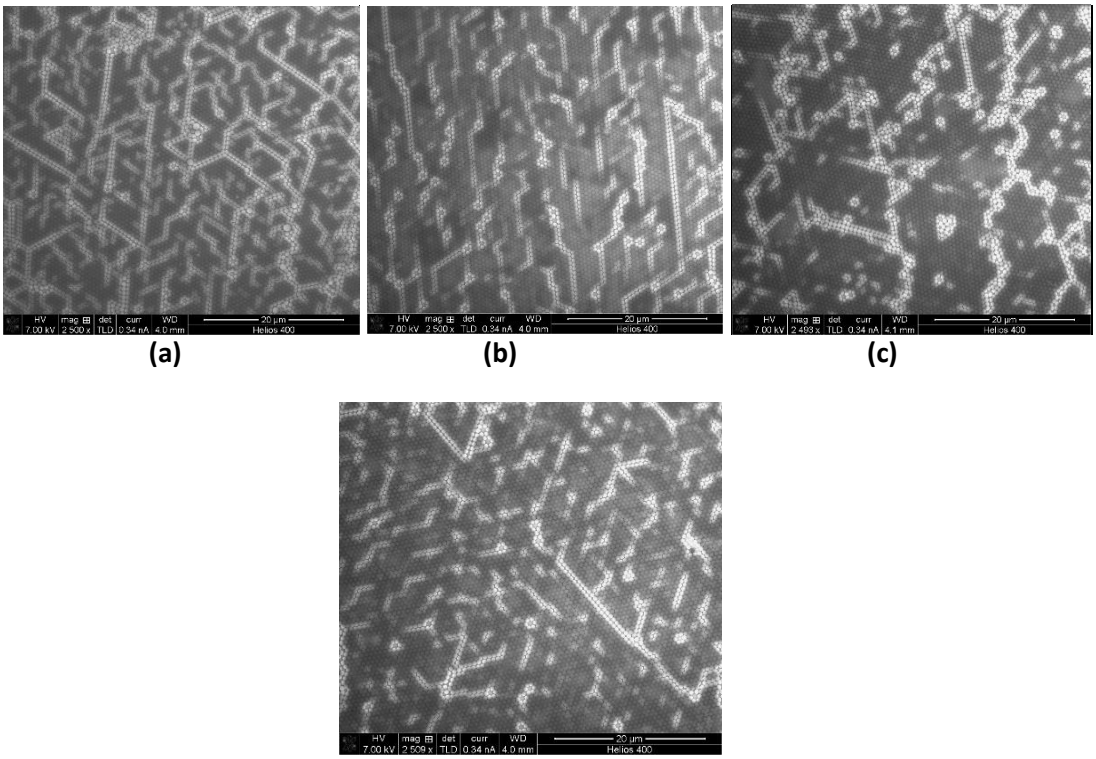

Figure 4.1.1.1.7 2500 X Magnification Scanning electron micrograph of 600 nm Polystyrene for film quality analysis with respect to % SDS precoated on substrate.(a) 0% SDS (b)0.1% SDS,(c) 0.5% SDS, (d) 1% SDS

The SDS concentrations were varied between 0.1 and 1 vol. %. Using a spin coater, these different loading of SDS are coated on a pre-cleaned and plasma etched Silicon substrate. Characteristic optical micrograph of monolayers of 600 nm (diameter) polystyrene particles self-assembled on top of these SDS coated substrate is shown in Fig 4.1.1.1.6. SEM is also presented at low magnification (Figure 4.1.1.1.7) to bolster the optical image results (Figure 4.1.1.1.6). Significant reduction of line defects were observed with highest concentration of SDS on the surface, a higher magnification Scanning Electron Micrograph shows the higher packing density of particles with SDS (See Figure 4.1.1.1.8).

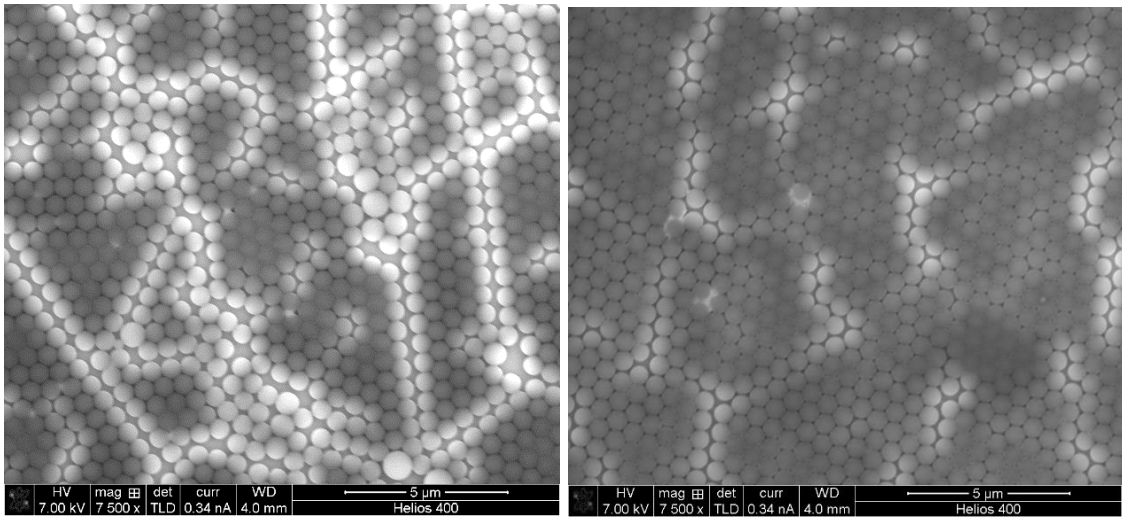

(a) **(b)**

Figure 4.1.1.1.8 Scanning electron micrograph of 600 nm Polystyrene on SDS coated Silicon substrate (a) 0% SDS (b) 0.1% SDS

4.1.1.3 Conclusion

In brief, using the reverse convective self-assembly method, close packed monolayers for monodispersed particles were developed. As thinning of meniscus and evaporation onsets loosely packed monolayers were observed, on further evaporation and onset of capillary interaction force close packed monolayers are formed. This process continued until the entire liquid on the three-phase contact line is used up over the entire region. For a particular solid loading with different diameter of particle, it is found that the optimal coating speed for monolayer coverage over the surface is higher for smaller particles than the large particles. Defects were significantly reduced by coating SDS surfactant to the substrate prior to assembly of colloids.

4.1.2 Production of Close Packed Monolayers via Inkjet Printing

4.1.2.1 Introduction

In addition to producing large areas of closely packed monolayer of colloidal particles, it is also very important to provide complex and precise surface patterning. Drop on Demand piezo inkjet printers are capable of depositing precise Pico liter droplets of solutions (ink) at a desired location. Inkjet printing enables reduced waste, non-contact deposition that minimizes contamination and provide efficient use of varied materials on any desired substrate. The high precision printing capability allows direct printing of materials (ink) without any intermediate masking processes, resulting in cost savings. In this study, a direct patterning of colloidal particles on desired substrates were performed using a commercially available drop on demand piezo actuated inkjet printer. The colloidal suspension of particular polystyrene particles were used as ink to produce desired patterns over any substrates. Producing larger areas of homogeneous 2D layers was the primary focus of this work. The investigations were performed on chemical compositions of the ink, particle concentration, substrate modification and effect of externally induced vibration during self-assembly. We have developed a process of using a combination of varied chemical composition of the ink, with substrate modification and application of external vibration during self-assembly to produce the largest possible monolayer coverage with reduced defects via Inkjet printing.

4.1.2.2 Results and Discussion

At first, our focus was to use a single drop from the print head to find the optimal ink composition and optimization of other parameters for a uniform deposition over the entire deposit on the surface.

Figure 1 shows the comparison of morphologies of the different sized polystyrene nanoparticle deposits obtained from the single ink droplets after drying on the hydrophilic silicon substrate. The solid loading of the colloidal solution/ink held fixed at 1% vol. The average diameter of the polystyrene particles used are 150nm, 300nm and 600 nm.

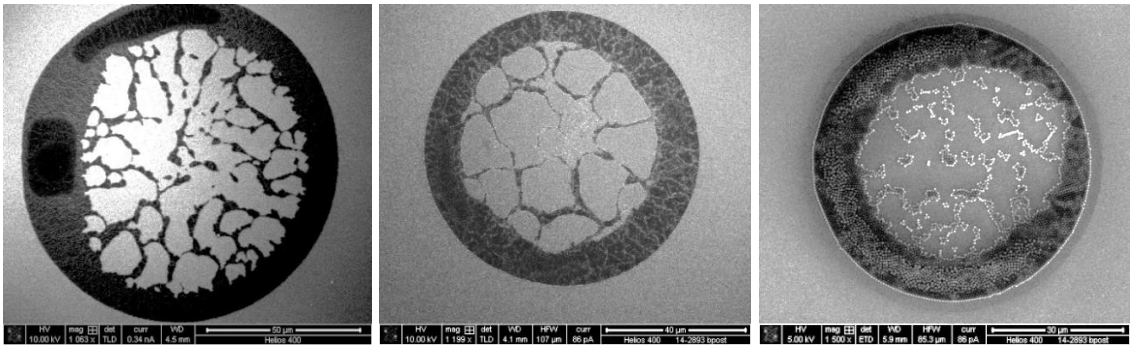

(a) (b) (c)

Figure 4.1.2.2.1 Morphologies of different sized Polystyrene particles on hydrophilic Silicon.(a) 150nm,1% solid loading, (b) 300 nm, 1% solid loading, (c) 600 nm, 1% solid loading.

A few things are noteworthy about figure 4.1.2.2.1: (a) the pattern of particle deposits for all three sizes are very similar; the coffee ring effect is predominant in all three cases, (b)

although coffee ring like deposit is prevalent, the center voids formed are indicative of concentration of particles not being sufficient for entire coverage of the surface uniformly.

To understand if concentration is the sole issue in inhibition of homogeneous coverage on the surface, we varied the particle concentration for a particular size and performed the deposition of a single ink droplet on hydrophilic surfaces.

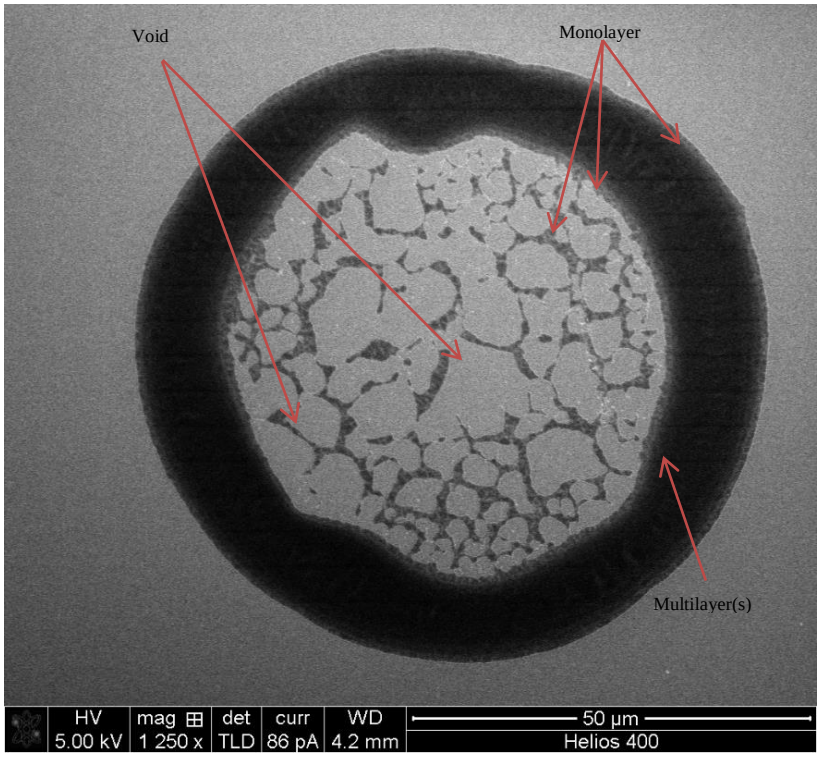

Figure 4.1.2.2.2 Morphology of 150 nm (Diameter) Polystyrene particle with 2% solid loading.

As seen in figure 4.1.2.2.2 the central void with a ring like deposit with higher loading of the particle is still present, and buckling (multilayer) is enhanced on the edges.

It is our understanding that the high evaporative flux from the outer edge of the droplet causes a high radial flow of particles towards the outer edge, which causes inhomogeneity in the coating.

Next, ink composition was varied and high boiling point inks were used in combination with low boiling point inks to see if the rate of radial flow can be lowered to form homogeneity across the coating. Here, we used mixed solvents of water/DEG, water/FA and water/NMP with various loading of colloidal particles (150 nm diameter) ranging from 2-5vol. %. See figure 4.1.2.2.3 for few notable results.

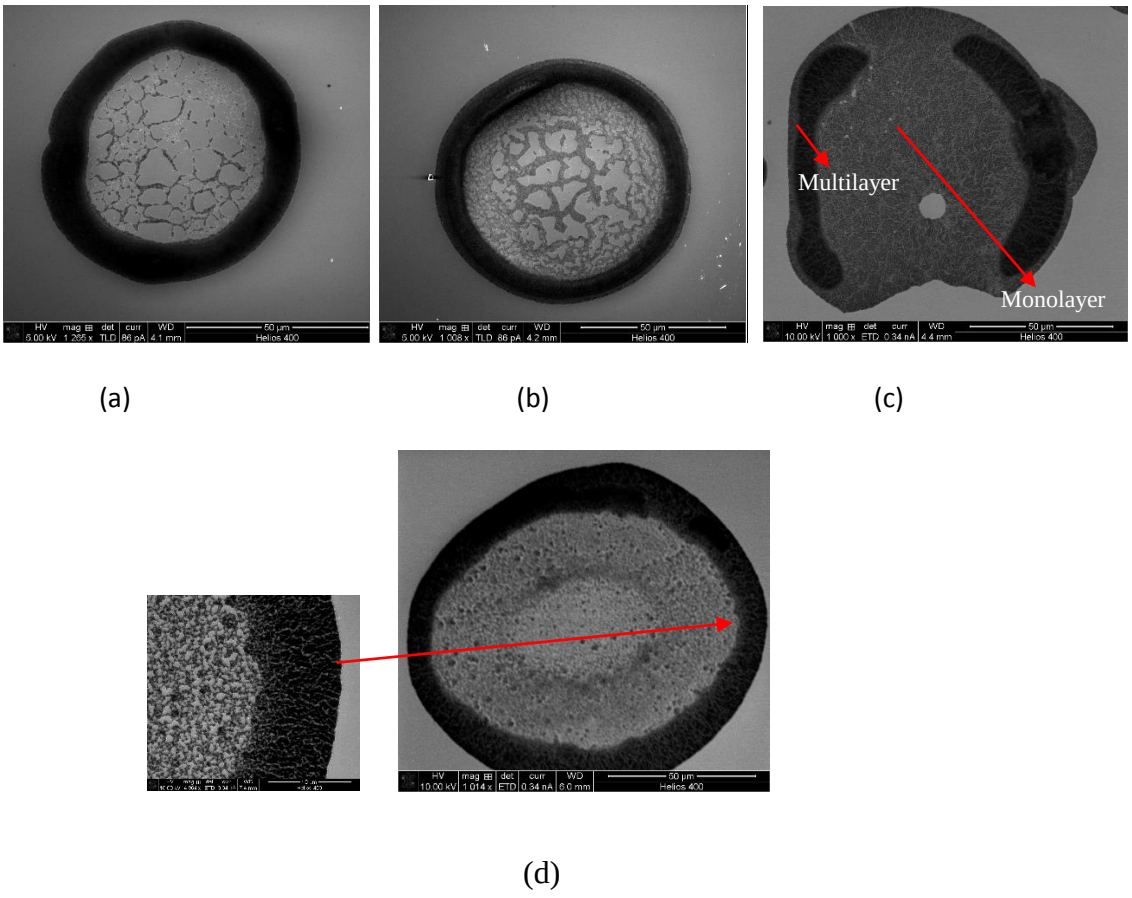

Figure 4.1.2.2.3 Morphology of 150 nm (Diameter) Polystyrene particle with various ink composition and solid loading.(a) 2% Polystyrene + 0.5 vol.% Diethylene Glycol(DEG) (b) 2% Polystyrene + 0.5 vol.% Formamide(FA), (c) 4% Polystyrene + 0.5 vol.% Formamide(FA), (d)4% Polystyrene +0.5 vol.% N-methyl pyrolidone. The substrate used was hydrophilic Silicon.

The results clearly indicate that with mixed solvents we have higher uniformity. Comparing Figure 4.1.2.2.3 (a) and (b) for DEG based ink it is seen that the coverage is not as uniform as FA with similar loading of the particle. We pursued different loadings

of the particles with 0.5 vol. % FA as ink. As seen in Figure 4.1.2.2.3 (c), the maximum area of monolayer coverage is found to exist with 4 vol. % loading of the 150 nm PS particles. With higher loading of particles (five vol. %) creates more multilayers around the edges. With N-methyl pyrolidone 0.5 vol. % and 4% PS particles, as seen in Fig 4.1.2.2.3(d) indicates non uniformity in the coating with sparse monolayers in the center, and edges covered with partial monolayers and multilayers. If concentration of N-methyl pyrolidone is increased above 0.5%, we have observed significant dissolving of the Polystyrene particles, leading to structural deformation.

It is observed with a mixed solvent based ink composition that the shape of the single droplet is varied which is indicative of dissimilar drying rate/mechanism. The high boiling point (DEG, FA, and NMP) and low boiling point (water) solvent mixture possibly induces two different drying rates. After the impact of the droplet from the inkjet onto the surface, the low boiling point (water) liquid enables spreading of the droplet and water having a very high vapor pressure compared to FA (two orders of magnitude higher than FA). The water starts to evaporate at first from the contact line of the droplet, which induces convective flows of particles to the drying front. After the evaporation of water completes, the composition of the solvent changes only to the high boiling point solvent, and the edge evaporation almost ceases, minimizing the radial flow of the particles. FA enables more uniform coating than DEG or NMP because it is to be understood that at the very first impact of the droplet when convective flow is high FA also induces a higher counter convective flow of the particle, than other solvent. This is a characteristic of low surface tension of the solvent in comparison to water (enabling counter radial flow towards the center of the coating). After the surface tension gradient ceases due to

complete evaporation of the water, the radial flow also ceases and the drying process gets slower at this stage, enabling more uniform coating over the entire region. Hence, a combination of proper particle loadings and solvent choices of a high boiling point with low surface tension and low enough viscosity with high diffusion coefficient is crucial to form uniform coating over a desired region.

We further examined the water/FA ink for large areas of coatings by decreasing the dot-to-dot distance, which caused the individual droplets to coalesce on the hydrophilic surface. When the interdot distance is less than the single drop diameter, continuous coating can be formed.

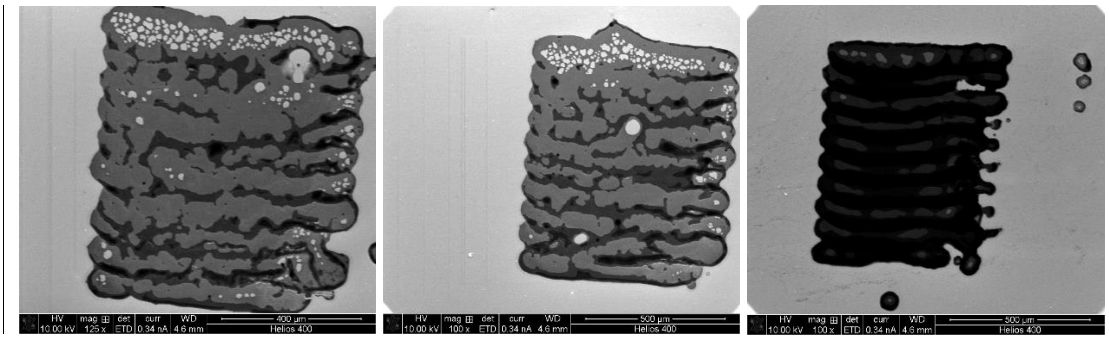

(a) (b) (c)

Figure 4.1.2.2.4 Scanning Electron micrograph of PS particle deposit morphology, produced by the inkjet printing of 10 X 10 array with water/FA ink at different dot-to-dot distances (a) 83µm and (b) 80µm, (c) 76µm.The substrate used are hydrophilic Silicon. Very light gray/white indicates voids, light gray indicates monolayers and dark gray indicates multilayers.

For the 4 vol. % PS + 0.5 vol. % FA based ink the maximum uniformity in coverage is obtained with dot to dot spacing around 80µm. With dot-to-dot spacing above 80µm, there is onset of voids that takes place whereas below 80µm dot to dot spacing produces high percentage of multilayers (See Figure 4.1.2.2.4).

In order to reduce the multilayers and void formations during the large area coating, we changed the ink compositions by adding polyvinyl pyrolidone (PVP) at different loadings to the water/FA based ink. Fig 4.1.2.2.5 indicates that the voids are eradicated from the coating, but the multilayers between two continuous lines were still present.

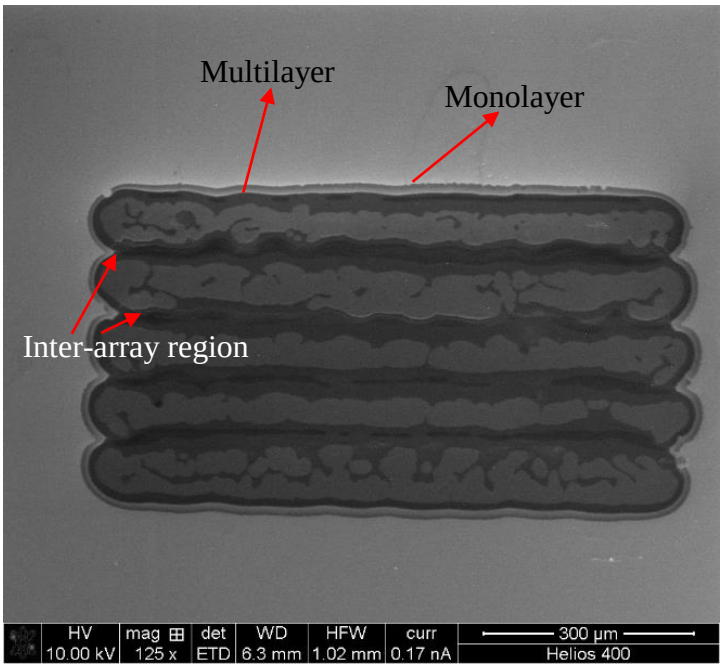

Figure 4.1.2.2.5 Scanning Electron micrograph of PS particle deposit morphology produced by the inkjet printing of 10 X 5 array with water/FA+PVP ink at a dot-to-dot distance of 80µm. The substrate used is hydrophilic Silicon

For large area of coating it is seen as the drops coalesce in the horizontal direction, the choice of proper dot to dot spacing is crucial. However, the problem of multilayer formation arises when the second array is printed beneath the first array. At the interface of the first and the second array, multilayers are formed, several attempts with different solvents were tried to reduce the buckling of the particle at the interarray region. One of the inherent issue with the DMP Dimatix Inkjet printer is the incapability of printing in multiple directions. Our understanding is while the first array is printed and the outer

edge of each droplet dries out, the dried edge of the first array impedes the spreading of the second array droplets that induces multilayer formations at the inter-arrayed region. Using PVP/water/ FA as ink reduces voids, but multilayers at the inter-arrayed region is observed (See Figure 4.1.2.2.5). PVP has low surface tension and has higher boiling point than water that helps further reduce the particles radial flow, enabling reduced void formations.

Next, we studied the effect of external vibration and substrate modification on water based ink to enable monolayer production and reduce the defects formed. We applied external vibration to the substrate while it is being printed. We connected the piezoelectric element to a function generator to generate vibrations at different frequencies. We also, pre-coated the substrate using 2 vol.% PVP using a spin coater (with following specification: 250 rpm;30sec, 0rpm;45 sec, 1500rpm;30 sec), and applied vibrations to see the differences, we printed large areas of 2mm X 2mm and used optical image and image J analysis to analyze the film quality. Defect reduction via substrate modifications and external vibrations during assembly of particles is shown using Scanning Electron Micrograph images.

A hydrophilic silicon wafer mounted on top of the piezo element is placed on the platten where the printing takes place for the 600 nm (dia.) PS particle of 1 vol.% loading, the frequency of the piezo element is varied using a function generator, and varied drop spacings were used. As seen in Figure 4.1.2.2.6, clearly with an increase in frequency to the substrate the ammount of monolayer coverage increases.

Next with an addition to vibration we used 2 vol.% PVP coated substrate instead of bare Silicon substrate. As seen in figure 4.1.2.2.7 and 4.1.2.2.8 and 4.1.2.2.9 precoated silicon with PVP enhanced the monolayer coverage significantly.

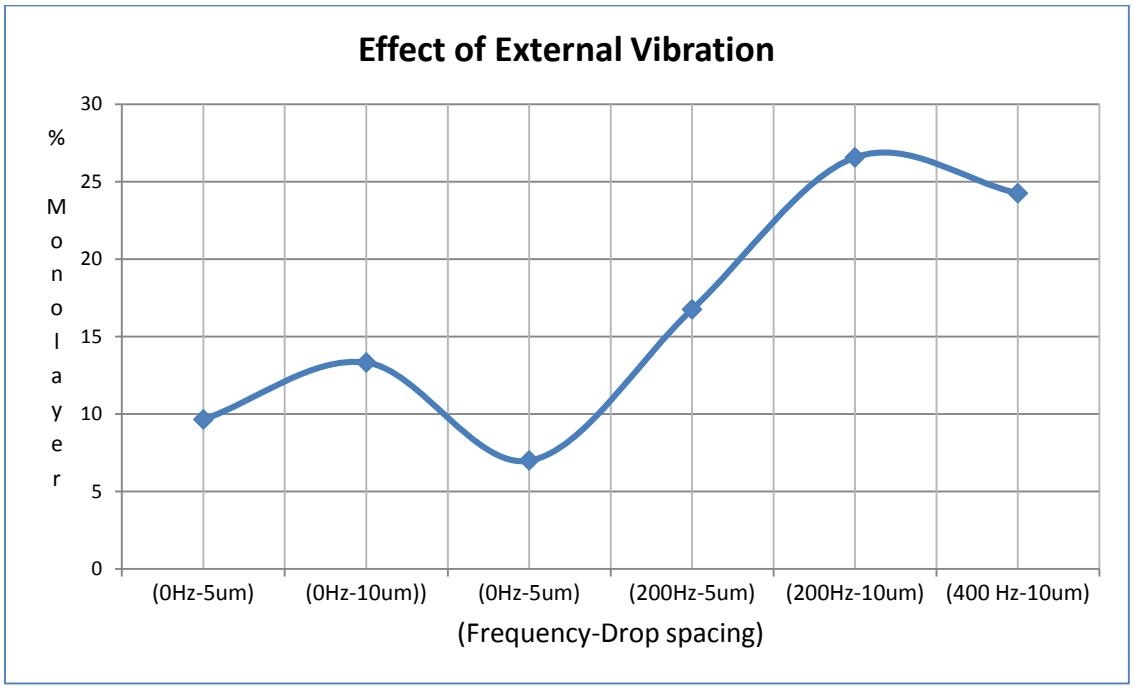

Figure 4.1.2.2.6 Effect of external vibration on monolayer coverage with varying dot-to-dot spacing and frequency

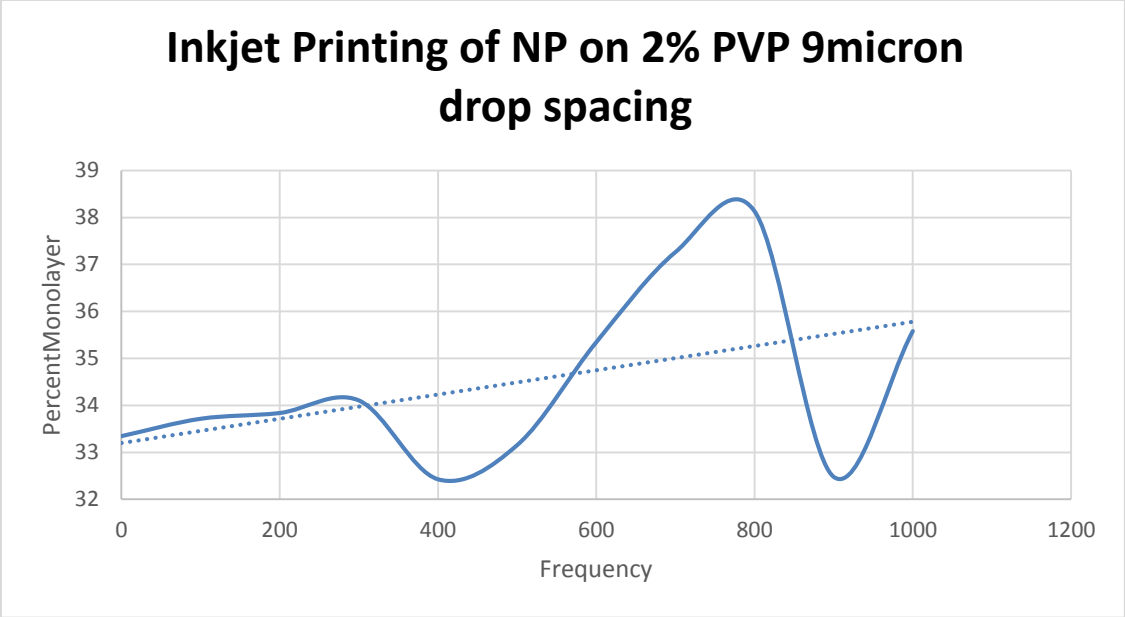

Figure 4.1.2.2.7 Effect of external vibration on 900 nm (dia.) monolayer coatings with 9 micron drop spacing.

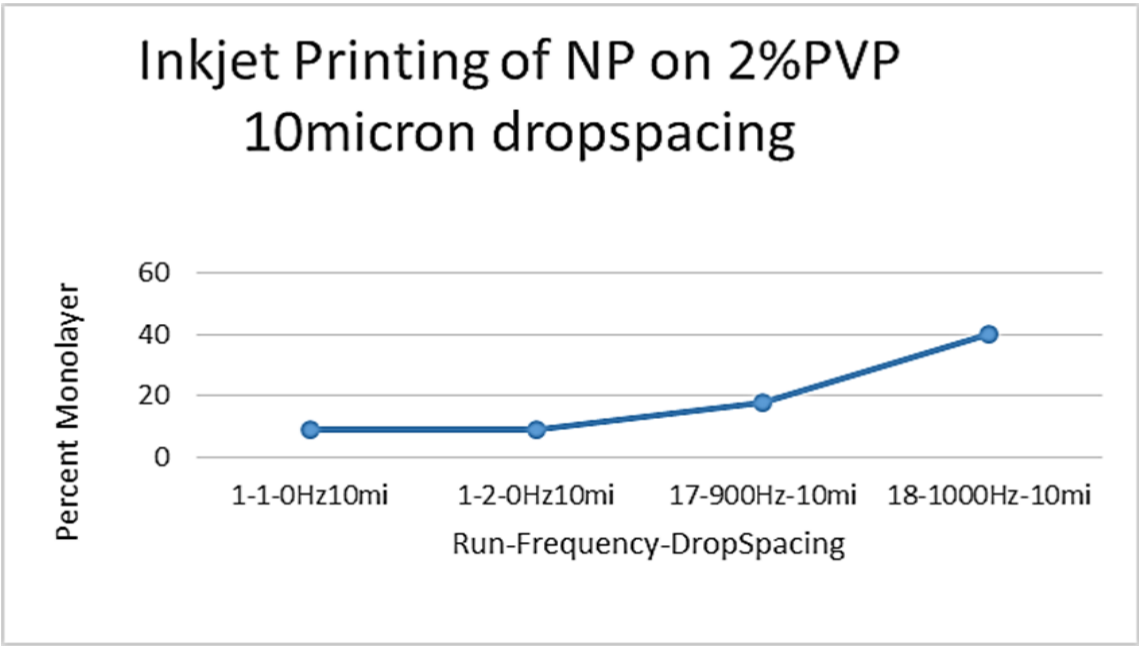

Figure 4.1.2.2.8 Effect of external vibration on 900 nm (dia.) monolayer coatings with PVP modified substrate. Monolayer coverage using pre-modified substrate enhanced by 33% in comparison to just vibration.

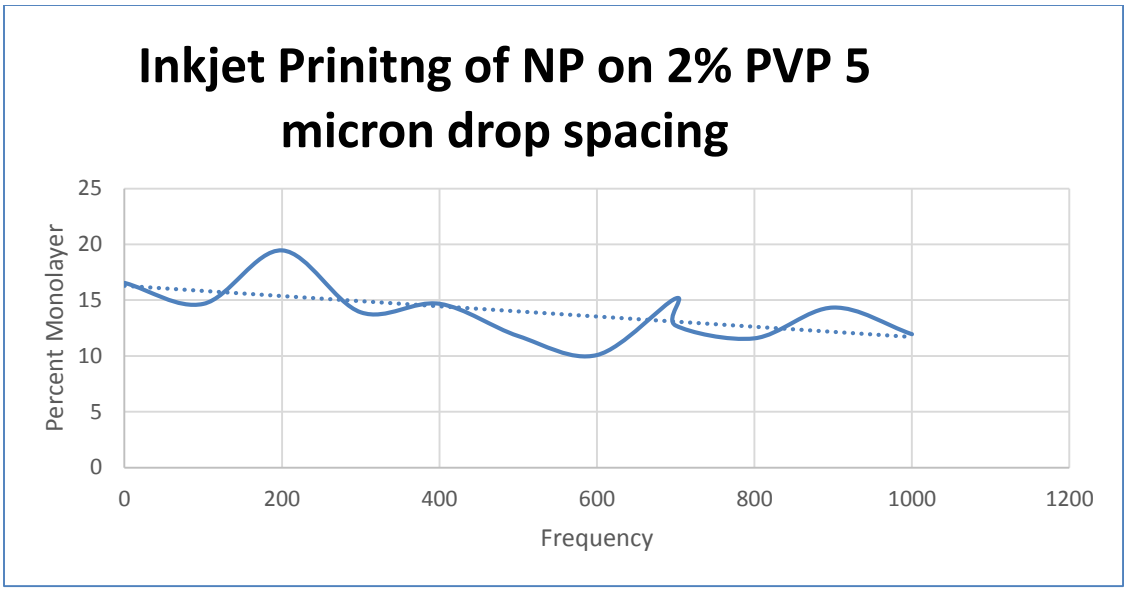

Figure 4.1.2.2.9 Effect of external vibration on monolayer 900nm (dia.) coverage with 5 micron drop spacing. Maximum monolayer coverage for 200Hz. Monolayer coverage using pre-modified substrate enhanced by 50% in comparison to just vibration.

For 1 vol. % loading of 900 nm particles as ink, for inkjet printing, the highest monolayer coverage for a 2mm X 2mm area is obtained using a 10µm dot to dot spacing with external vibrations and pre modified substrates.

Using mechanical vibrations at different frequencies we found less multilayers with higher percentage of monolayer over the entire region in comparison to when no vibration was applied. We suspect lesser buckling of particles due to external vibration is because the external vibration induces extra energy to the particles that in turn enables higher kinetic energy to the particles during self-assembly processes. This allows the particles to overcome the radial convective flow during drying of the edges and during the onset of capillary interaction for ordering of particle, the energy induced due to vibration to the particles enables them to have enough energy required to reach its energy minima state. Hence by adding external vibrations during the self-assembly

process helps better packing. In particular, a significant decrease of point defects is realized with vibration on modified surfaces, as seen in Figure 4.1.2.2.10.

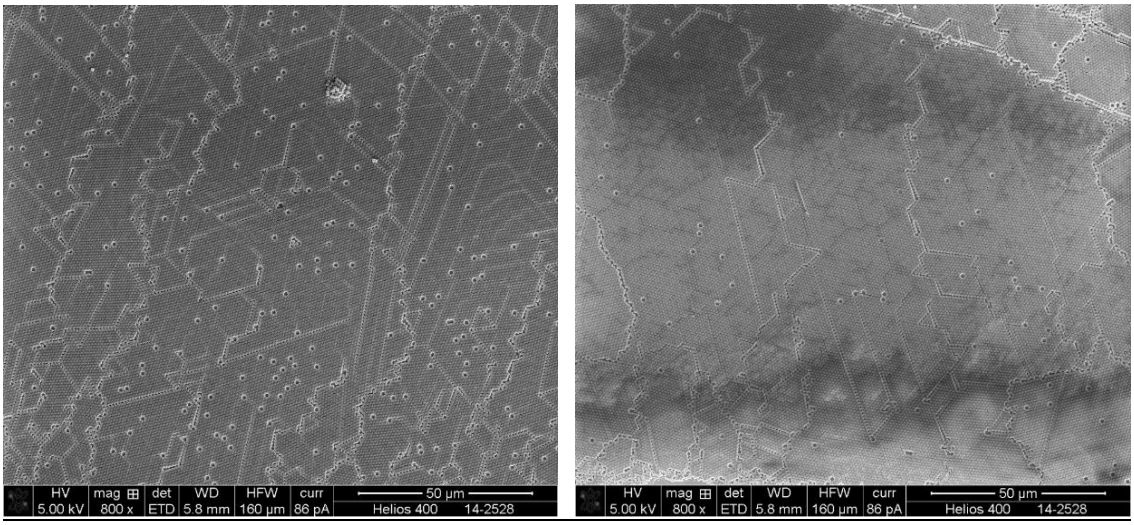

Figure 4.1.2.2.10 Effect of external vibration on monolayer 900nm (dia.) coverage with 9 micron drop spacing.(a) 1% 900 nm colloidal assembly with defects on bare silicon without vibration;0 Hz,(b)1% 900 nm colloidal assembly with less defects on 2%PVP with 700Hz.

4.1.2.3 Conclusion

In brief, ink compositions of FA/water has enabled to suppress the coffee ring effect of a single droplet. When large area was coated, buckling is noticed in the inter-arrayed region with sparse voids over the entire region. Using ink composition of FA/water/PVP we have enabled to reduce void formation but buckling at the interarray region is still prevalent. Although, extensive study with various loadings of ink and external vibrations is necessary to optimize the monolayer coverage. We have also successfully utilized the

external vibrations on pre-modified surfaces with water-based ink to present large area monolayer coverage and reduce the defects in particle packing.

4.1.3 Nano Sized Hierarchical Structures on Surfaces

4.1.3.1 Introduction

Fabrication of nano-structures in colloidal lithography using close packed monolayers is widely used for various applications. These close packed structures are only capable of creating structures that reflect the contour of the interstitial sites (triangular shape) of the close packed monolayers (99) (100). However, building of complex structures like disks, crescents, rings from individual colloids is usually accomplished by using expensive technology and time-consuming processes.

There are several methods to create non-close packed monolayers as discussed in the earlier section. Using oil- water and air-water interface in past, a few researchers have been successful in creating non-close packed monolayers, with a high degree of control on the spacing (101) (102) (103). A fairly inexpensive and faster process known as plasma etching can also be used to form non-close packed packing from close packed arrays (104) (66) (105). Construction of the nanostructures via this method has been the primary focus of the researchers for various applications. Recently Nicolas Vogel et al (75) has carefully examined this process using a commercially available plasma cleaning apparatus under several conditions: varying substrate temperature, plasma power, plasma composition and particle compositions. They successfully demonstrated an etching

process that led to non-close packed structures. Although, formation of complex surface patterns using plasma etching on different substrates for a prolonged period is not well known.

In this study, a commercially available plasma etching apparatus was used to create different hierarchical structures and different substrates for different time periods. Besides the etching conditions of the polystyrene particles to from non-close packed structure , the formation of interesting patterns via prolonged etching of the colloidal monolayer is presented and the nucleation of structures from a thin film using plasma etching is also presented. Plasma etching was carried out on three systems for different time intervals. First system consists only of polystyrene particles on silicon substrate, second system is a combination of polystyrene particles and functionalized graphene on silicon and finally, functionalized graphene (Graphenol) pre-coated on silicon.
Here main goal is to present different structures possible by using a simple method (plasma etching) which enables more structural possibilities than only non-close packed monolayers. These structures can be used as masks during lithography processes. In this work the surface patterns are presented, further investigation of these structures for various applications is not presented.
We have used colloidal particles as a template to produce nanocones, via a process well known as Nano sphere lithography (106). Colloidal lithography since first reported (107) has grown into a widely used technology. The process flow of Nano sphere lithography is shown in Figure 4.1.3.1. We present different structures obtained via Nano sphere lithography process using different metal depositions.

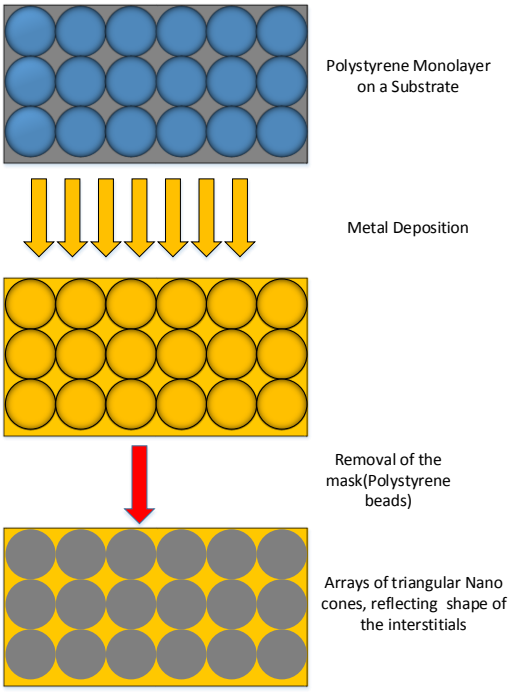

Figure 4.1.3.1.1 Nano sphere Lithography process flow diagram

4.1.3.2 Results

For polystyrene particles on Silicon substrate, the diameter of the particles decreased linearly with increasing etching time (Figure4.1.3.2.1). Etching parameters used were 25 SCCM oxygen flow, 100RF power on 900 nm (diameter) Polystyrene particles, it is found that the etching rate is 3.106 nm/sec.

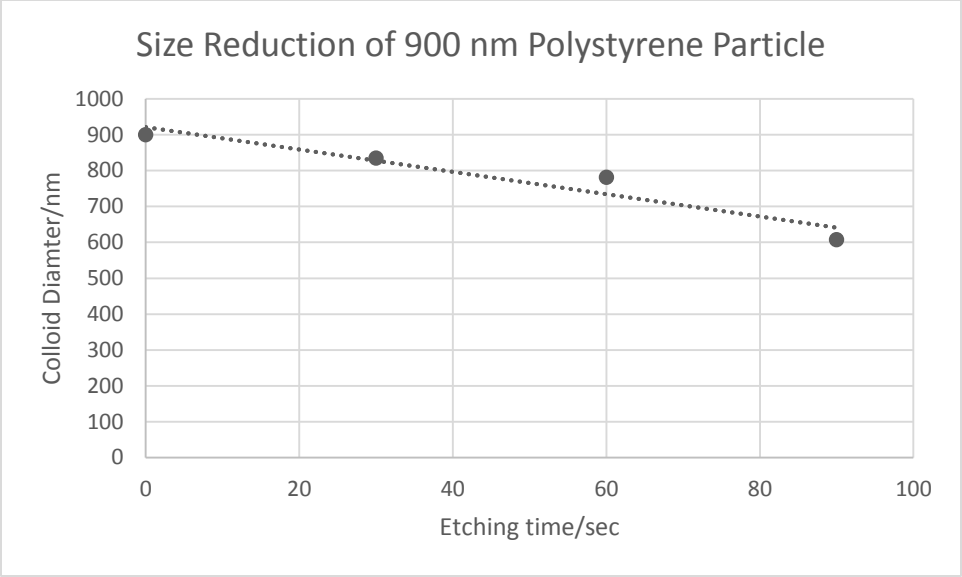

Figure 4.1.3.2.1 Size Reduction of polystyrene (900nm dia.) monolayers with respect to time

If the etching period is continued past 20 minutes, we were successful in creating different structure formation on top of the substrates (See figure 4.1.3.2.2).

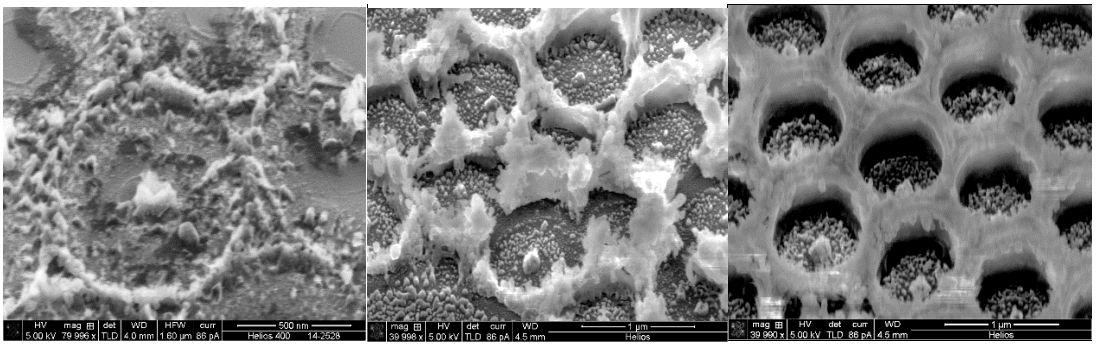

(a) (b) (c)

Figure 4.1.3.2.2 Surface Patterns after prolonged Plasma Etching (a) 20min Plasma Etching on 900nm Polystyrene monolayer on Silicon (b)20 min Plasma Etching on 900 nm Polystyrene monolayer on Graphenol coated Silicon Substrate (c) 30 min Plasma Etching of 900 nm Polystyrene monolayer on Graphenol coated Silicon Substrate

With polystyrene monolayer on functionalized graphene (Graphenol) pre-coated silicon substrate, if prolonged etching for more than 20 minutes is performed a similar surface patterning is observed with polystyrene on bare Silicon. As seen in Fig4.1.3.2.2 (b) with

functionalized graphene coated substrates the growth of these structures formed were significantly increased and with further increase in etching time (See figure 4.1.3.2.2 (c)) uniformity is observed. Finally, via plasma etching on functionalized graphene (Graphenol) film on silicon we observed nanocone structure nucleating from the surface (See figure 4.1.3.2.3).

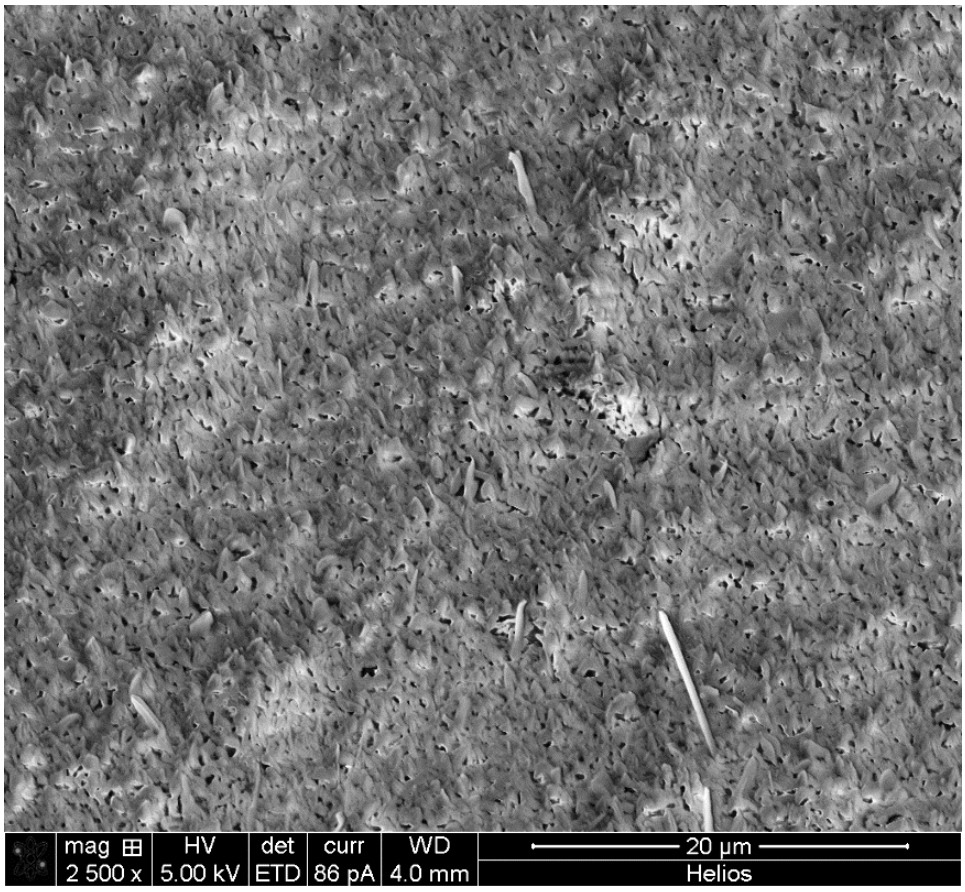

Figure 4.1.3.2.3 Nucleation of nano-structure after Plasma Etching Graphenol coated Si substrate

Production of triangular nanocones were achieved by metal deposition on colloidal monolayer followed by etching of the colloidal masks. Metals like gold and aluminum were coated using ebeam evapoaration onto the colloidal monolayers. Etching of the polystyrene particles were carried out by ultrasonicating the polystyrene particle coated

metals in ethanol bath for a period of 5 minute. Scanning electron micrograph images are presented in Figure 4.1.3.2.4& 4.1.3.2.5.

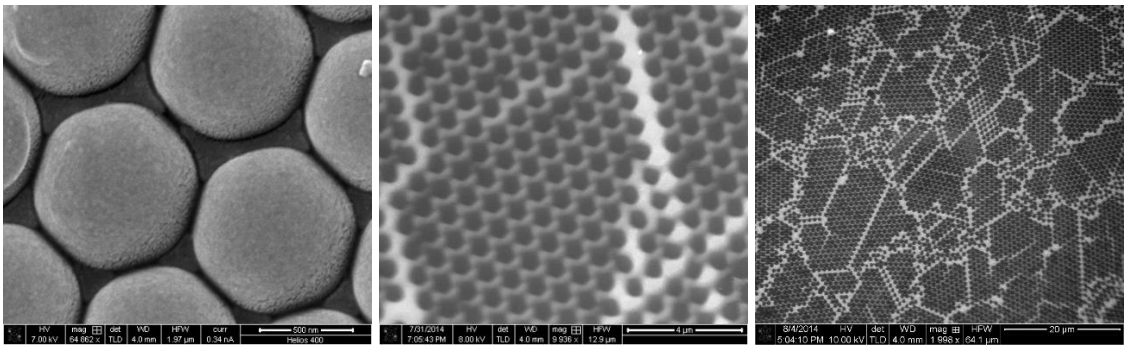

(a) (b) (c)

Figure 4.1.3.2.4 Colloidal Lithography using gold deposition (~20 nm). (a) After Gold deposition on Polystyrene Monolayer. Etching of Polystyrene mask done using Ethanol and ultra-sonication for 5 min (b) &(c) Low magnification images indicating triangular nanocones from different packing colloids. Thicker lines indicates gold deposition onto the defected region of the monolayers

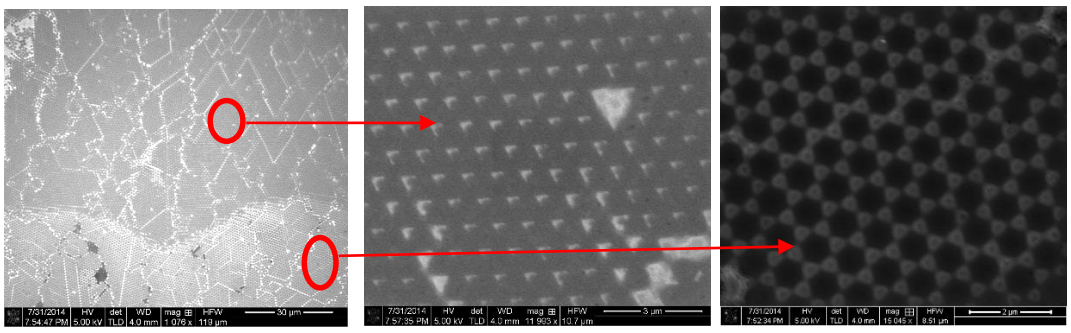

(a) (b) (c)

Figure 4.1.3.2.5 Colloidal Lithography using Aluminum deposition (~250 nm). (a) After etching of Polystyrene mask using Ethanol and ultra-sonication for 5 min (a) Low magnification SEM image indicating aluminum nanocones of two different structure. (b) High Magnification SEM image of the interstitial cones of the face centered packed colloids , and (c) High Magnification SEM image of the interstitial cones of the hexagonally close packed colloids.

4.1.3.3 Conclusion

In brief, plasma etching is used to create different patterns of nanostructures on the surface and effect of plasma etching on functionalized graphene is presented. Ease and simplicity of the plasma etching process over elongated period on different substrates clearly indicates a route for formation of various surface patterns, detailed discussion and study was not a focus of this work. Results are available for further research and development of different applications. Colloidal lithography with different metals is presented and different structure of triangular patterns are presented.

4.2 Binary Colloidal Monolayer Assembly and Control of Phase Segregated Patterns

4.2.1 Introduction

Recent studies indicate that binary colloidal assemblies exhibits more control and tunability of performance over mono-sized assemblies, which is highly advantageous for various applications. For example, when using binary colloidal assemblies high degree of band gap tunability was realized (108). Previous studies on binary particles were focused on forming different 2D and 3D, LS_N structures using several different techniques for specific applications. LS_N characterizes the pattern of the binary colloidal assemblies and N is the number ratio of the small to large spheres. However, very little work has been performed on the spontaneous phase segregation of binary colloids for industrial applications.

As mentioned in Section 3.4, previous work with binary colloids were performed under different conditions to understand the primary force of phase segregation. Although, no clear understanding of this phenomenon is yet available, the processes used in these studies were time consuming and not scalable.

Creation of colloidal surface pattern merely by the design of the process is very attractive, due to its simplicity and reduced production steps. For example, creating stripe-patterned monolayers of particles on surface can be useful for colloidal lithography. Currently, only two notable work had been done on stripe patterning formations. Watanabe et.al. (97) produced stripe patterns via convective assembly of monodispersed particles and reported the concavity of the meniscus (laplacian shape) in combination with low particle concentration as the driving mechanism behind the stripe

pattern formations on a hydrophilic substrate. Work by Retsch et.al (98) was done to prepare heterogeneous monolayer at the air water interface where combination of: inkjet printing on substrates, then floatation of the sparsely printed particle onto the air water interface and finally transfer of non-close packed heterogeneous particles on desired substrate was performed. After drying for a period of time, heterogeneous monolayers on the substrate was obtained.

In this chapter, directed self-assembly of binary colloids were done using the simple and scalable process (reverse convective assembly). As discussed earlier, this process is easy to implement without any use of expensive equipment.

In this section we will present monolayer patterns obtained via reverse convective assembly processes with binary colloids of size ratios (Small(S)/ Large (L)) ranging from 0.11-0.67. One particular size ratio of ($\frac{S}{L}$) 0.67 enabled phase segregation with distinct and periodic stripe patterns. Using this system, we further investigated the mechanism of spontaneous phase segregation and means to gain control over the phase segregation process enabling controllable stripe patterned coatings.

4.2.2 Results and Discussion

We used the process of reverse convective self-assembly with similar parameters as those used for monodispersed system (See Section 4.1.1.2), for investigating binary colloidal assemblies.

In this chapter, we will assess the different size ratios ranging from ($\frac{S}{L}$) 0.11-0.67 to detect phase segregation pattern. For one particular size ratio that provides distinct phase segregation, we will investigate the parameters required to control its pattern periodicity.

We will also present schematic and mathematical explanation for the mechanism behind the phase segregation of the particles.

Binary Colloids Structural Diversity

In order to investigate the range of particular size ratio of colloids that undergo phase segregation during assembly, a systematic variation of size ratio between the small (S) and the large (L) particles were carried out using reverse convective assembly (RCA) process. All other parameters for the process (RCA) were kept fixed for all different size ratio. Binary colloidal solutions were prepared by mixing suspensions of large particles (L) (1 vol. %) with small particles (1 vol. %) at volume ratio $\frac{\emptyset_S}{\emptyset_L} = 1$. Figure 4.2.2.1 shows variations in the patterns of binary colloidal assembly for different size ratios ($\frac{S}{L}$).

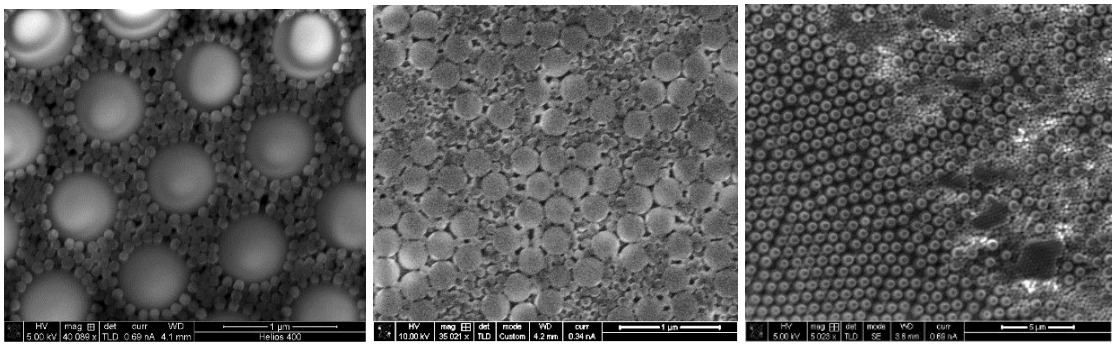

(a) (b) (c)

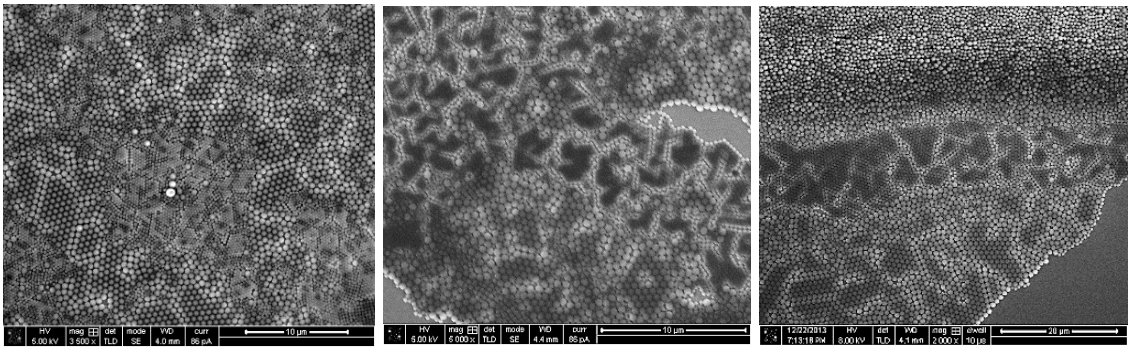

(d) (e) (f)

Figure 4.2.2.1 Binary Colloidal assembly structural diversity (a) Size Ratio(S/L:100/900)=0.11,(b) Size Ratio(S/L:100/300)=0.33,(c)Size Ratio(S/L:300/900)=0.33,(d) Size Ratio(S/L:300/600)=0.5,(e) Size Ratio(S/L:300/500)=0.6 (f) Size Ratio(S/L:600/900)=0.67

As seen from Figure 4.2.2.1, for size ratio $(\frac{S}{L})$ < 0.5 the entire region of self assembly was dominated by multilayers or mixing of particles with little to no sign of segregation. We further experimented with varied volume ratio for this particular size ratios ($(\frac{S}{L})$ < 0.5), no significant segregation was observed. In our understanding, when the evaporative flux occurs at the drying front, the meniscus thining leads to an increase in viscosity of larger particle. The larger particle becomes partially immobile on the surface while the smaller

particle still have enough room to move towards the drying front, for ($\frac{S}{L}$) < 0.5 the meniscus height is large enough to enable multiulayer formation of these smaller particle. In our case for similar volume loading of both small and large particles where the number of smaller particles is higher than number of larger particles, the smaller particle not only dominates the drying front but also fills the interstities between the immobilized larger particles. Finally, when capillary interaction onsets with the drying of the meniscus, multilayer assembly of smaller particle takes place and the smaller particles in between the intrerstities impedes the formation of monolayer of larger particle, hence an over all area of mixture and multilayers are observed. Clearly, it is important to choose proper size ratio and the volume loading for each particle size.

For size ratios above ($\frac{S}{L}$) ≥0.5 the phase segregation is clearly observed (distinct), it is our understanding with higher size ratio the meniscus thinning is just right enough for the particle flux to be restricted to form a monolayer. For some size ratios ($\frac{S}{L}$) ≥ 0.5 (See Figure 4.2.2.1), even though segregation of particles occur, the segregated patterns formed are random. For size ratio of ($\frac{S}{L} = \frac{600}{900} = 0.67$) the segregation is more uniform (parallel to the meniscus direction) and occurs periodically. Later in this section we will discuss how to control its width. Our findings on phase segregation for mixture of 600nm and 900nm particles were videographed during its assembly that correlates with our logical explaination for phase segregation mechanism (provided later in this section).

Control of the phase segregation patterns

The actual mechanism of phase segregation of these binary colloids during the self assembly process is described later in this section. Owing to the interest of control of colloidal self assembly, the next section is geared towards understanding the different parameters that affect the self assembly process of these binary colloids. Investigation of parameters such as volume fraction, effect of addition of solvent is performed to understand the factors that enable tunability of distinct periodic phase segregation over a considerable larger area. Here for initial study only size ratio ($\frac{S}{L} = \frac{600}{900} = 0.67$) is investigated.

1. **Effect of volume fraction**

Figure 4.2.2.2 shows each phase-segregated particle as a function of particle volume fraction. We varied the volume fraction for the 600 nm(S) and 900 nm (L) mixture with, $\frac{\emptyset_S}{\emptyset_L}$ ranging from 0.25 to 5. As seen in Figure 4.2.2.2, with $\frac{\emptyset_S}{\emptyset_L} < 1$ it is clear the phase segregation is present, but the patterns formed were highly random and lacks periodicity. For $\frac{\emptyset_S}{\emptyset_L} \geq 1$ we observe distinct stripe pattern formation along the direction parallel to the contact line. With $\frac{\emptyset_S}{\emptyset_L} = 1$, the stripe pattern was sporadically spotted on the substrate at various location, although the percent multilayer coverage were high in compared to individual colloidal assembly, which indicates higher particle concentration. For $1 < \frac{\emptyset_S}{\emptyset_L} > 3$ periodic repetition of stripe patterns were visible but the stripe length was not

consistent (i.e. not parallel with the contact line), rather perpendicular segregation (right angle to the direction of the contact line) were found to be intertwined with horizontal stripe formation (along the direction of contact line). For $\frac{\emptyset_S}{\emptyset_L} \geq 4$ we see more uniformity and segregation in one direction (along the direction of the contact line). It was also found that across the length of the coating the thickness of each stripe length (both 600 nm and 900 nm coating) decreased from the front to the end of the coating, which could be caused due to variation of local concentration of the particles during this coating process.

$\frac{\emptyset_S}{\emptyset_L} = 0.25$ $\frac{\emptyset_S}{\emptyset_L} = 0.33$ $\frac{\emptyset_S}{\emptyset_L} = 0.5$

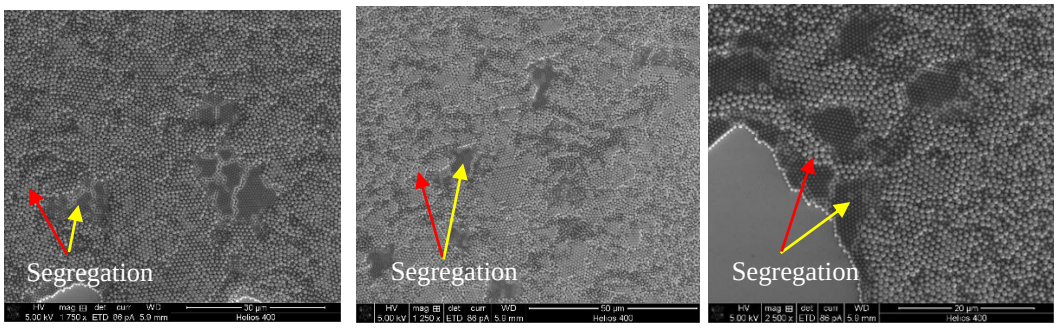

$\frac{\emptyset_S}{\emptyset_L} = 1$ $\frac{\emptyset_S}{\emptyset_L} = 2$ $\frac{\emptyset_S}{\emptyset_L} = 3$

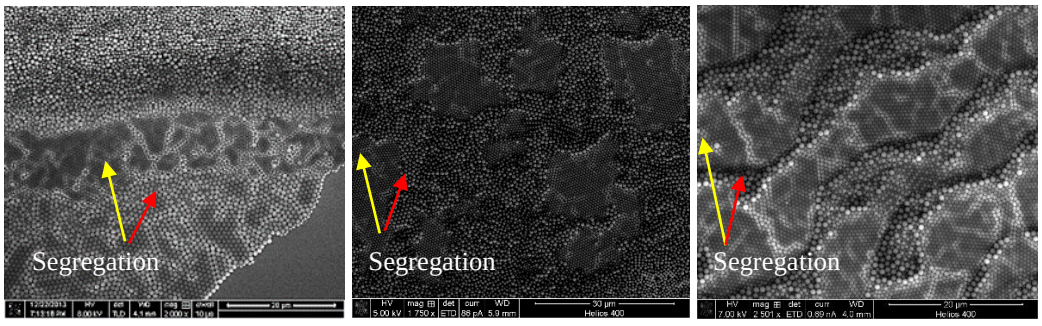

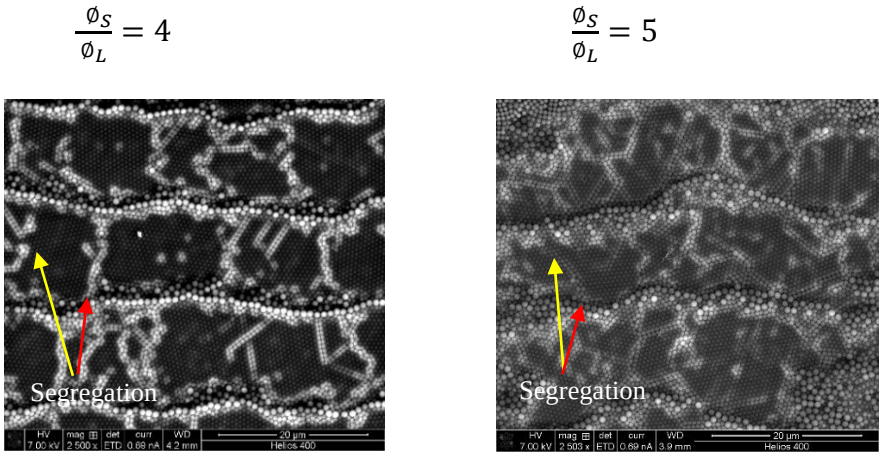

Figure 4.2.2.2 Binary Colloidal assembly structural diversity of varying volume fraction for Size Ratio ($\frac{S}{L} = \frac{600}{900} = 0.67$)

Hence, we conclude that (a) smaller particle concentration for size ratio ($\frac{S}{L} = \frac{600}{900} = 0.67$) is critical to stripe formation, and (b) for other size ratios($\frac{S}{L}$ >0.5) that shows presence of phase segregation, proper tuning of the volume fraction might reveal periodic phase segregation and stripe formations.

2. Solvent addition and its Surface Tension Effect

In this study, we investigated the effect of solvent on controlling the stripe lengths for the size ratio ($\frac{S}{L} = \frac{600}{900} = 0.67$) with volume fraction $\frac{\emptyset_S}{\emptyset_L} = 4$. We did a comparative study of the individual stripe length resulting on a silicon wafer with different concentrations of ethanol in the colloidal suspension.

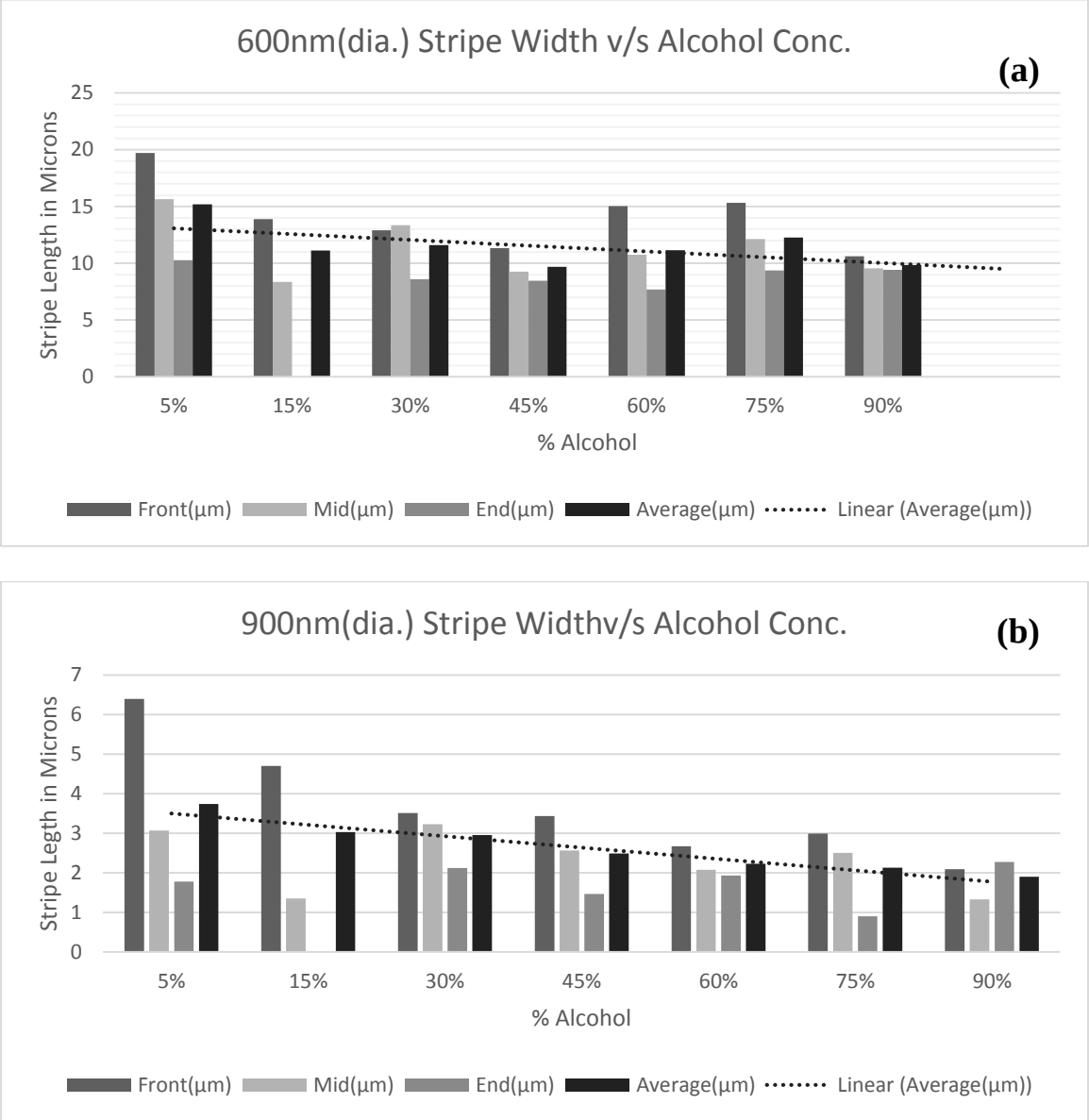

Figure 4.2.2.3 Stripe width as a function of alcohol concentration, (a) 600 nm polystyrene particle stripe width at different coating region v/s alcohol concentration. (b) 900 nm polystyrene particle stripe width at different coating region v/s alcohol concentration

Figure 4.2.2.3 shows stripe width as a function of alcohol concentration, within the concentration range required for the formation of phase segregation. Although it is evident that the stripe width for both 600 and 900 nm particles decreases with an increase in alcohol concentration. It is seen in figure 4.2.2.3 for a particular concentration the

stripe length varies from the start of the process (Front) to the end of the process. This is primarily due to the inherent issue of local concentration variation (higher concentration of particle at the front in compared to the end of the process) in a non-equilibrium process (i.e. Reverse Convective Assembly). These results clearly suggests that the length of the periodic stripe patterns can be controlled by changing the solvents , and, as seen in figure 4.2.2.4, the contact angle decreases with increase in alcohol concentration, indicating that the surface tension of the dispersing media possibly controls the stripe lengths for both the particle coating thickness. This indicates a correlation between the stripe widths; wider width of any one particle coating results in wider width of the other particle coating and the correlation strengthens with higher concentration of particles (comparison of coating thickness from front to end).

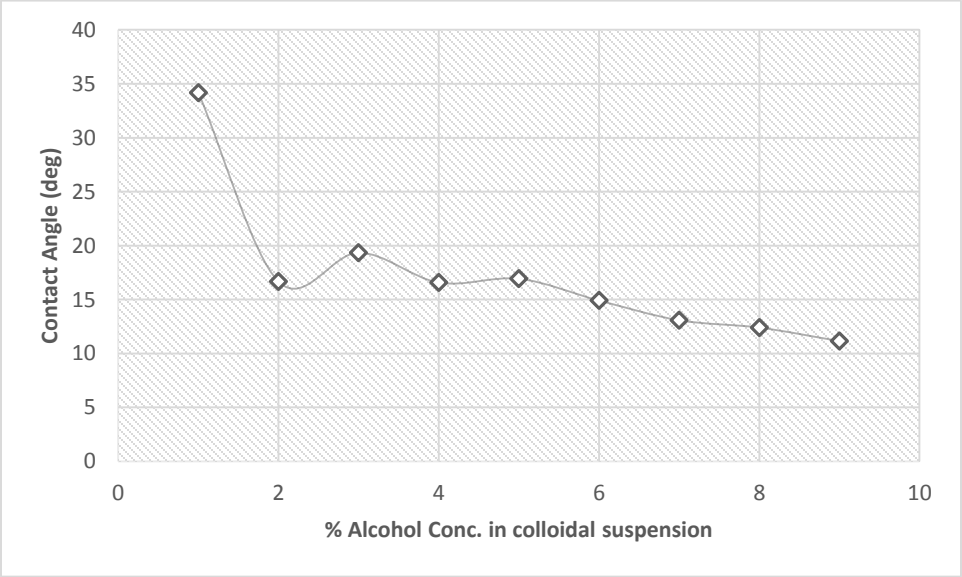

Figure 4.2.2.4 Contact angle as a function of alcohol concentration in the suspension, measured using a goniometer setup

Mechanism of Periodic Phase Segregated Pattern Formation on Hydrophilic surface

The Stripe pattern formed by binary colloids can be divided into two stages: particle separation at the drying front based on meniscus shape and particle(s) flow and the particle(s) segregation, which is the thermodynamic aspect of the system that aids in forming close packed structure among its similar sizes (phase segregation). For the particle kinetics based particle separation, we discuss a process flow for particle separation based on sizes. For complete segregation of particles in its own domain, we provide interaction energies at different separation length for different contact angle, which elucidates why they segregate among the similar sized particles rather than mixing at any stage of drying process.

To our findings, (See figure 4.2.2.5) the concavity of the meniscus while drying due to surface tension effect, and the concentration of particle near the drying front, and the size ratio drives the particle separation mechanism. Particle separation initiated via meniscus thinning leads to larger particle getting its particle head out of the water meniscus where it is immobilized to the adjacent surface. While the larger particle is immobilized smaller particles are still seeping through the inter particle region of the larger particles and moving to the drying front until the thinning of the meniscus is below the diameter of the smaller sized particle.

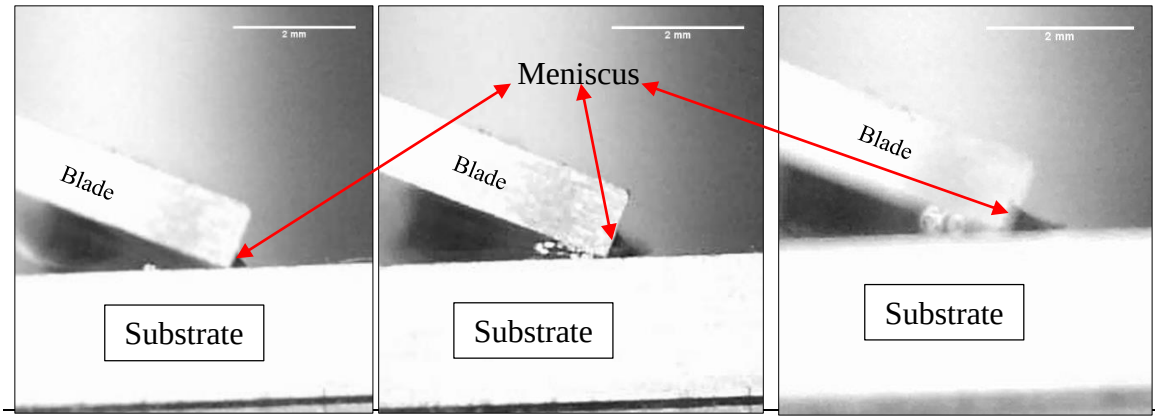

(a) (b) (c)

Figure 4.2.2.5 Shape evolution of the meniscus while Reverse Convective Assembly at (a) Time T1, (b) Time. T2, (c) Time, T3.Here, T1<T2<T3.Images Captured using a CCD Camera.

A process flow is also presented in Figure 4.2.2.6 to provide a logical conclusion to mechanism of particle separation. At first, as the solvent evaporates, enabling lowering of the liquid level, this induces a convective flow for the particles towards the drying front. With further evaporation and lowering of the liquid film from the drying front, the liquid film reaches a height that becomes equal or lower than the large sized particle diameter (a). Hence the larger particle ceases to move laterally and gets pinned onto the substrate in a non-close packed manner. While the larger particle are immobilized (b), the smaller particles that are still beneath the liquid film is capable of Brownian motion, but under the influence of the convective flow, the smaller particles move towards the drying front of the film. Under the condition of reasonably low concentration of larger particle compared to smaller particle (i.e. volume fraction) , the particle flux for combined two different size becomes equal to the relative rate of the withdrawal for the blade enabling to form monolayers. It is well known that shape of a meniscus must satisfy the Laplace

equation for a quasi-static process, (109) which means the shape of the meniscus has to be concave against the substrate (as seen in Figure 4.2.2.4) to satisfy the Laplace equation. Now, when the liquid film is attached to the tail end of the larger particle (c) and the liquid film meniscus becomes concave against the surface, the meniscus concaves more due to evaporation and withdrawal of the blade. The larger particle that first comes out of the liquid film determines the width of the stripe of the smaller particle assembly. As the larger particles flow to the drying front completely ceases (d), the meniscus, while being thinned and concaved, can only allow certain sized particles to flow towards the drying front. At this stage, the meniscus is allowing the smaller sized particles to come close to the edge of the new drying front. Finally, flow of any particle to the drying front ceases when the meniscus concaves and thins below the height of the smallest particle. The meniscus, after being thinned and pulled away from the drying front, again reattaches to the next pinned larger sphere next to the previous band of smaller particles, and the process repeats. As per the proposed mechanism, the width of the stripe of smaller particle is dependent on the particle concentration and the concavity of the meniscus at drying front and the height of the larger particle. If the particle size difference is too large and smaller particles can move towards the drying front, the smaller particles will form multilayer and occupy the inter-particle spaces of the larger ones that in turn will cause mixing and buckling, as seen for size ratio below 0.5.

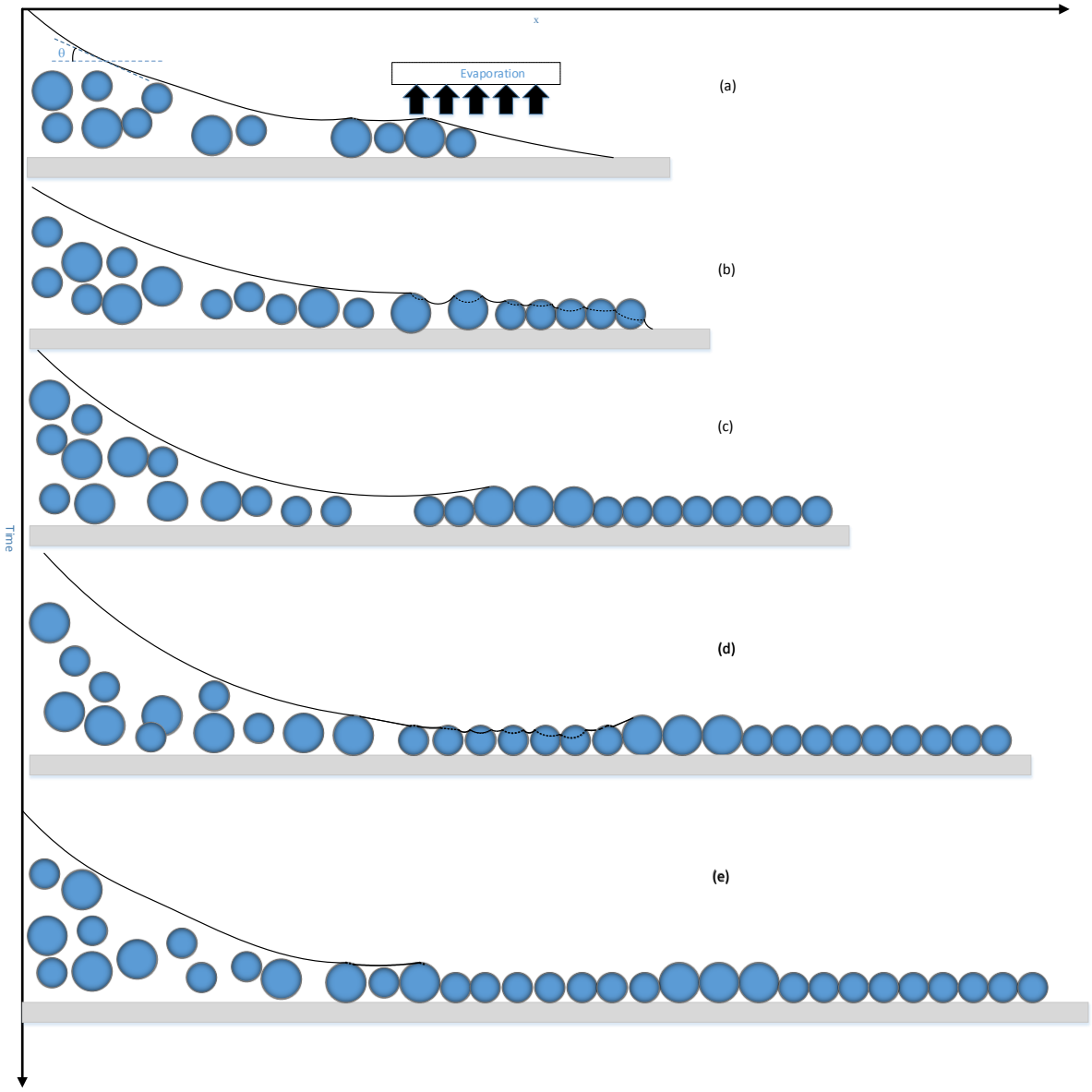

Figure 4.2.2.6 Illustration of Mechanism of Particle Separation and Periodic Stripe Formation

Capillary Interaction Energy induced Phase Segregation of Particles

As the particles separate out during the convective flow, the question is what happens when the capillary interaction onsets. To understand the mechanism, we simulated the capillary interaction energy between particles with different contact angles, representing different drying stages.

In our case for simplicity, we have considered cylinders (See figure 4.2.2.7).

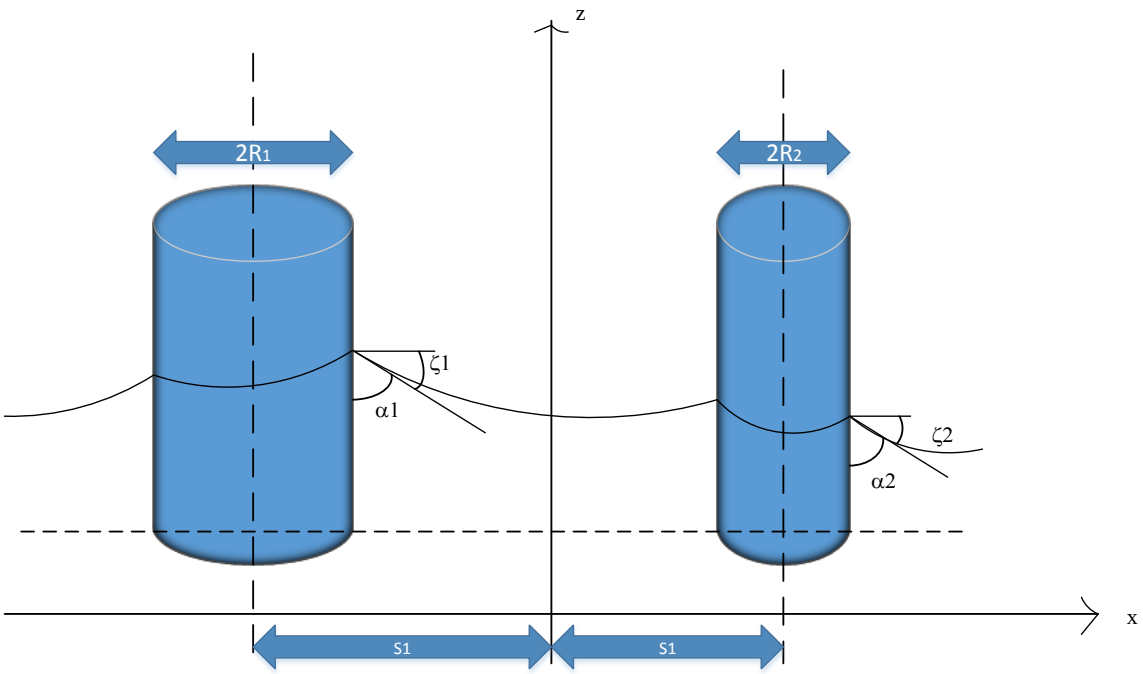

Figure 4.2.2.7 Capillary Meniscus Sketch for two vertical cylinders of radii R1 and R2. α1, α2 are the three phase contact angle

According to Kralchevsky et.al. (110), the capillary interaction energy for any system of particles attached to an interface is given by:

$$\Delta E = E - E_{\infty}$$

$$E = Interparticle\ Interaction\ Energy\ ,$$

$$E_{\infty} = Interparticle\ Interaction\ Energy\ E\ at\ infinite\ separation\ of\ particle$$

Where,

$$\Delta E = -\pi\gamma \sum_{k=1}^{2}(z_k - z_{k\infty})R_k \sin\zeta_k \tag{4.1}$$

$$z_k = R_k \sin\zeta_k\,[\Gamma_k + 2\ln(1 - e^{-2\Gamma_k})] - (R_1 \sin\zeta_1 + R_2 \sin\zeta_2)\ln(\gamma q a) + (R_1 \sin\zeta_1 - R_2 \sin\zeta_2) * [A - (-1)^k \sum_{n=1}^{\infty}\frac{2}{n}\frac{e^{-n\Gamma_k}\sinh n\Gamma_j}{\sinh n(\Gamma_1+\Gamma_2)}] \tag{4.2}$$

$$q^2 = \frac{g(\rho_1-\rho_2)}{\gamma}; \tag{4.3}$$

ρ_1 & ρ_2 = mass densities of two neighboring fluid phases, g = gravity, γ = interfacial tension

Here, j, k =1, 2 with j≠k

$$\Gamma_k = \ln(\frac{a}{R_k} + \sqrt{(\frac{a^2+{R_k}^2}{{R_k}^2})}), \text{ with k=1, 2} \tag{4.4}$$

And,

$$a^2 = \frac{\frac{b}{4}(b+2R_1)(b+2R_2)(b+2(R_1+R_2))]}{(b+(R_1+R_2))^2} \tag{4.5}$$

$$b = s_1 + s_2 - (R_1 + R_2) \tag{4.6}$$

$$A = \sum_{n=1}^{\infty}\frac{1}{n}\frac{\sinh n(\tau_1-\tau_2)}{\sinh n(\tau_1+\tau_2)} \tag{4.7}$$

$$z_{k\infty} = R_k \sin\zeta_k\, ln\frac{4}{\gamma q R_k(1+\cos\zeta_k)}; \text{ k=1, 2 and for } qR_k << 1 \tag{4.8}$$

Substituting (4.2-4.8) into 4.1 using Mathematica software we solved for ΔE with respect to interparticle distance b, with different contact angle (psi) ζ_k, (See figure4.2.2.7) with k=1, 2). Given; cylinders with diameters of 900 nm and 600 nm, $\Delta\rho$=1gm /cm^3, and γ=40 mN/m, we obtain the following:

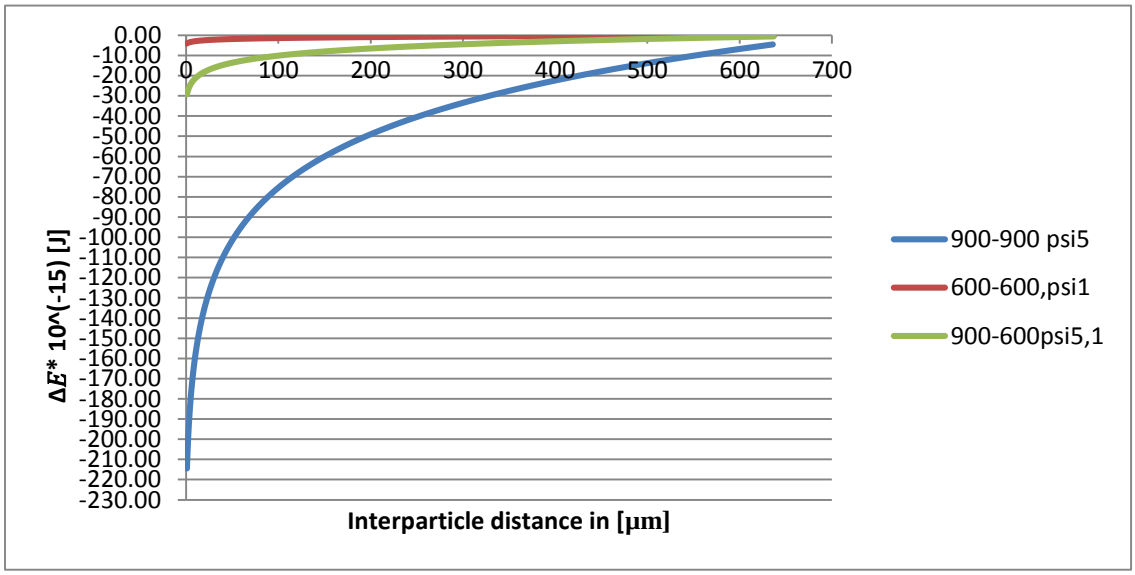

Figure 4.2.2.8 Interaction energy with respect to Interparticle distance for similar and dissimilar sized particles with ζ_1=5º and ζ_2=1º.

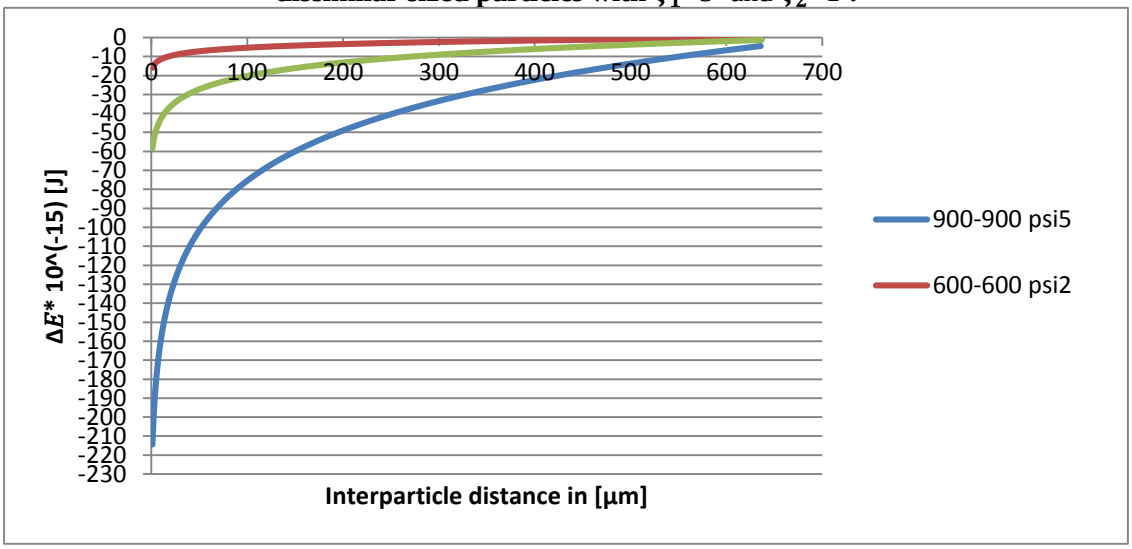

Figure 4.2.2.9 Interaction Energy with respect to Interparticle distance for similar and dissimilar sized particles with ζ_1=5º and ζ_2=2º.

In our case of binary systems , as discussed earlier(with schematic) the larger particle comes out of the water meniscus first, and the smaller particles comes out of water later , which justifies the choice of difference in contact angle for two different sizes during drying. As seen in fig 4.2.2.8 and 4.2.2.9, the interaction energy between the large size particles is significantly higher at any instant of the drying process. This clearly explains why binary phase segregation happens during capillary interaction of particles.

4.2.3 Conclusion

In brief, method and mechanism of fabricating periodic phase segregated stripe pattern using binary colloidal films were presented; also, we have investigated the mechanism of phase segregation process by varying experimental process/parameters. Phase segregated stripe pattern of each sized colloids were formed spontaneously for size ratios (S/L) >0.5. Using one particular binary system, we have studied the effect of addition of solvent and surface tension effect to enable control over the periodic width of the stripes of two sizes by varying volume fraction of the colloids we identify different segregation patterns. Logical explanation with a schematic were presented for the mechanism of phase segregation based on videography of the 600 and 900 nm binary colloids during its self-assembly. Finally, a mathematical simulation using Mathematica is presented to unravel the capillary interaction based segregation of particles.

V. EXPERIMENTAL

5.1 General Procedures

5.1.1 Treatment of Silicon Substrate Prior-use

All Silicon wafers were first cut to desired dimension. The cleaning was done in a beaker immersed in an ultrasonic bath (Ultrasonic Cleaner, DSA 50-SK 2-2.51). Deionized water was used to rinse the silicon wafers. Then for 1 min each, the silicon wafer were cleaned to remove any surface contaminants using the ultrasonic bath with DI water, followed by Methanol (99%) and Iso propanol alcohol (99%). Finally, rinsed with running DI water and dried using nitrogen gas. Then the substrate were plasma etched for 5 min at 25sccm Oxygen and 100RF power, this final step increased the surface energy and induces very low ($<20^{o}$) water contact angle.

5.1.2 Production of Nanostructures

The evaporations were carried out in a physical vapor deposition chamber; Angstrom Engineering Evo Vac. Commercially available plasma etcher was used with Oxygen gas with flow rate of 25 sccm and RF power of 100 Watts.

5.1.3 Scanning Electron Microscopy

All scanning electron micrographs were carried out in FEI Helios Nano Lab 400 SEM.

5.1.4 Optical Characterization

All optical videography and imaging were carried out in Olympus BX 60 Optical Microscope, 20-50X infinity corrected lens with high working distance.

5.1.5 Inkjet Printing

All inkjet printing were carried out using FujiFilm Dimatix Inkjet Printer # DMP 2831.

5.2 Materials

Unless otherwise stated all other chemicals were purchased and obtained from Sigma Aldrich, VWR and it was used as received. Water of high purity (milliQ garde; resistivity =18.2MΩ cm) were obtained from (Milipore, Direct Q3UV).

5.3 Experimental Details of Reverse Convective Self-Assembly

All polystyrene nanoparticles were commercially available and obtained from Thermo Fischer Scientific with added surfactant. Monodispersed polystyrene particles with a mean diameter of 100-900 nm with a polydispersity of <4% were dispersed or redispersed in Ultrapure water at required solid loading. The dispersed solution was ultrasonically treated for 2-5 min (Ultrasonic Cleaner, DSA 50-SK 2-2.5l).

The particle suspension were deposited between the substrate and glass blade. To ensure the proper angle of the blade and to monitor the evolution of the meniscus shape during coating; a video camera was used (Digi micro, AGPtEK iT7B-150112, 2 MP USB Digi Camera, 30 fps, 24 bit RGB, 110 mm (L) X 33 mm(R))

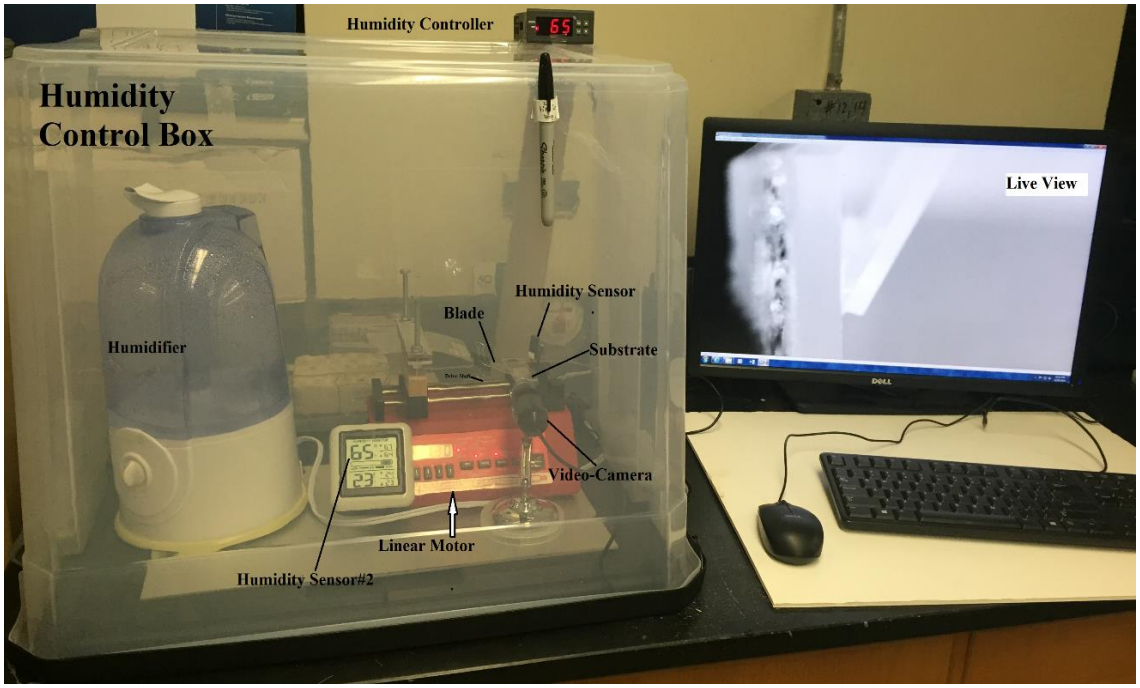

Figure 5.3.1 Reverse Convective Assembly Setup

Unless otherwise stated, the substrate consisted of a P-type Si wafer of [100] orientation (Wacker Siltronic Corp.,525 μm ± 20 μm,10-15 Ω-cm) and plain precleaned glass slides and all chemicals were purchased from Fisher Scientific (Pittsburgh, PA). The Silicon wafer were first cut into desired sizes and then pre-cleaned in an ultrasonicating bath to remove any organic or macro particles by using methanol, and Iso propyl alcohol followed by rinsing with ultrapure water. To obtain hydrophilic surface both chemical and physical methods were used. Chemical cleaning with piranha solution (3:1 Sulfuric acid: Hydrogen Peroxide heated to 100^{o}C) was performed for 30 minutes followed by rinsing with ultrapure water. Physical Cleaning was done using Oxygen Plasma Etcher (RF power of 100W, 25 SCCM of Oxygen for 300 seconds).

Just before the use, each substrate were rinsed with DI water and dried with Nitrogen gas, and then mounted on the stage of the linear motor. The entire setup was kept in a humidity controlled box, a humidifier (Safety first, 360º Ultrasonic Humidifier) was controlled via a humidity controller (WILLHI Digital Humidity Controller, Model# WH8040, control accuracy 1%, sensor Type HM 40, humidity measurement Error 3%, working temperature: 0-50ºC), with hysteresis set at 5%) with the humidity and temperature sensors were attached close to the coating area (shown in Figure 7.3.1), to monitor the region of interest. If needed $CaSO_4$ desiccant were placed inside the enclosure for required time to adjust the humidity as desired. The temperature in the laboratory was maintained at 23±2ºC. Using a micropipette (Volumate LiquiSystems, 20-200µl) desired microliter of suspension was then placed between the blade and the substrate.

Characterizations of the coated surface were done using optical microscope and Scanning electron microscope followed by image J analysis.

5.4 Experimental Details for Inkjet Printing

Monodispersed polystyrene particles with a mean diameter of 100-900 nm with a polydispersity of <4% were obtained from Fischer Scientific. The Polystyrene particles were dispersed or redispersed in ultrapure water at required solid loading. The dispersed solution (ink) were ultrasonicated for 2-5 min (Ultrasonic Cleaner, DSA 50-SK 2-2.5l). Unless otherwise stated, the polystyrene nanoparticles were concentrated by centrifugation (Eppendorf, Centrifuge 5424) as per required loading.

A P-type Si wafer of [100] orientation (Wacker Siltronic Corp., 525 μm ± 20 μm, 10-15 Ω-cm), and glass microscope slides (Fischer Scientific ,25 X 75 X 1 mm) was used as substrates. The Silicon wafer were at first cut into desired sizes and then pre-cleaned in an ultrasonicating bath to remove any organic or macro particles by using Iso propyl alcohol, methanol followed by rinsing with ultrapure water. To obtain hydrophilic surface both Chemical and physical methods were used. Chemical cleaning with piranha solution (3:1 Sulfuric acid: Hydrogen Peroxide heated to 100^{o}C) was performed for 30 minutes followed by rinsing with ultrapure water. Physical Cleaning was done using Oxygen Plasma Etcher (RF power of 100W, 25 SCCM of Oxygen for 300 seconds). Plasma cleaning was preferred due to less contamination on the surface. After the hydrophilic treatment of the silicon wafer, if needed it was spin coated with PVP (poly vinyl pyrolidone) solution of 0.1-3 vol. %. The coating thickness measured by filmetrics (Filmetrics F20-UV film thickness measurement systems) were around 150 nm in the middle and 114 nm on the outer edges. The contact angle of the polystyrene bead solution

of 0.5-1 vol. % were 16º. All the above contact angle measurements were carried out using Ramehart Contact angle Goniometer, Model 200 DS.

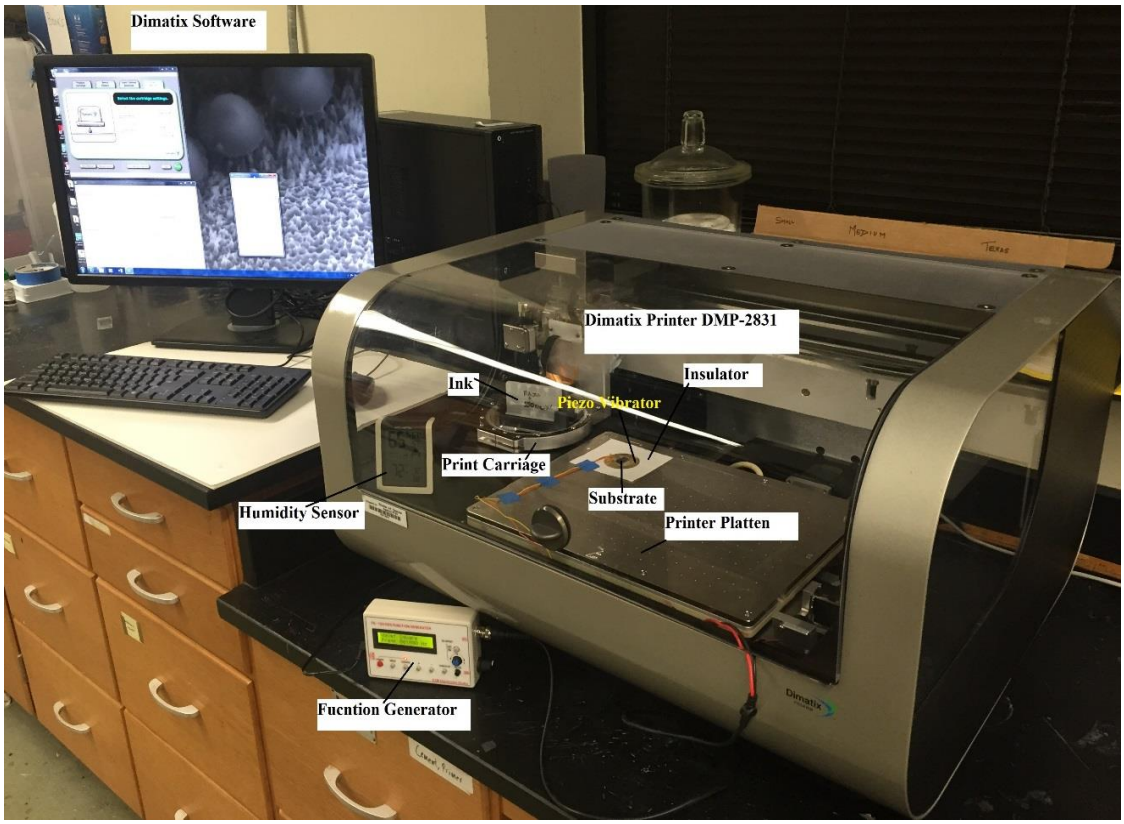

Figure 5.4.1 Inkjet Printer Setup

The colloidal solution consisting of monodispersed polystyrene spheres were coated on various substrate using an ink-jet printer manufactured by Dimatix a FujiFilm company DMP 2831. The printer works using a drop on demand technology with piezoelectric nozzle of orifice 21 um. The distance between the substrate and the nozzle was varied from 0.5mm to 1.5 mm and temperature of the substrate was kept fixed at 28ºC, the temperature of the print head was varied from 30-45ºC. Uniform ejection of the colloidal solution from the nozzle was obtained at 34V, jetting frequency of 1 kHz were used consistently due to low viscosity of the ink enabling higher reproducibility of the droplet. The volume of the ejected droplets were dependent on the absolute voltage.

A piezoelectric transducer from (Multicomp-piezo, 27mm dia., resonant frequency: 4400±500Hz, rated maximum voltage :20 V_{p-p}, resonant impedance > 300Ω, operating temperature: 20 to 60ºC) coupled with a function generator (ZJ Chao 1Hz-500KHz DS Function Signal Generator Module, maximum output amplitude is ±10Vpp (no-load), output impedance of 50Ω ± 10% DC bias of ± 10V (no-load) . 1 Hz power supply, DC 3.5-10V, output frequency range: sine wave ranging 1Hz-500KHz , square-wave ranging 1 Hz - 20kHz) is used to introduce mechanical vibration during the inkjet printing for frequencies ranging from 0-3000Hz at $10V_{p-p}$, with square wave .

We used the Dimatix inkjet printer to print the colloidal solution onto the hydrophilic surfaces with mechanical vibrations. An array of the droplets were deposited with varied dot to dot spacing ranging from 5 μm to 150 μm. Characterizations of the coated surface were done using optical microscope and Scanning electron microscope followed by image J analysis.

VI. APPLICATION

Current and future display devices benefits highly from the structural color property obtained from colloidal assembled films. Pixelated photonic crystal films producing green, red, blue and white is well known for replacing color filters and backlight of a liquid crystal displays. This enables higher picture quality and lower energy consumption (111). Current methods used for pixilation using colloidal particles are top down approaches namely micro molding in capillaries (MIMIC), UV etching via photolithography process (Figure 6.1), and selective photo polymerization in colloidal crystal films (112) .

These methods eventually enables one to pixelate more than one distinct structures with different band gap positions which can be used directly as color reflector in display devices (See Figure 6.2). Multiple steps of production and high cost is involved in these top down processes. Undoubtedly, a cheaper alternative to produce these structures will be very useful for this market segment. According to a materials report on TFT-LCD by Jurichich (113) , color filters is one of the most expensive component in display devices and accounts mostly due to its high manufacturing cost involved during the process of photolithography. If potential technology can replace the photolithography process, almost 20% decrease in manufacturing cost of display devices will be realized.

Lee et al (114) have reported formation of pixelated inverse opal giving red, blue and green colors. They produced inverse opal via multiple steps using a combination of top

down and bottom up approach. The sizes used to produce the inverse opal were 343, 278 and 249nm for red, blue and green color, respectively.

The size ratio(S/L) of the particle used to produce red, blue and green color is clearly above 0.5. According to our findings, phase segregation of these particles is possible via mere design of the reverse convective assembly process, which can significantly reduce the manufacturing cost to produce pixelated color.

According to a market research on global display market (2012-2017), the market is said to reach $164.24 billion by the year 2017, at a compound annual growth rate (CAGR) of 3.12% (115) . Anticipated CAGR of LCD and LED display is 20% (116). In addition, expected revenue from LCD display market alone is approximately $90 billion by 2016 (117).

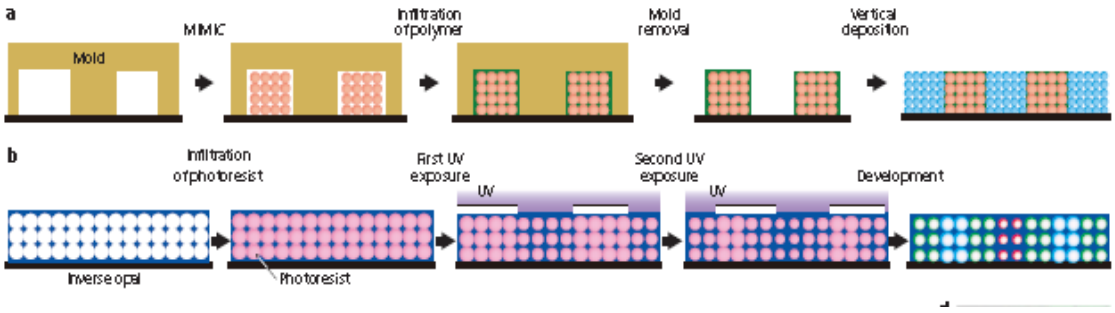

Figure 6.1 Patterning technique of photonic crystals (a) Contemporary MIMIC and vertical deposition technique for patterning of more than one sized colloidal particles (b) The different sized inverse opal formation for pixilation to produce red, green and blue (RGB) colors. Picture taken from reference (111).

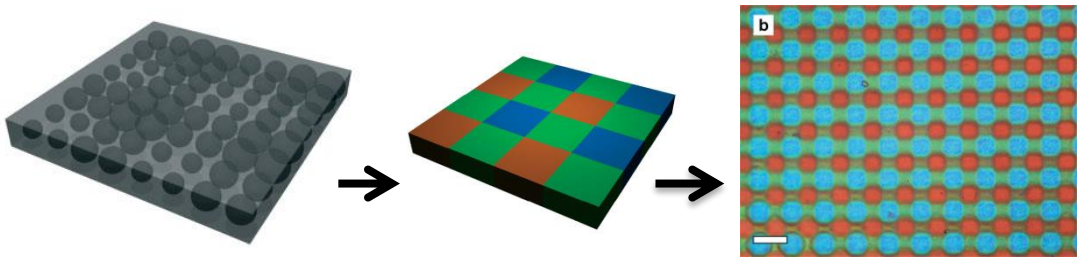

Figure 6.2 (i) Capping of patterned structure with liquid-crystal control layer (105). (ii) Animated picture of the expected color pattern (iii) a real optical image of a patterned film (Scale bar=100 um).Picture taken from reference (112)**.**

APPENDIX SECTION

Inkjet Printer*

FUJIFILM

Dimatix Materials Printer DMP-2831

System Description

- Flat substrate, xyz stage, inkjet deposition system
- Low cost, user-fillable piezo-based inkjet print cartridges
- Built-in drop jetting observation system
- Fiducial camera for substrate alignment and measurement
- Variable jetting resolution and pattern creation PC-controlled with Graphical User Interface (GUI) application software
- Capable of jetting a wide range of fluids
- Heated vacuum platen
- Cartridge cleaning station
- Includes PC, monitor, and software

Mechanical System

- Printable area
  - Substrate < 0.5 mm thickness: 210 mm x 315 mm (8.27 in x 12.4 in)
  - Substrate 0.5 - 25 mm thickness: 210 mm x 260 mm (8.27 in x 10.2 in)
- Repeatability: ± 25 µm (± 0.001 in)
- Substrate holder
  - Vacuum platen
  - Temperature adjustable; ambient to 60° C
- System Footprint: 673 mm x 584 mm x 419 mm (26 in x 23 in x 16 in)
- Weight approximately 43 kg (95 lbs)
- Power 100-120/200-240 VAC 50/60 Hz 375 W maximum
- Operating range 15-40° C at 5-80% RH non-condensing
- Altitude up to 2000 m
- Safety and EMC compliance
  - Safety: NRTL Certified to EN 61010-1, UL 61010-1, CSA 22.2 No. 61010-1
  - EMC: EN61326-1 Class A, FCC Part 15 Class A

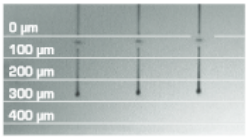

Drop Watcher View

Fiducial Camera

- Allows substrate alignment using reference marks
- Allows positioning a print origin or reference point to match substrate placement
- Provides measurement of features and locations
- Provides inspection and image capture of printed pattern or drops
- Provides cartridge alignment when using multiple cartridges
- Allows matching drop placement to previously patterned substrate

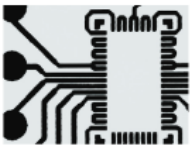

Fiducial Camera View

Cartridge

- Type: Piezo-driven jetting device with integrated reservoir and heater
- Usable Ink Capacity: Up to 1.5 ml (user-fillable)
- Materials Compatibility: Many water-based, solvent, acidic or basic fluids
- Number of Nozzles: 16 nozzles, 254 µm spacing, single row
- Drop Volume: 1 (DMC-11601) and 10 (DMC-11610) picoliter nominal

Control PC and Application Software

- Pre-loaded patterned templates
- Pattern preview
- Editors: Pattern, piezo drive waveform, cleaning cycle, substrate setting
- Bitmap (1 bit) files accepted
- DXF, Gerber, GDSII and OASIS file conversion to Bitmap

Replaceable Items

- Print cartridge with one-time user-fillable reservoir
- Cleaning station nozzle blotting pad
- Drop watcher fluid absorbing pad

Source*: https://www.fujifilmusa.com/shared/bin/PDS00085-DMP2831.pdf

Syringe Pump **

Specifications

Mechanical & Electrical

Syringe sizes:	Up to 60 mL (140 mL partially filled)
Number of syringes:	1
Motor type:	Step motor
Motor steps per revolution:	400
Microstepping:	1/8 to 1/2 depending on motor speed
Advance per step:	0.2126 uM to 0.8504 uM depending on motor speed
Motor to drive screw ratio:	15/28
Drive screw pitch:	20 revolutions/"
DC connector:	2.1 mm, center positive
Voltage at DC connector:	12V DC at full load
Amperage:	750 mA at full load
Power supply type:	Unregulated linear external wall adapter, country and power source specific
Power supply output rating:	12V DC @ 800 mA
Dimensions:	8 3/4" x 5 3/4" x 4 1/2" High (22.86 cm x 14.605 cm x 11.43 cm)
Weight:	3.6 lbs. (1.63 kg)
Allen Wrench	3/32 Hex

Operational

Maximum speed:	5.1005 cm/min
Minimum speed:	0.004205 cm/hr
Maximum pumping rate:	1699 mL/hr with a B-D 60 cc syringe
Minimum pumping rate:	0.73 µL/hr with a B-D 1 cc syringe
Maximum force:	35 lbs. at minimum speed, 18 lbs. at maximum speed
Number of Program Phases:	41
RS-232 pump network:	100 pumps maximum
RS-232 selectable baud rates:	300, 1200, 2400, 9600, 19200
Syringe inside diameter range:	0.100 to 50.00 mm

Custom Applications

For specialized and OEM applications, contact your dealer or New Era Pump Systems Inc. Custom modifications can be made to the mechanics or the firmware.

Source**: http://www.syringepump.com/download/NE-1000Brochure.pdf

Sample Mathematica Code:

```
rhop = 1.781 × 10^3;
rhol = 0.781 × 10^3;
g = 9.80665;
T = 0.4 / 10^2;
q = Sqrt[((rhop - rhol) g) / T];
bb = 0.0000001;
alpha1 = Pi / 6;
R1 = 900 / 10^9;
R2 = 900 / 10^9;
l0 = 400 / 10^9;
E1 = 1.781072418 ;
alpha2 = Pi / 6;

(*r2 =Re[ Sqrt[(l0 -h)  (2 R2 - l0 + h)]];*)
For[h1 = 400 / 10^9, h1 < 1.2 R1 - l0, h1 = h1 + 10 / 10^9,
  Psi1 = ArcSin[r1 / R1] - alpha1;
 Psi2 = ArcSin[r2 / R2] - alpha2;
  r1 = Sqrt[(l0 + h1) (2 R1 - l0 - h1)];
 r2 = r1;
 h = h1;
a = Sqrt[bb * (bb + 2 * r1) * (bb +
   2 * r2) * (bb + 2 * r1 + 2 * r2) / (4 * (bb + r1 + r2) ^2)];
T1 = Log[(a / r1) + Sqrt[(a^2 / r1^2) + 1]];
T2 = Log[(a / r2) + Sqrt[(a^2 / r2^2) + 1]];
A = ∑_{k=1}^{2} (1 / k) * ((Sinh[k * (T1 - T2)]) / (Sinh[k * (T1 + T2)]));
B = ∑_{k=1}^{2} (2 / k) * ((Exp[-k * T2 * Sinh[k * T1]]) / (Sinh[k * (T1 + T2)]));
  (*= r1*Sin[
      Psi1]*(T1 + 2*Log[1 - Exp[-2*T1]]) - (r1*Sin[Psi1] +
       r2*Sin[Psi2])*
     Log[E1*q*a] + (r1*Sin[Psi1] -  r2*Sin[Psi2])*(A +  B) - h ;
 (*Plot[k,{h,-1/(5*10^6),3000*1/(5*10^6)}] ]*)*)

Print["{r1,r2,h1,h, Energy}=", {N[r1], N[r2], N[h1], Re[Abs[N[h]]], Re[(- ((Pi *
     T) ((2 h1 R1 Cos[alpha1] - r1 h1 Sin[Psi1] +
      r1^2) + (2 Re[Abs[h]] R2 Cos[alpha2] - r2 Re[Abs[h]] Sin[Psi2] +
      r2^2)) - ((rhop - rhol) g) (
    ( Pi / 2) * (- (h1^2) / 2) (2 l0 (2 R1 - l0) - h1^2) + ((4 /
      3) (R1 - l0) (-h1^2) + r1^2 h1^2) +
    (Pi / 2) * (-h^2 / 2) (2 l0 (2 R2 - l0) - h^2) + ((4 /
      3) (R2 - l0) (-h^2) + r2^2 h^2))) / (10^(-14)))]}]](*/.
  FindRoot[r2*Sin[
      Psi2]*(T2 + 2*Log[1 - Exp[-2*T2]]) - (r1*Sin[Psi1] +
       r2*Sin[Psi2])*
     Log[E1*q*a] + ((r1*Sin[Psi1] -  r2*Sin[Psi2])*(A -  B) )- h== 0,
    {h,300*10^(-9)+I 10^(-9)}]]]*)
```

Sample Mathematica Output:

$$\{r1,r2,h1,h,\ \text{Energy}\}=\{8.94427\times10^{-7},\ 8.94427\times10^{-7},\ 4.\times10^{-7},\ 4.\times10^{-7},\ -3.10718\}$$

$$\{r1,r2,h1,h,\ \text{Energy}\}=\{8.95489\times10^{-7},\ 8.95489\times10^{-7},\ 4.1\times10^{-7},\ 4.1\times10^{-7},\ -3.09858\}$$

$$\{r1,r2,h1,h,\ \text{Energy}\}=\{8.96437\times10^{-7},\ 8.96437\times10^{-7},\ 4.2\times10^{-7},\ 4.2\times10^{-7},\ -3.12774\}$$

$$\{r1,r2,h1,h,\ \text{Energy}\}=\{8.97274\times10^{-7},\ 8.97274\times10^{-7},\ 4.3\times10^{-7},\ 4.3\times10^{-7},\ -3.15651\}$$

$$\{r1,r2,h1,h,\ \text{Energy}\}=\{8.97998\times10^{-7},\ 8.97998\times10^{-7},\ 4.4\times10^{-7},\ 4.4\times10^{-7},\ -3.18491\}$$

$$\{r1,r2,h1,h,\ \text{Energy}\}=\{8.9861\times10^{-7},\ 8.9861\times10^{-7},\ 4.5\times10^{-7},\ 4.5\times10^{-7},\ -3.21295\}$$

$$\{r1,r2,h1,h,\ \text{Energy}\}=\{8.99111\times10^{-7},\ 8.99111\times10^{-7},\ 4.6\times10^{-7},\ 4.6\times10^{-7},\ -3.24066\}$$

$$\{r1,r2,h1,h,\ \text{Energy}\}=\{8.995\times10^{-7},\ 8.995\times10^{-7},\ 4.7\times10^{-7},\ 4.7\times10^{-7},\ -3.26805\}$$

$$\{r1,r2,h1,h,\ \text{Energy}\}=\{8.99778\times10^{-7},\ 8.99778\times10^{-7},\ 4.8\times10^{-7},\ 4.8\times10^{-7},\ -3.29513\}$$

$$\{r1,r2,h1,h,\ \text{Energy}\}=\{8.99944\times10^{-7},\ 8.99944\times10^{-7},\ 4.9\times10^{-7},\ 4.9\times10^{-7},\ -3.32192\}$$

$$\{r1,r2,h1,h,\ \text{Energy}\}=\{9.\times10^{-7},\ 9.\times10^{-7},\ 5.\times10^{-7},\ 5.\times10^{-7},\ -3.34844\}$$

$$\{r1,r2,h1,h,\ \text{Energy}\}=\{8.99944\times10^{-7},\ 8.99944\times10^{-7},\ 5.1\times10^{-7},\ 5.1\times10^{-7},\ -3.3747\}$$

$$\{r1,r2,h1,h,\ \text{Energy}\}=\{8.99778\times10^{-7},\ 8.99778\times10^{-7},\ 5.2\times10^{-7},\ 5.2\times10^{-7},\ -3.41379\}$$

$$\{r1,r2,h1,h,\ \text{Energy}\}=\{8.995\times10^{-7},\ 8.995\times10^{-7},\ 5.3\times10^{-7},\ 5.3\times10^{-7},\ -3.45315\}$$

$$\{r1,r2,h1,h,\ \text{Energy}\}=\{8.99111\times10^{-7},\ 8.99111\times10^{-7},\ 5.4\times10^{-7},\ 5.4\times10^{-7},\ -3.49279\}$$

$$\{r1,r2,h1,h,\ \text{Energy}\}=\{8.9861\times10^{-7},\ 8.9861\times10^{-7},\ 5.5\times10^{-7},\ 5.5\times10^{-7},\ -3.53273\}$$

$$\{r1,r2,h1,h,\ \text{Energy}\}=\{8.97998\times10^{-7},\ 8.97998\times10^{-7},\ 5.6\times10^{-7},\ 5.6\times10^{-7},\ -3.57298\}$$

$$\{r1,r2,h1,h,\ \text{Energy}\}=\{8.97274\times10^{-7},\ 8.97274\times10^{-7},\ 5.7\times10^{-7},\ 5.7\times10^{-7},\ -3.61354\}$$

$$\{r1,r2,h1,h,\ \text{Energy}\}=\{8.96437\times10^{-7},\ 8.96437\times10^{-7},\ 5.8\times10^{-7},\ 5.8\times10^{-7},\ -3.65443\}$$

$$\{r1,r2,h1,h,\ \text{Energy}\}=\{8.95489\times10^{-7},\ 8.95489\times10^{-7},\ 5.9\times10^{-7},\ 5.9\times10^{-7},\ -3.69567\}$$

$$\{r1,r2,h1,h,\ \text{Energy}\}=\{8.94427\times10^{-7},\ 8.94427\times10^{-7},\ 6.\times10^{-7},\ 6.\times10^{-7},\ -3.73725\}$$

$$\{r1,r2,h1,h,\ \text{Energy}\}=\{8.93252\times10^{-7},\ 8.93252\times10^{-7},\ 6.1\times10^{-7},\ 6.1\times10^{-7},\ -3.7792\}$$

$$\{r1,r2,h1,h,\ \text{Energy}\}=\{8.91964\times10^{-7},\ 8.91964\times10^{-7},\ 6.2\times10^{-7},\ 6.2\times10^{-7},\ -3.82151\}$$

$$\{r1,r2,h1,h,\ \text{Energy}\}=\{8.90562\times10^{-7},\ 8.90562\times10^{-7},\ 6.3\times10^{-7},\ 6.3\times10^{-7},\ -3.86421\}$$

$$\{r1,r2,h1,h,\ \text{Energy}\}=\{8.89044\times10^{-7},\ 8.89044\times10^{-7},\ 6.4\times10^{-7},\ 6.4\times10^{-7},\ -3.90729\}$$

$$\{r1,r2,h1,h,\ \text{Energy}\}=\{8.87412\times10^{-7},\ 8.87412\times10^{-7},\ 6.5\times10^{-7},\ 6.5\times10^{-7},\ -3.95078\}$$

$$\{r1,r2,h1,h,\ \text{Energy}\}=\{8.85664\times10^{-7},\ 8.85664\times10^{-7},\ 6.6\times10^{-7},\ 6.6\times10^{-7},\ -3.99467\}$$

$$\{r1,r2,h1,h,\ \text{Energy}\}=\{8.83799\times10^{-7},\ 8.83799\times10^{-7},\ 6.7\times10^{-7},\ 6.7\times10^{-7},\ -4.03899\}$$

REFERENCES

1. *Self-assembly at all scales.* **GM Whitesides and B Grzybowski. 295(5564):2418–2421, March 2002.** 5564, 2002, SCIENCE, Vol. 295, pp. 2418-2421.
2. *Toward smart nano-objectsby self assembly of block co-polymersin solution.* **J. Rodrguez-Hernndez, F. Chcot, Y. Gnanou, and S. Lecommandoux.** 7, 2005, Progress in Polymer Science, Vol. 30, pp. 691-724.
3. *Self healing and thermo reversible rubber from supramolecular assembly.* **hilippe Cordier, Francois Tournilhac, Corinne Soulie-Ziakovic, and Ludwik Leibler.** 7181, 2008, Nature, Vol. 451, pp. 977-980.
4. *Folding DNA to create nanoscale shapes and patterns.* **Rothemund., Paul W. K.** 7082, 2006, Nature, Vol. 440, pp. 297-302.
5. *Logical Computation using algorithmic self-assembly of DNA triple-crossover molecules.* **Chengde Mao, Thomas H. LaBean, John H. Reif, and Nadrian C. Seeman.** 6803, 2000, Nature , Vol. 407, pp. 493-496.
6. *Synthesis, Modification, Organization and Utilization of Colloid Particles.* **F. Caruso, Colloids and Colloid Assemblies:.** 2004., 1st ed., Wiley-VCH Verlag GmbH & Co. KGaA, Weinheim, .
7. ***Y.A. Vlasov, X.Z. Bo, J.C. Sturm, D.J. Norris,.*** *2001, Nature, Vol. 414 , pp. 289–293.*
8. ***A.N. Shipway, E. Katz, I. Willner.*** *2000, ChemPhysChem, Vol. 1, pp. 18-52.*
9. ***Joannopoulos, J.D.*** *2001, Nature, Vol. 414, pp. 257-258.*
10. ***Velev, O.D.*** *2001, Handbook of Surfaces and Interfaces of Materials, Academic Press, pp. 1-43.*
11. ***Shimmin, G. R.*** *Evaporation driven self-assembly as a route to photonic materials,. University of Illinois at Urbana-Champaign, Urbana, Illinois,USA. : s.n., (2007).*
12. ***T.A. Taton, D.J. Norris.*** *685, 2002, Nature, Vol. 416.*
13. ***A. Imhof, D.J. Pine.*** *948, 1997, Nature, Vol. 389.*
14. ***Rabideu, D.*** *the self assembly of colloidal particlesinto 2D arrays. Austin, TX : s.n., 2007.*
15. Perfectly hydrophobic surfaces with patterned nanoneedles of controllable features. ***Park, S.G., Lee,S.Y.,Jang S.G.,Yang,S.M.*** *s.l. : Langmuir, 2010, Vol. 26.*
16. Bioinspired self cleaning antireflection coatings. ***Min, W.L.,Jiang,B.,Jiang,P.*** *3914, s.l. : Advanced Materials, 2008, Vol. 20.*
17. Cell adhesion strength is controlled by intermolecular spacing of adhesion receptors. ***Selhuber-Unkel, C.,Erdmann,T.,Lopez-Garcia,M.,Kessler,H.,Schwartz,U.S.,Spatz,J.P.*** *s.l. : Biophysical Journal, 2010, Vol. 98.*
18. ***S.M. Yang, H. Miguez,G.A. Ozin.*** *12, 2002, Adv. Funct. Mater., Vol. 425.*
19. ***P. Yang, T. Deng, D. Zhao, P. Feng, D. Pine, B. F. Chmelka, G. M.Whitesides, G. D. Stucky,.*** *282, 1998, Science , Vol. 2244.*
20. A new measurement method for ultrasonic surface roughness measurement. ***F. Forouzbakhsh, J. Rezanejad Gatabi and I. Rezanejad Gatabi.*** *s.l. : Measurement,Elseiver, 2008.*

21. Light diffraction from opal-based photonic crystals with growth-induced disorder: Experiment and theory. ***AV Baryshew, Va Kosobukin,KB Samusev,DE Usvyat, MF Limonov.*** *20, s.l. : Physical Review B, 2006, Vol. 73.*
22. Physics and chemistry of interfaces. ***Butt, H.J., Graf,K.,&Kappl, M.*** *s.l. : Weinham Wiley, 2006.*
23. ***Stern, O.*** *s.l. : Zeitschrift fur Angewande Physik und Chemie, 1924, Vol. 30.*
24. ; Capillary forces and structuring in layers of colloid particles,. ***Peter A. Kralchevsky, Nikolai D. Denkov.*** *6, s.l. : Current Opinion in Colloid & Interface Science , 2001, Vol. 383401.*
25. ***Li, Q., Jonas,U., zhao, X.S., & Kapp,M.*** *s.l. : Asia Pacific Journal of Chemical Engineering, 2008, Vol. 3.*
26. ***J.B. Perrin.*** *5-114, s.l. : Ann.Chem.Phys, 1909, Vol. 18.*
27. ***M. Trau, D. A. Saville, and I. A. Aksay.*** *13, s.l. : Langmuir , 1997, Vol. 6375.*
28. ***B. Gates, D. Qin, Y. Xia,.*** *11, s.l. : Adv. Matter. , 1999, Vol. 466 .*
29. ***Nagayama., A.S.Dimitrov and K.*** *12, s.l. : Langmuir , 1996, Vol. 1303.*
30. ***Denkov. N, Velev. O, Karalchevsky. P, K. Nagayama,.*** *8, s.l. : Langmuir , 1992, Vol. 3183.*
31. ***Hulteen. J, Van. Duyne. R. J. Vac.*** *13 , s.l. : Sci. Techno A , 1995, Vol. 1553. 3.*
32. ***Malaquin, L.,Kraus, T., Schmid, H.,Delamarche,E., & Wolf, H.*** *s.l. : Langmuir, 2007, Vol. 23.*
33. ***Park, S.H.,Qin,D., Xia ,Y.*** *10, s.l. : Adv. Mater., 1998, Vol. 1028.*
34. ***Chen, K.M., Jiang,X.,Kimerling,L.C., & Hammond,P.T.*** *s.l. : Langmuir, 2000, Vol. 16.*
35. ***Weekes, S.M.,Orgin,F.Y.,Murray,W.A.,& Keatley,P.S.*** *s.l. : Langmuir, 2007, Vol. 23.*
36. Engineered deposition of coatings from nano- and micro-particles: A brief review of convective assembly at high volume fraction. Colloids and Surfaces . ***B.G. Prevo, D.M.Kuncicky, O.D.Velev,.*** *2-10, s.l. : A: Physicochem. Eng. Aspects , 2007, Vol. 311.*
37. ***P. Jiang, J.F. Bertone, K.S. Hwang, V.L. Colvin,.*** *s.l. : Chem. Mater. , 1999, Vol. 11.*
38. Steady-state unidirectional convective assembling of fine particles into 2-dimensional arrays. ***A.S. Dimitrov, K. Nagayama,.*** *s.l. : Chem. Phys. Lett., 1995, Vol. 243.*
39. ***A.S. Dimitrov, K. Nagayama,.*** *s.l. : Langmuir , 1996, Vol. 12.*
40. ***C.J. Brinker, Y.F. Lu, A. Sellinger, H.Y. Fan,.*** *s.l. : Adv. Mater., 1999, Vol. 11.*
41. ***N.D. Denkov, O.D. Velev, P.A. Kralchevsky, I.B. Ivanov, H. Yoshimura, K.Nagayama,.*** *s.l. : Nature , 1993, Vol. 361.*
42. Steady-state unidirectional convective assembling of fine particles into 2-dimensional arrays, . ***A.S. Dimitrov, K. Nagayama,.*** *s.l. : Chem. Phys. Lett., 1995, Vol. 243.*
43. Effect of Nanoparticle Concentration on the Convective Deposition of Binary Suspensions . ***Pisist K., and James F. G.,.*** *s.l. : Langmuir, 2009.*
44. ***Prevo B.G., & Velev,O.D.*** *s.l. : Langmuir, 2004, Vol. 20.*
45. Restricted meniscus convective self assembly. ***Kai Chen, Stefan V. Stoianov, Justin Bangerter, Hans D. Robinson.*** *s.l. : Journal of Colloid and Interfacial Science, 2010, Vol. 344.*
46. ***De Gans, B. J., Duineveld, P. C. and Schubert, U.S.*** *s.l. : AdV. Mater. , 2004.*
47. ***P., Calvert.*** *13, s.l. : Chem. Mater., 2001, Vol. 3299.*

48. ***Sirringhaus, H. and Shimoda, T.*** *28, s.l. : MRS Bull, 2003, Vol. 802.*
49. Highly ordered self-assembling polymer/clay nanocomposite barrier film. ***Ray Cook, Yihong Chen, and Gary W. Beall.*** *20, s.l. : ACS Appl. Mater. Interfaces, 2015, Vol. 7.*
50. ***Sirringhaus, H., et al.*** *s.l. : Science, 2000, Vols. 290,2123.*
51. ***Shimoda, T.,Inbasekaran, Seki, S. and Kiguchi, H.*** *28, s.l. : MRS Bull. , 2003, Vol. 821.*
52. ***Reis, N, Ainsley, C,Derby, B. Am.*** *82, s.l. : Ceram. Soc. Bull. , 2003, Vol. 9101.*
53. ***Katstra, W.E., Palazzolo,R.D. Rowe, C. W., et al.*** *1, s.l. : J. Controlled Release , 2000, Vol. 66.*
54. Using convective flow splitting for the direct printing of fine copper lines. ***Cuk, T., Troian, S. M., Hong, C. M. and Wagner, S.*** *77, s.l. : Applied Phys. Lett., 2000, Vol. 2063.*
55. Drawing a single nanofibre over hundreds of microns. ***Ondarcuhu, T. and Joachim, C.*** *s.l. : Europhysics Letters, , 1998, Vol. 42.*
56. Rings and Hexagons made of nanocrystals. . ***Maillard, M., Motte, L. and Pileni, M.-P.*** *s.l. : Advanced Materials, 2001, Vol. 13.*
57. ***J. F. Dijksman.*** *s.l. : J. Fluid Mech., 1984, Vols. 139,173.*
58. ***Fromm, J. E.*** *s.l. : IBM J. Res. Dev., 1984, Vols. 28,322.*
59. ***D. B. van Dam and C. L. Clerc.*** *s.l. : Phys. Fluids, 2004, Vols. 16,3403.*
60. ***S. Magdassi, M. Grouchko, D. Toker, A. Kamynshny, I. Balberg andO. Millo.*** *21, s.l. : Langmuir, 2005, Vol. 10264.*
61. ***E. Tekin, B.-J. de Gans and U. S. Schubert,.*** *14, s.l. : J.Mater. Chem., , 2004, Vol. 2627.*
62. ***H.-Y. Ko, J. Park, H. Shin and J. Moon,.*** *16, s.l. : Chem. Mater., , 2004, Vol. 4212.*
63. ***J. Park and J. Moon.*** *22, s.l. : Langmuir, 2006, Vol. 3506.*
64. Superadhesion: Attachment of Nanobacteria to Tissues-Model Simulation. ***Sommer, A. P., Cehreli, M., Akca, K., Sirin, T. and Piskin, E.*** *s.l. : Crystal Growth and Design, 2005, Vol. 5.*
65. ***Sommer, A. P. Suffocation of Nerve Fibers by Living Nanovesicles:.*** *3, s.l. : A Model Simulation - Part II. Journal of Proteome Research, 2004, Vol. 1086.*
66. ***Plettl, A., Enderle, F.,Saitner,M., Manzke,a., Pfahler,C., Wiedemann,S., et.al.*** *s.l. : Adv. Funct. Mater., 2009, Vol. 19.*
67. ***Yan, X.,Yao,J.,Lu,G.,Li,X., Zhang,J.,Han,K.,et. al.*** *s.l. : Journ. of the American Chem. Soc., 2005, Vol. 127.*
68. ***Li, X., Wang,T.Q., Zhang,J.H.,Yan,X., Zhang, X.M., Zhu,D.F., et. al.*** *s.l. : Langmuir, 2010, Vol. 26.*
69. ***Pan, F.,Zhang,J.Y., Cai,C.& Wang,T.M.*** *s.l. : Langmuir, 2006, Vol. 22.*
70. ***Venkatesh, S.,Jiang,P.,& Jiang,B.*** *s.l. : Langmuir, 2007, Vol. 23.*
71. ***Aveyard, R.,Clint,J.H.,Nees,D.,& Paunov,V.N.*** *s.l. : Langmuir, 2000, Vol. 16.*
72. ***McGorty, R.,Fung,J.,Kaz,D.,&Manoharan,V.N.*** *s.l. : Materials Today, 2010, Vol. 13.*
73. ***Horozov, T.S., Aveyard,R.,Clint,J.H.,& binks,B.P.*** *s.l. : Langmuir, 2003, Vol. 19.*
74. ***Horozov, T.S., Aveyard,R., binks,B.P.& Clint,J.H.*** *s.l. : Langmuir, 2005, Vol. 21.*
75. ***Vogel, N.*** *Surface Patterning with colloidal monolayers. Doctoral thesis . The University of Mainz, Germany : Springer Theses, 2012.*

76. Two-dimensionally patterned nanostructures based on monolayer colloidal crystals: Controllable fabrication, assembly, and applications. ***Xiaozhou Ye, Limin Qi,.*** *s.l. : Nano Today , 2011, Vol. 6.*
77. ***Velikov, K.P.,Christova,C.G.,Dullens,R.P.A.,& van Blaaderen,A.*** *s.l. : Science, 2002, Vol. 296.*
78. ***Kim, M.H.,Im, S.H.,&Park,O.O.(.*** *17, s.l. : Advanced Materials, 2005, Vol. 2501.*
79. Fabrication of Binary Colloidal Crystals and Non Close Packed Structures by a sequential Self Assembly Method. ***Zhou, Z. C., et al.*** *2007, Langmuir, Vol. 23, pp. 1473-1477.*
80. ***Huang, X.G.,Zhou,J.,Fu,M.,Li,B.,Wang, Y.H.,Zhao,Q., et al.*** *s.l. : Langmuir, 2007, Vol. 23.*
81. ***Kitaev, V., & Ozin, G.A.*** *16, s.l. : Advanced Materials, 2003, Vol. 244.*
82. ***Cong, H.L., & Cao,W.X.*** *s.l. : The Journal of Physical Chemistry B, 2005, Vol. 109.*
83. ***Sanchez-Iglesias, A., Grzelczak, M., Perez-Juste, J., & Liz-Marzan, L. M.,.*** *s.l. : Angewandte Chemie. International Edition, 2010, Vol. 49.*
84. ***Kumnorkaew, P., & Gilchrist, J.F.*** *s.l. : Langmuir, 2009, Vol. 25.*
85. ***Sing, G., Pillai,S.,Arpanaei,A., & Kingshott,P.*** *s.l. : Advanced Materials, 2011, Vol. 23.*
86. ***Yu, J., Yan, Q. F., &Shen, D.Z.*** *s.l. : ACS Applied Materials & Interfaces, 2010, Vol. 2.*
87. ***Wang D., & Mohwald, H.*** *15, s.l. : Advanced Materials, 2004, Vol. 75.*
88. Segregation Phenomena in Monodisperse Colloids. ***al., Hachisu et.*** *3, s.l. : Journal of Colloid and Interface Science, 1976, Vol. 55.*
89. Size Dependent Separation of colloidal particles in Two-Dimensional Convective Self Assembly. ***Yamaki, M., Higo, J., & Nagayama, K.*** *s.l. : Langmuir, 1995, Vol. 11.*
90. Simulation of self assemblies of colloidal particles with different sizes by using a lattice boltzman pseudo solid model,International . ***al., Gongyu Liang et.*** *12, s.l. : Journal of Modern Physics C, , 2013, Vol. 24.*
91. ***Barrat J L, Baus M and Hansen J P.*** *56, s.l. : Phys. Reu. Lett. , 1986, Vol. 1063.*
92. ***J, Murray M J and Saunders.*** *42, s.l. : Phil.Mag. A, 1980, Vol. 721.*
93. ***Bartlett P, Ottewill R H and Pusey P N.*** *s.l. : J. Chem. Phys, 1990.*
94. Phase behaviour of deionized binary mixtures of charged colloidal spheres . ***Nina J Lorenz et al., N.*** *Institute for Colloidal Organization, Hatoyama 3-1-112 Uji, Kyoto 611-0012 Japan. : s.n.*
95. Entropically driven surface phase segregation in binary colloidal mixtures. ***P.D. Kaplan, J.L. Rouke, & A.G. Yodh.*** *4, s.l. : Physical Review Letters, 1994, Vol. 72.*
96. Phase Diagram, Design of Monolayer Binary Colloidal Crystals, and Their Fabrication Based on Ethanol-Assisted Self-Assembly at the Air/Water Interface. ***Zhengfei .D., Yue L., Guotao D., Lichao J., & Weiping C.*** *2012.*
97. ***Thermo Fischer Scientific.*** *Derivation of Count per Milliliter from Percentage of Solids, Technical Note TN-017.04.*
98. ***Reynaert, S.,Moldeneaers,P., & Vermant, J.*** *s.l. : Langmuir, 2006. Vol. 22.*
99. ***Hulteen, J.C.,Vanduyne,R.P.*** *s.l. : Journal of Vaccum Science and Technology A-Vaccum Surface Films, 1995, Vol. 13.*
100. ***Fischer U.C., & Zingsheim, H.P.*** *s.l. : Journal of Vaccum Science and Technology, 1981, Vol. 19.*

101. ***Isa, L., Kumar,K.,Muller,M.,Grolig,J.,Textor,M& Reimhult,E.*** *s.l. : ACS Nano, 2010. Vol. 4.*
102. ***Ray, M.A.,Jia,&L.*** *19, s.l. : Advanced Materials, 2007, Vol. 2020.*
103. ***Bhawalkar, S.P., Qian,J.,Heiber,M.C.,& Jia,L.*** *s.l. : Langmuir, 2010, Vol. 26.*
104. ***Retsch, M.Tamm,M.,Bocchio,N.,Horn,N.,Forch,R.,Jonas,U., et.al.*** *s.l. : Small Weinheim an der Bergstrasse,Germany, 2009, Vol. 5.*
105. ***Choi, D.G..,H.K.,Jang, S. G., & Yang, S. M.*** *s.l. : Journal of American Chemical Society, 2004, Vol. 126.*
106. ***Harkins, W.D.*** *s.l. : Journal of American Chemical Society, 1947, Vol. 69.*
107. In film formations in coatings. ***Tang, J.,DanielsEric,S.,Dimonie Victoria,L.,Klein,A.,& El-Aaser Moham,S.*** *s.l. : ACS, 2001, Vol. 790.*
108. ***K. M. Ho, C. T. Chan, and C. M. Soukoulis.*** *1990, Phys. Rev. Lett. , Vol. 65, p. 3152.*
109. Mechanism for Stripe Pattern Formation on Hydrophilic Surfaces by using Convective Self Assembly . ***Watanabe, S., et al.*** *s.l. : Langmuir , 2009, Vol. 25.*
110. Energetical and Force Approaches to the Capillary Interactions between particles attached to a liquid-fluid interface. ***et.al., Kralchevsky.*** *s.l. : Journal of Colloid and Interfacial Science, 1993, Vol. 155.*
111. Self-assembled colloidal structures for photonics. ***Shin-Hyun Kim1, Su Yeon Lee, Seung-Man Yang and Gi-Ra Yi,,.*** *1, s.l. : NPG Asia Mater, 2011, Vol. 3.*
112. ***I. Lee et al.*** *22, s.l. : Adv. Mater. , 2010, Vol. 4973.*
113. ***Jurichich, Steve.*** *Summary of The TFT LCD Materials Report.*
114. ***Su Yeon Lee, Shin-Hyun Kim,Hyerim Hwang,Jae Young Sim, Seung-Man Yang.*** *15, 2014, Vol. 26, pp. 2391-2397.*
115. ***[Online] http://www.marketsandmarkets.com/Market-Reports/display-market-925.html.***
116. [Online] http://www.marketsandmarkets.com/PressReleases/display.asp.
117. [Online] http://www.dolcera.com/wiki/index.php?title=LCD_Technologies.